Noninvasive Assessment of Cardiovascular Health

By

Xinshu Xiao

B.S., Precision Instrument (1998)
Tsinghua University, P.R.China

Submitted to the Department of Mechanical Engineering
in Partial Fulfillment of the Requirements
for the Degree of

Master of Science
in Mechanical Engineering

at the

Massachusetts Institute of Technology
August 2000
[September 2000]

Signature of Author.................................
Department of Mechanical Engineering
August 20, 2000

Certified by...................................... ι   ....
Roger D. Kamm
Professor of Mechanical Engineering and BEH
Thesis Supervisor

Accepted by...
Ain A.Sonin
Chairman, Departmental Committee on Graduate Studies
Department of Mechanical Engineering
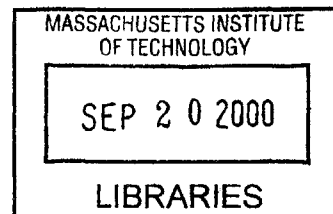
Noninvasive Assessment of Cardiovascular Health

By

Xinshu Xiao

Submitted to the Department of Mechanical Engineering on August 2000
in Partial Fulfillment of the Requirements for the

Degree of Master of Science in Mechanical Engineering

Abstract

Cardiovascular health is currently assessed by a collection of hemodynamic parameters many of which can only be measured by invasive methods often requiring hospitalization. A non-invasive approach of evaluating some of these parameters, such as systemic vascular resistance (SVR), maximum left ventricular elasticity (E_{LV}), end diastolic volume (V_{ED}), cardiac output and others, has been established. The method has three components: (1) a distributed model of the human cardiovascular system (Ozawa) to generate a solution library that spans the anticipated range of parameter values, (2) a method for establishing the multi-dimensional relationship between features computed from the arterial blood pressure and/or flow traces (e.g., mean arterial pressure, pulse amplitude, mean flow velocity) and the critical hemodynamic parameters, and (3) a parameter estimation method that provides the best fit between measured and computed data. Sensitivity analyses are used to determine the critical parameters that must be allowed to vary, and those that can be assumed to be constant in the model. Given the brachial pressure and velocity profiles (which can be measured non-invasively), this method can estimate SVR with an error of less than 3%, and E_{LV} and V_{ED} with less than 10% errors.

Measurements on healthy volunteers and patients were conducted in Brigham and Women's Hospital, Boston, MA. Carotid, brachial and radial pressures were measured by tonometry and velocities at corresponding locations were measured by ultrasound. Reasonable agreement is found between the measured pressure and velocity curves and the reconstructed ones. Invasive measurements of hemodynamic parameters are available for two of the patients, which are compared to predictions to evaluate the performance of parameter estimation routines.

Thesis Supervisor: Roger D. Kamm, Ph.D.

Title: Professor of Mechanical Engineering and the Division of Bioengineering and Environmental Health

Acknowledgement

There are lots of people I would like to acknowledge who have helped me in my work. First, I am forever grateful to my thesis advisor, Prof. Roger D. Kamm, for his careful guidance, continuous inspiration and support. His excellent management style and great concern for students have created a very exciting and friendly working environment in the research group, in which I have enjoyed greatly for the past two years. I could not have asked for a better advisor.

I would like to thank Dr. Richard T. Lee and Dr. Nancy Sweitzer in Brigham and Women's Hospital, Boston, for doing all those experiments and for always giving insightful thoughts and advice to my work.

I am grateful to all members of the Fluid Mechanics Laboratory for their help and friendship over the years, which will always be cherished.

I also want to thank Prof. C. F. Dewey and Prof. Roger G. Mark in HST for giving me invaluable advice and encouragement when they employed our cardiovascular model in their projects. Thanks also go to Dr. David Kass and Barry Fetics in John Hopkins University for answering my questions regarding the left ventricle elasticity curve.

I would like to thank Claire Sasahara and Leslie Regan for their expert administrative assistance.

I owe a debt of gratitude to my sister and my parents for their love, understanding and fully support throughout my education. I would like to thank Zhuangli, my devoted and wonderful husband, for all the wise advice and encouragement to my work and for sharing the extraordinary life experience with me.

Finally, and with great emphasis, thanks go to the Home Automation and Healthcare Consortium in MIT who funded this project and the Rosenblith fellowship who supported my stay during the past year.

Table of Contents

1. Model- based Noninvasive Assessment of Cardiovascular Health

Abstract

Cardiovascular health is currently assessed by a collection of hemodynamic parameters many of which can only be measured by invasive methods often requiring hospitalization. A non-invasive approach of evaluating some of these parameters, such as systemic vascular resistance (SVR), maximum left ventricular elasticity (E_{LV}), end diastolic volume (V_{ED}), cardiac output and others, has been established. The method has three components: (1) a distributed model of the human cardiovascular system (Ozawa) to generate a solution library that spans the anticipated range of parameter values, (2) a method for establishing the multi-dimensional relationship between features computed from the arterial blood pressure and/or flow traces (e.g., mean arterial pressure, pulse amplitude, mean flow velocity) and the critical hemodynamic parameters, and (3) a parameter estimation method that provides the best fit between measured and computed data. Sensitivity analyses are used to determine the critical parameters that must be allowed to vary, and those that can be assumed to be constant in the model. Given the brachial pressure and velocity profiles (which can be measured non-invasively), this method can estimate SVR with an error of less than 3%, and E_{LV} and V_{ED} with less than 10% errors. Extensive simulations were performed to test the ability of the approach to predict changes of SVR and E_{LV} using computer-generated data.

Keywords: Parameter estimation, feature extraction, computational model, sensitivity analysis, hemodynamic parameters

Introduction

In patients suffering from a variety of cardiac diseases, the cardiovascular state is typically assessed by the measurement of hemodynamic parameters such as HR (Heart Rate), SVR (Systemic Vascular Resistance), E_{LV} (Left Ventricle Elasticity), V_{ED} (End Diastolic Volume), V_{ES} (End Systolic Volume), P_{ED} (End Diastolic Pressure), C.O. (Cardiac Output), S.V. (Stroke Volume), EF (Ejection Fraction = S.V./V_{ED}), and CI (Cardiac Index) [1,2,3,4,5,6]. Many of these parameters must be measured invasively and can therefore only be monitored in the hospital. For example, SVR is an important parameter used clinically to adjust vasodilatory medication [7]. It is usually calculated by (P_{MA} - P_{RA})/C.O., where P_{MA} and P_{RA} are Mean Arterial Pressure and mean Right Atrial Pressure (approximated by central venous pressure), respectively. Of these at least two, C.O. and P_{RA}, must be measured invasively.

However, the rising need for home health monitoring systems or systems capable of continuous patient assessment has led to recent efforts to develop reliable, noninvasive methods to estimate these parameters.

Noninvasive cardiovascular assessment in the home is currently limited primarily to the simple measurements of blood pressure and heart rate. The potential exists to monitor the ECG as well, but few devices are capable either of continuous monitoring or of data interpretation beyond the obvious. Yet, even these simple measures contain additional useful diagnostic information that could be gleaned from the data by subsequent analysis. Few studies have explored this possibility for obtaining more comprehensive, and more useful, information concerning the cardiovascular state of the individual.

Continuous measurement of blood pressure is now a reality with the recent development of systems that can be worn, either on the wrist or even the finger [8,9]. Miniaturized sensors and on-board electronics enable the device to convert the measured signal to a form more easily transmitted to a central computer for further processing and analysis. The processing of this information is designed to extract all the useful information contained in the signal. In the case of the blood pressure pulse, clinicians have known and made use of the fact that various aspects of the waveform contain information about the state of the heart or the peripheral vascular network. For example,

9

the maximum rate of pressure rise at the beginning of systole is indicative of the strength of cardiac contraction while the rate of decay of pressure during end diastole is a measure of peripheral vascular resistance; both of these are important parameters used in cardiovascular diagnoses.

Inference of cardiac parameters from peripheral measurements, however, is complicated by the changes in pulse shape that occur as the pressure wave propagates through the intervening arterial tree. Others have sought to overcome this problem by establishing the transfer function that relates changes in pulse shape at the aortic root to changes at a peripheral measurement site [10]. This method suffers, though, from the need for periodic calibration requiring arterial catheterization. An alternative approach, presented in this paper, involves the use of a comprehensive model of the entire arterial system and left heart. This computational model is used to create a *solution library* consisting of an extensive collection of peripheral pressure and/or flow traces, each corresponding to a different set of system parameters, covering the entire range of possible parameter values. The solution library is further condensed by a two-step process. First, each curve is represented by some small number of features (*feature extraction*). These features are selected so that they describe the shape and magnitude of the pressure waveform, and correspond to the set of *critical parameters*, those we seek to predict by our parameter estimation technique. Second, the dependence of each feature on the critical parameters is viewed as an *N*-dimensional surface and is mathematically represented by a *surrogate function*. The surrogate function itself is represented by a set of coefficients that are stored for later use in the parameter estimation procedure.

Parameter estimation begins with the measurement of arterial pressure by one of several non-invasive methods. The measured trace is processed in the identical manner as the computed waveforms to extract the features. An initial seed is chosen (a particular point in parameter-space) and a measure of the relative error between the features calculated from the measurement and the features corresponding to the initial seed point. Beginning at this point, a minimization routine is used to march down the error surface to eventually identify the point in parameter-space having the smallest error and therefore corresponding to the set of parameters that most closely match those of the subject from whom the measurements are taken.

10

In this way, the values of the critical parameters are estimated. In METHODS, it will be discussed how these critical parameters are selected from all the hemodynamic parameters specified in the computational model. Although these parameters are only a small subset of the ones measured clinically, many other parameters can be calculated by inputting the estimated critical parameters into the model.

Methods

Model Theory

The distributed cardiovascular model of Ozawa, *et al* [11,12] is used to generate the solution library. This model consists of a distributed arterial system and boundary conditions to simulate the left ventricle, bifurcations, and peripheral vessels. The arterial system contains thirty main arterial segments. The proximal and distal boundary conditions for the arterial system are, respectively, the left ventricle and the lumped parameter windkessel model for the smaller branching peripheral vessels. Given specific hemodynamic parameter values, the one-dimensional fluid dynamic equations can be solved numerically to obtain estimates for blood pressure, flow velocity and cross-sectional area at each location in the arterial tree as a function of time. Details about the modeling theory and computational methods are described in Ozawa, *et al* [11,12]. Only changes to the model are presented here.

Modified Left Ventricle Wall Elastance Curve

In the cardiovascular model, the left ventricle is approximated by a chamber with an entrance (mitral) and an exit (aortic) valve, whose compliance changes as a function of time, thus driving flow. Ozawa et al. assumed the ventricular wall elastance $E(t)$ to be a pure half-sinusoid, whose duration as a fraction of the entire cardiac cycle was denoted as Ω. Since the shape of the ventricular contraction curve strongly influences the arterial pulse profile, we have utilized the results of Senzaki, et al who provide a more accurate form for $E(t)$ [13]. Their study showed that the mean normalized elastance curves $E_n(T_n)$ (where $E_n = E(t)/E_{max}$, and $T_n = t/T_{systole}$) were remarkably similar over a wide range of patients in varying degrees of cardiovascular health as given in Figure 1.

Averaged Normalized Elastance Curve

E_N

T_N
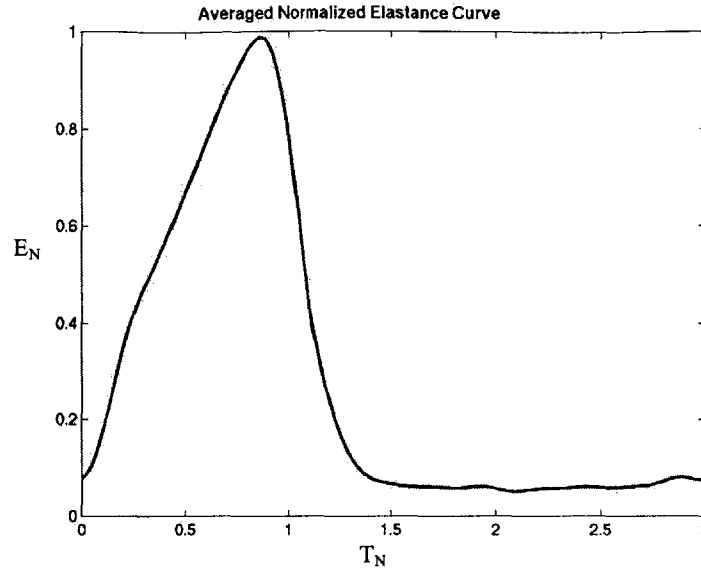
Fig. 1: Averaged normalized elastance curve

Identification of the Parameter Set

In its current form, the model requires the specification of over 200 parameters. While the number of parameters in parameter estimation routines should be a reasonably small value to achieve computational efficiency, it is necessary to make certain simplifying assumptions. Obviously, the validity of these assumptions will need to be further evaluated.

One of the most important assumptions is that of geometric self-similarity. We assume that the branching pattern of the larger vessels in the arterial system is self-similar in terms of the length of each segment, the distribution of branches, and branching angles. Therefore, the arterial tree geometry (i.e. lengths, cross-sectional areas at a reference pressure, artery wall thickness) can be expressed in terms of a single length scale (e.g. subject height) along with a large number of dimensionless ratios. In addition to geometrical similarity, we assume structural similarity in the sense that the normalized distribution of wall thickness and arterial elasticity is similar in all individuals. Consequently, arterial elastance is characterized by a single parameter, the Young's modulus at one specified location, and this single parameter is allowed to vary between subjects. This assumption has important implications in the application of the parameter

estimation technique. For example, its accuracy will likely be adversely affected in patients with arterial stenosis in the vicinity of the site of pressure and/or velocity measurement.

Self-similarity is also assumed in the distribution of cardiac output. Although the overall level of systemic vascular resistance is allowed to vary, the relative resistance of one peripheral vascular bed to another is held constant.

Together with the parameters associated with calculations of both the left and right ventricles and the lumped model of venous and pulmonary circulation, which can be found in the fluid dynamic equations of the cardiovascular model [11,12], the final parameter set identified for this work has 21 parameters in total. Table 1 lists the nominal values and ranges of these parameters, which were estimated based on available data.

Table 1 List of model parameters, nominal, maximum and minimum values

#	Name	Nominal Value	Minimum Value	Maximum Value
1	Heart Rate	72BPM	40	160
2	Left Ventricle E_{max}	6000dyn/cm^5	300	15000
3	Left Ventricle E_{min}	133dyn/cm^5	50	500
4	Left Ventricle 0-Pressure Vol	15ml	0	100
5	End Diastolic Volume	120ml	30	400
6	Right Ventricle E_{min}	133dyn/cm^5	50	500
7	Right Ventricle 0-Press Vol	15ml	0	100
8	Transthoracic Pressure	(-)5 mmHg	-20	0
9	Sinus of Valsalva C_{sinus}	0.00005cm^5/dyn	1.00E-05	3.00E-04
10	Venous Pressure	8mmHg	0	30
11	Venous Cv	0.075cm^5/dyn	0.01	0.1
12	Venous Rv	13.3dyn-sec/cm^5	1.00	100.00
13	Pulmonary Rro	4 dyn-sec/cm^5	1.00	10.00
14	Pulmonary Cpa	0.0032cm^5/dyn	1.00E-03	1.00E-02
15	Pulmonary Rpa	106.7 dyn-sec/cm^5	10	500
16	Pulmonary Cpv	6.30E-03	1.00E-03	1.00E-02
17	Pulmonary Rpv	13.3 dyn-sec/cm^5	1	100
18	Blood Viscosity	0.04cp	0.01	0.10
19	Length Scale	1.00	0.5	1.5
20	Artery Wall Stiffness E	1.00	0.50	2.00
21	Systemic Vascular Resistance	1000dyn-sec/cm^5	300	3500

Parameter Reduction

The complete set of hemodynamic parameters (table 1) that reflect the unique state of a given patient still contains many more parameters than can reasonably be predicted and must therefore be substantially reduced. Two schemes for parameter reduction are used here: Dimensional Analysis and Sensitivity Analysis.

Dimensional Analysis: This approach reduces the number of parameters by taking advantage of non-dimensionalization, and by using a subset of the total parameters to define dimensionless parameters from the remaining subset. We chose to use the density of blood, a characteristic length (the length between distal points of brachial and radial artery), and the Young's Modulus of the arterial wall to non-dimensionalize all remaining parameters. By this means, the dimension of the parameter space (number of independent parameters) is decreased by two.

Initial Sensitivity Analysis: To reduce the number of parameters further, the relative contribution of each is assessed in terms of its morphological and quantitative effects on the model output. For this purpose, each parameter was varied in turn over its dimensionless scale from the nominal value (in Table 1) to $\pm 10\%$ of the total operating range, while holding all other parameters constant. A root mean square error function was then defined so that the deviation of each new run with its single adjusted parameter could be compared with the solution using the nominal value (standard case). Denoting the data set of length n taken from the aortic root pressure/velocity of the standard case as p_m, and comparing it with a set of calculated data p_c taken from the same location, where both share the same time axis, then the error may be written as:

$$\varepsilon_{rms} = \frac{1}{n\bar{p}_m} \sum_{j=1}^{n} (p_c^j - p_m^j)^2 \tag{1}$$

where

$$p_m = \{p_m^1, p_m^2, ..., p_m^n\} \text{ and } p_c = \{p_c^1, p_c^2, ..., p_c^n\} \tag{2), (3}$$

and the mean of the standard set is indicated by the over bar. Additionally, both curves

were made dimensionless so that the pressure/velocity values were normalized in both curves by the minimum and maximum values from the standard case, as shown in equations 4 and 5.

$$p_m = \frac{p_m' - \min(p_m')}{\max(p_m') - \min(p_m')} \tag{4}$$

$$p_c = \frac{p_c' - \min(p_m')}{\max(p_m') - \min(p_m')} \tag{5}$$

where p_m' is the dimensional standard case, and p_c' is the dimensional test case to be compared against.

Additional values for errors at other locations can be calculated by repeating the analysis. These locations are determined by taking into consideration the methods available to the clinician to non-invasively measure both pressure (using a tonometer) and velocity (using Doppler ultrasound) in a patient. These locations include the carotid arteries (both pressure and velocity), the brachial artery (velocity), the radial artery (pressure), the femoral artery (velocity), and the tibial artery (velocity). By taking the average deviation from all of the measurement locations and aortic root, a single composite ranking of the error as a function of parameter deviation taken at the eight locations can be constructed and summarized in table 2.

Based on table 2, a reduced parameter set can be defined. The parameters contributing to large RMS errors are: venous pressure, length scale, heart rate, systemic vascular resistance, left ventricle E_{min}, right ventricle E_{min}, arterial wall stiffness E, left ventricle E_{max} and end diastolic volume (V_{ED}). Since for purpose of parameter estimation, one is only interested in parameters that have direct effects on the arterial waveforms generated by the model, we decided to eliminate the venous and pulmonary circulations from the simulation (thus eliminating right ventricle E_{min}), replacing them with V_{ED} and P_V. The parameter set can be further simplified by assuming that venous pressure varies little in comparison to the large amplitude pressure changes seen in the arterial system. Thus, variations in venous pressure can be neglected. Additional

15

simplifications can be made if one assumes that the only effect that left ventricular E_{min} has on the arterial system is in determining the final steady state diastolic volume of the left ventricle. Therefore, this parameter can be condensed into the parameter V_{ED}.

Table 2. Results of initial sensitivity analysis

Parameter #	Parameter Name	Mean RMS Error
10	Venous Pressure	1.70
19	Length Scale	1.19
1	Heart Rate	1.10
21	Systemic Vascular Resistance	1.05
3	Left Ventricle E_{min}	0.91
6	Right Ventricle E_{min}	0.84
20	Artery Wall Stiffness E	0.40
2	Left Ventricle E_{max}	0.36
5	End Diastolic Volume	0.21
12	Venous Rv	0.20
15	Pulmonary Rpa	0.18
9	Sinus of Valsalva C_{sinus}	0.18
17	Pulmonary Rpv	0.18
14	Pulmonary Cpa	0.17
16	Pulmonary Cpv	0.17
8	Transthoracic Pressure	0.17
4	Left Ventricle 0-Pressure Vol	0.17
13	Pulmonary Rro	0.17
7	Right Ventricle 0-Press Vol	0.17
11	Venous Cv	0.17
18	Blood Viscosity	0.15

Using this initial sensitivity analysis, four parameters are recognized as having relatively large effects on model outputs, in addition to the two parameters used to non-dimensionalize other parameters, length scale and arterial wall stiffness E. They are Heart Rate (HR), Peak Left Ventricle Elasticity (E_{LV}), End Diastolic Volume (V_{ED}), and Systemic Vascular Resistance (SVR).

Table 3 gives the ranges of the four parameters varied over which the calculations are conducted.

Table 3. Ranges of four parameters

Parameters	HR (/min)	E_{LV} (dyn/cm^5)	V_{ED} (ml)	SVR (PRU)
Minimum	40	300	30	0.225
Maximum	160	15000	400	2.625

The initial sensitivity analysis completed prior to generating a solution library from the model helped to identify the parameters that needed to be systematically varied in the library. Another sensitivity analysis was conducted to evaluate the effects of all parameters on parameter estimation accuracy after the library and the parameter estimation routines have been established, which will be discussed in RESULTS and DISCUSSION.

Parameter Estimation Scheme

Extensive work in parameter estimation has been done in the field of engineering and the application of "surrogates" to describe the behavior of a system, as a function of its parameters, is well established. We use techniques similar to those developed by Yesilyurt and Patera [14]. A solution library is first constructed with the cardiovascular model consisting of a collection of hemodynamic parameters (*model inputs*) and pressure, velocity traces (*model outputs*) at each node of the arterial network. An N-dimensional interpolation routine is used to generate the surrogates that describe the relationship of the model output to the inputs. Next, an objective function ε_{obj} is defined to give an indication of the "error" between the output of the model for a given parameter set and the actual patient data:

$$\varepsilon_{obj} = \sqrt{\sum_{i=1}^{n} (1 - f_e / f_m)^2} \qquad (6)$$

where f_e is the feature of *model output* and f_m is the feature from the actual patient data.

Given measured patient pressure and/or velocity data at any location of the

arterial tree, using the surrogate, the "best fit" can be located and the corresponding estimated patient hemodynamic parameters associated with the point of minimum "error" can be reached.

1. Feature Selection

Features are defined to quantitatively characterize pressure and velocity profiles. One assumes that each pulse is specific to each given set of parameter values, and that the features selected are adequate to uniquely specify one pulse. Thus, feature selection is crucial to the accuracy of parameter estimations. Over the course of this study, different methods for feature extraction have been compared, such as wavelet analysis, Fourier transform, etc. Ultimately, we found that the features typically used by clinicians yielded the most accurate parameter estimations. These offer the added advantage that they are familiar to the clinician and more likely to gain acceptance in clinical practice. As a matter of convenience in measurement, parameter estimations were made using pressure and velocity profiles in the carotid, brachial and radial arteries.. Errors of parameter estimations for model-generated pressure and/or velocity using different combinations of all extracted features are compared, and the optimal set of features for our purpose is taken as the set that gives the least estimation error. As will be shown below, the optimal feature set is: [P_{mean}/V_{mean} $(dp/dt)_{max}$ P_{mean} $\Delta P(= P_{max} - P_{min})$]. When only pressure data is available, the parameter estimation scheme can also give small errors when using feature set [$(dp/dt)_{max}$ P_{mean} ΔP P_{max}]. Detailed discussions will be given in RESULTS. Figure 2 defines these features.
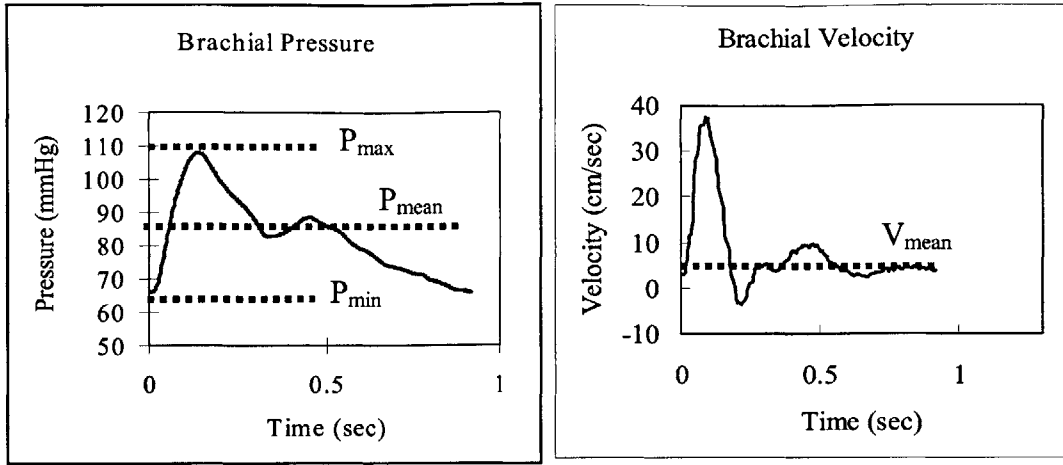
Figure 2 Feature selections

2. Shepard Interpolation Method

As mentioned above, the solution library generated from the model contains a collection of peripheral pressure and velocity traces, each corresponding to a different set of system parameter values. Since the range of possible parameter values is broad, while only sparse points in the space can be generated and stored in the library (because of computational limitations), we employ an interpolation method to describe the relationship between parameters and features.

Shepard quadratic interpolation is used here because it minimizes storage requirements and is easily generalized for multidimensional interpolation. The original detailed presentations of this method were given by Franke and Nielson and Renka for the two- and three-dimensional cases [15,16]. Given that we have a dataset D which contains N input-output pairs:

$$D = \{(p_1, f_1), \ldots, (p_N, f_N)\} \tag{7}$$

Where p_j and f_j are parameters and features, respectively, $j=1\ldots N$ and

$$f_j = F(p_j) \tag{8}$$

$$p_j = (p_j^1, \ldots, p_j^n) \tag{9}$$

19

where n is the total number of parameters in p. Thus, an interpolation function of the following form can be defined:

$$\tilde{F}(p) = \sum_{k=1}^{N} W_k(p) Q_k(p) \tag{10}$$

where $Q_k(p)$ are quadratic nodal functions acting as local approximations to $F(p)$ of the form:

$$Q_k(p) = f_k + (\sum_{i=1}^{n} c_k^i(p^i - p_k^i)) + \sum_{j=1}^{n}\sum_{m=1}^{n} c_k^l(p^j - p_k^j)(p^m - p_k^m) \tag{11}$$

where:

$$l(j,m;n) = m + \sum_{p=1}^{j}(n - j + p) \tag{12}$$

and c_k^l are coefficients that minimize:

$$\sum_{\substack{i=1 \\ i \neq k}}^{N} \omega_i(p_k)[\ (\sum_{i=1}^{n} c_k^i(p^i - p_k^i)) + \sum_{j=1}^{n}\sum_{m=1}^{n} c_k^l(p^j - p_k^j)(p^m - p_k^m) + f_k - f_i\ ]^2 \tag{13}$$

$W_k(p)$ are weighting functions defined based on the distance between points p_k and p.

The Shepard routine is implemented to determine coefficients for the surrogate using library points generated by the model. Thus, a set of parameters may be sent to the surrogate, which then returns a single value (the corresponding feature) based upon interpolation between the library points. This process is repeated for each defined feature. In application, given a set of pressure and velocity curves, initial parameter values are input to the surrogate, generating a set of feature values, which are compared with the real feature values extracted from the curves (the numbers of parameters and features are not necessarily the same). Then, a minimization algorithm is employed to minimize the objective function (equation 6) that is defined based on the difference between the estimated features and the real features. When this minimization routine converges, the optimal parameter values are determined.

20

3. Minimization Routine

The Nelder-Mead Simplex Method, a direct search method [17] available as a MATLAB function, was used to minimization the objective function. Its advantages are that derivatives of the fitting function (dependent variable) need not be calculated and that it is insensitive to small local perturbations.

Results and Discussion

Parameter Estimation Errors

1. Parameter estimation errors using 2 feature sets

The first step in performance evaluation is to compute model generated pressure and velocity profiles, estimate their corresponding parameters and compare predictions with the original values used in the model simulation. The parameter estimation error (E) is defined as the following:

$$E = (P_{est} - P_{real}) \Big/ ((P_{max} - P_{min})/2 + P_{min}) \tag{14}$$

Figure 3 depicts the parameter estimation errors using two different feature sets that give small estimation errors as mentioned in feature selection. Feature set 1 is composed of features from both pressure and velocity profiles and feature set 2 comes from pressure curve only. Note that only three parameters are estimated, since Heart Rate (HR) can be easily measured.

As can be seen from the figure, feature set 1 gives the smallest estimation errors for model-generated data in the brachial artery. Errors for brachial artery waveforms using feature set 2 are slightly higher. These results indicate that both pressure and velocity are needed to achieve lower estimation errors. Parameter estimations for radial artery pressure and velocity have somewhat larger errors than estimations from the brachial artery (Fig. 3-b). Of the three parameters estimated, the error for SVR is always the smallest.

In the following discussions, only estimation results using brachial pressure

and/or velocity are presented.

2. Number of features

As mentioned above, the number of features and parameters are not necessarily the same and from the scheme of parameter estimation, it can be seen that the fewer the features, the faster the parameter estimation process proceeds. However, the features must be adequate to identify changes of parameters. For example, if only 3 features are used, parameter estimation errors will increase as shown in Figure 4.

In this figure, feature set 3 contains the same three features as feature set 1, without $(dp/dt)_{max}$, feature set 4 contains the same three features as feature set 2 without P_{max}. Feature set 5 will be discussed later. It can be seen that the errors using feature sets 3 and 4 are larger than those using feature sets 1 and 2, respectively. (Note, however, that errors using feature set 4 are only slightly larger than those using feature set 2 suggesting that P_{max} is a redundant feature. Given P_{mean} and ΔP, one can not calculate P_{max} since P_{max} can always be changed by changing the shape of the curve while keeping P_{mean} and ΔP constant.). Other calculations show that using five features or more fails to reduce parameter estimation errors, perhaps because the relationship becomes overspecified. Therefore, in this paper, feature sets 1 and 2 are considered optimal within the range of those tested.

3. Effects of $(dp/dt)_{max}$

In the selection of features, we also need to consider our ability to obtain accurate estimates in the clinical setting. Current measurement methods provide a means of determining, P_{mean} , ΔP, P_{max} with reasonable accuracy. However, $(dp/dt)_{max}$ may be subject to greater errors since the pressure curve used in estimation is usually the mean of several cycles to reduce the non-invasive measurement disturbance. If the measurement is adequate to give consistent cycles so that one of these cycles can be used directly in feature extraction, this problem will not exist.

Parameter estimation errors using feature sets that do not contain $(dp/dt)_{max}$ are evaluated, as shown in figure 4, using feature sets 3 and 5. In feature set 5, a new feature, T_{peak}^{*} (the ratio of time needed for pressure curve to reach the peak and the period, i.e.

T_{peak}/T) replaces $(dp/dt)_{max}$ in feature set 4. It can be seen that parameter estimation errors increase when $(dp/dt)_{max}$ is not used. This is not surprising since, $(dp/dt)_{max}$ is an important feature related to the strength of cardiac contraction. Thus, in measurement of pressure curves, it is desirable that the instrument have an adequate frequency response to capture $(dp/dt)_{max}$ and efforts should be made to ensure consistent cycles so that $(dp/dt)_{max}$ can be relatively accurately calculated.

4. Fixing V_{ED}

In parameter estimations, E_{LV} usually has the largest estimated errors. We found that it is difficult to discriminate the effects of V_{ED} from those of E_{LV}, due to the fact that they both appear only in the equation for ventricular function. Moreover, V_{ED} can be measured by the cardiologist using standard ultrasound methods. Therefore, it is reasonable if taking V_{ED} as a known parameter and as an input to parameter estimations in the conditions that it can be measured accurately and it remains constant during a specific period. Figure 5 shows the estimation errors when V_{ED} is specified. The errors for E_{LV} are significantly reduced (to less than 10% for both feature sets) in this way.
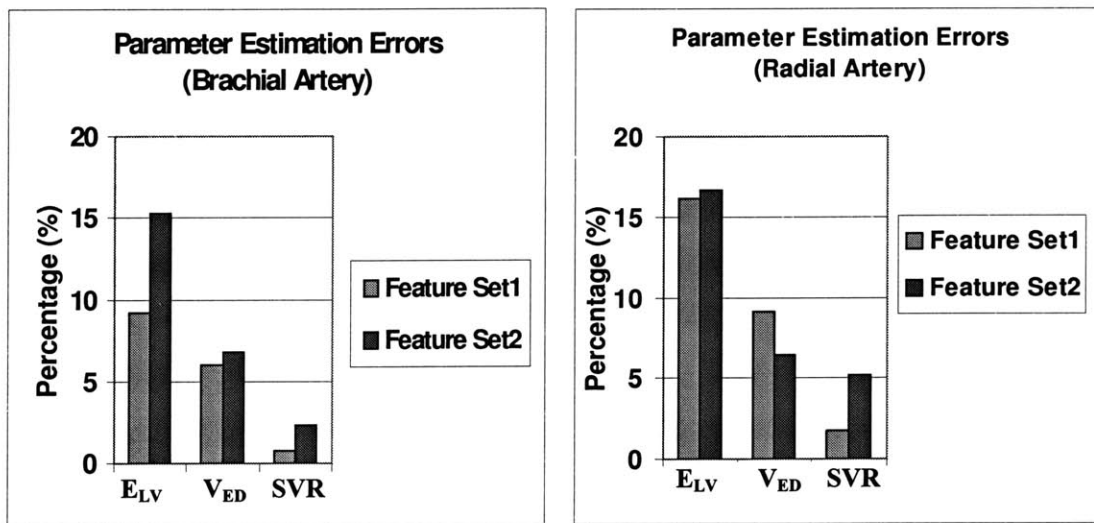

Figure 3. Parameter estimation errors

(Feature Set1: P_{mean}/V_{mean} $(dp/dt)_{max}$ P_{mean} ΔP

Feature Set2: $(dp/dt)_{max}$ P_{mean} ΔP P_{max})
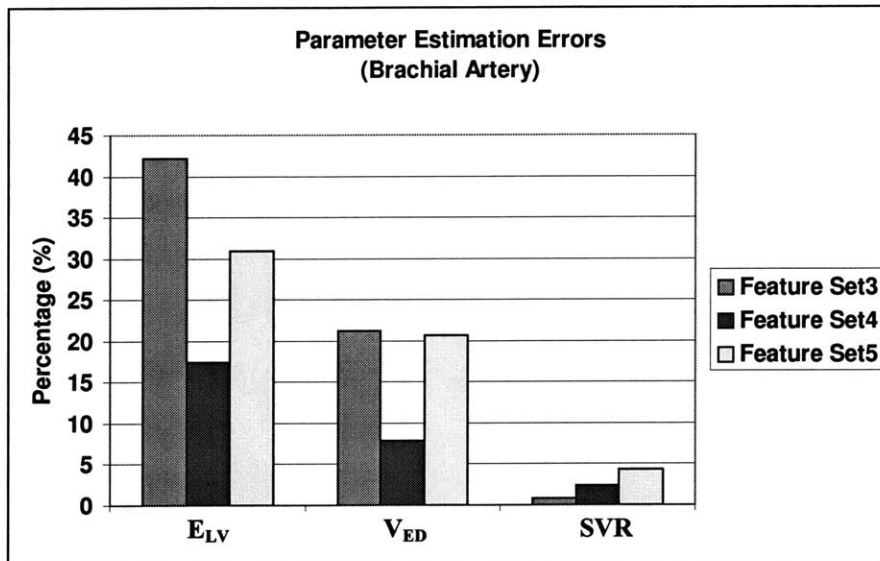
Figure 4. Parameter estimation errors

(Feature Set 3: P_{mean}/V_{mean} P_{mean} ΔP

Feature Set 4: $(dp/dt)_{max}$ P_{mean} ΔP
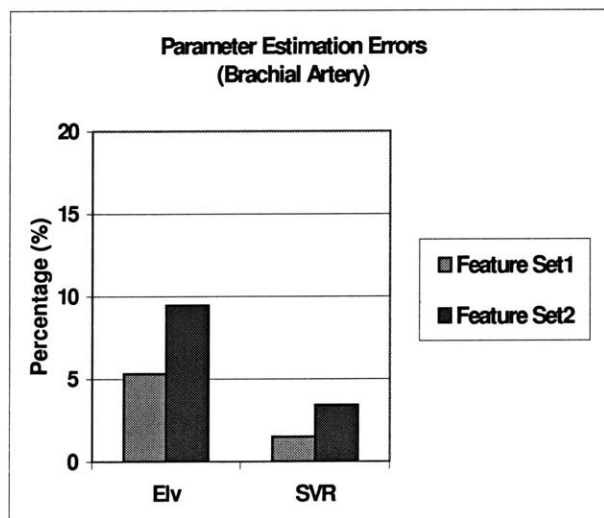
Feature Set 5: T_{peak} P_{mean} ΔP)

Figure 5. Parameter estimation errors with V_{ED} as known

Reconstruction and calculation of additional system parameters

Parameters in addition to those determined from parameter estimation can be calculated by performing a reconstruction, that is, using the estimated parameter values as inputs to the cardiovascular model to do simulation. In addition, this provides more opportunity for validation of the method. Figure 6 gives a sample comparison of two such sets of curves showing excellent agreement. The parameter values and estimation errors using the original brachial pressure and velocity are listed in Table 4.

When performing a reconstruction, other variables such as Cardiac Output (C.O.) and cardiac stroke volume (SV) can be calculated using the model. Since neither C.O. nor SV are required input parameters of the model, they can not be estimated using parameter estimation routines. However, given a set of patient's pressure and/or velocity curves, both can be calculated through the reconstruction procedure using the estimated parameter values of this patient. For example, in the reconstruction demonstrated in figure 6, the calculated C.O. is 5.36 l/min and SV is 67.35 ml.

Sensitivity Analysis

1. Method

As mentioned in METHODS, before setting up the solution library, an initial sensitivity analysis was performed for all parameters to compare their effects on *model outputs*. As a result of that analysis, only four parameters are allowed to change, all other parameters being fixed in generating solution library. Now we conduct a sensitivity analysis for the formerly fixed parameters to examine the effect that uncertainty in their values has on *parameter estimations*. Table 5 lists the five fixed model parameters that exert significant influence on parameter estimation based on preliminary analysis (other model-fixed parameters listed in table 1 have little influence on parameter estimation). Their nominal values and the possible ranges were estimated from available data.
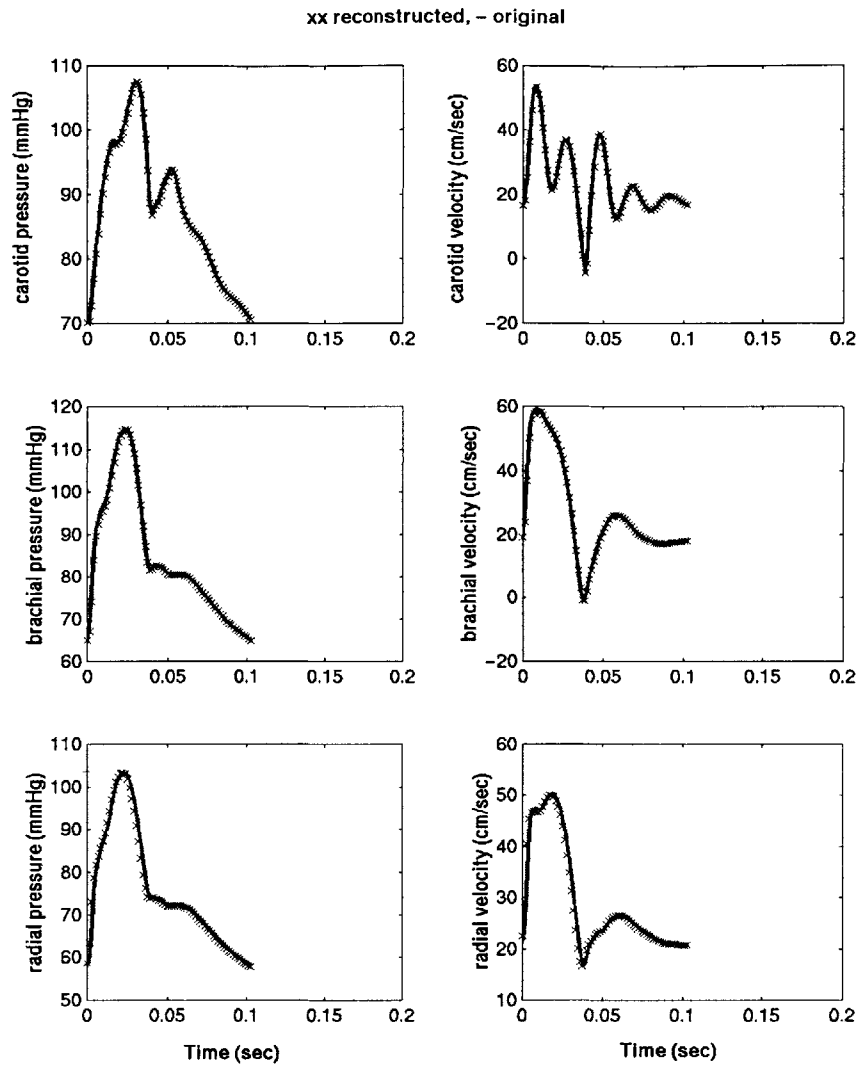
Figure 6. Reconstruction Example

Table 4. The parameter estimation errors

	HR (/min)	E_{LV} (dyn/cm^5)	V_{ED} (ml)	SVR (dyn/cm^5.sec)
Real Value	80.0	7500.0	120	1200
Esti	80	6618.1	126.866	1202.3
Error		11.53%	3.19%	0.20%

Table 5. Fixed model parameters

|	P_V (mmHg)	V_0 (ml)	P_{th} (mmHg)	C_{sinus} (cm^5/dyn)	Blood Viscosity (cp)
Nominal	5.0	15	-5	0.00005	0.04
Minimum	0	0	-20	1.00E-05	0.01
Maximum	30	100	0	3.00E-04	0.10

To analyze their sensitivity, simulations were done with each "fixed" parameter (minor parameter) varied from the standard value by ±10% and with the critical parameters (E_{LV}, V_{ED}, SVR) unchanged. The difference of estimated critical parameter values between the case where no minor parameters are changed (base case) and the case with variation is then calculated, as,

$$S_{i,j} = {\partial P_{i,est}} \Big/ {\partial P_{j,fix}}$$

(15)

where $\partial P_{i,est}$ is the difference between estimated dimensionless critical parameter value of a base case and the corresponding estimated parameter in the case with variation, $\partial P_{j,fix}$ is the change of minor parameters (±10%).

2. Results

Figure 7 presents the results for the sensitivity of the three critical parameters to all five minor parameters using feature sets 1 and 2. Note that when this ratio is near zero, the change of the minor parameter has little effect on parameter estimation and the errors resulting from holding it constant are insignificant. To evaluate the overall performance, we did not assume V_{ED} to be known, but rather, estimated it.
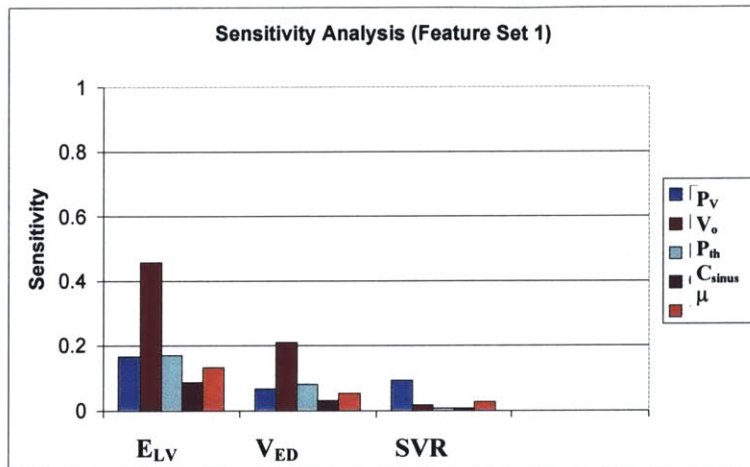
(a) Feature Set 1
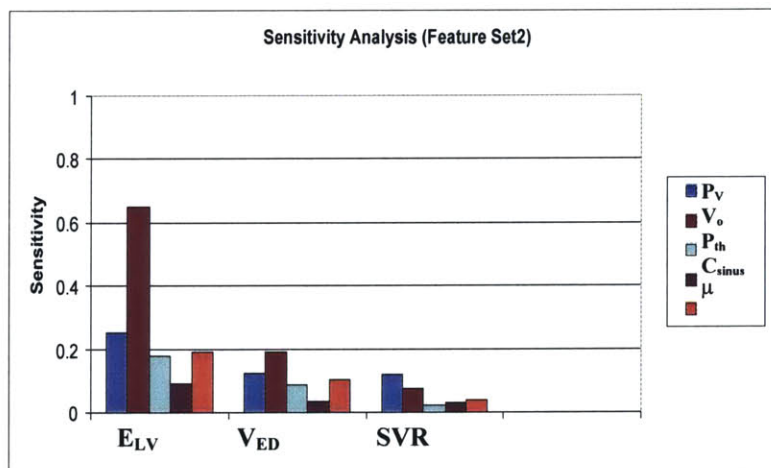
(b) Feature Set 2

Figure 7. Sensitivity analysis for 6 fixed parameters.

From these results, the following conclusions can be drawn. (1). Feature set 1 leads to predictions that are less sensitive to variations in the 5 parameters, though the sensitivity of feature set 2 is not much larger. Since in practice these 5 parameters likely vary for different persons, feature set 1 may turn out to be more effective in clinical applications. However, since feature set 2 only needs pressure measurement, it is more convenient to use especially when velocity measurements are not obtainable under some circumstances. (2). Ventricular volume at zero pressure (V_0) exerts a relatively large

effect on E_{LV} and V_{ED}. More work is needed to establish its value and take its effect into account. (3). None of the 5 parameters exert much effect on SVR. This is encouraging since SVR is one of the most desirable parameters from a clinical perspective.

3. Results when V_{ED} is known

As an example for sensitivity analysis when V_{ED} is taken as known, figure 8 gives the results using feature set 1. Much smaller sensitivities are achieved, which shows the advantage in parameter estimation when V_{ED} is known.
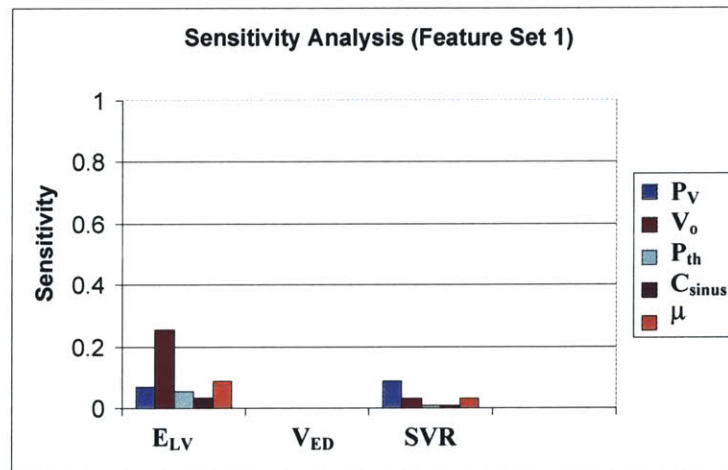
Figure 8. Sensitivity analysis with V_{ED} known

Prediction of Change of SVR

In practice, there may be many factors, such as measurement inaccuracy, person to person variability, etc., affecting the accuracy of final parameter estimation results. On the other hand, the amount of *change* in SVR is often of greater interest to clinicians than its absolute value. In these cases, although the absolute estimated parameter values may not be accurate, our approach can still be used if it can predict *changes* in SVR accurately. To test the ability of predicting changes in SVR, we performed simulations with SVR varied ±10% and with all other parameters fixed, and compared parameter estimation results with the known change in SVR. That is, we evaluated the ratio:

$$\partial P_{estimated}\Big/\partial P_{real} \qquad\qquad (16)$$

If this ratio equals unity, the change of SVR is captured perfectly. From the estimation results in Table 6, it can be seen that the mean ratio is very near unity with small standard deviations, especially for feature set 1. The ability of parameter estimation in predicting changes of SVR seems promising.

Table 6. Prediction of change of SVR

$\partial P_{est}\Big/\partial P_{real}$	ΔSVR (-10%)	ΔSVR (+10%)	Mean of $\pm$ 10% cases	Standard Deviation
Feature Set1	1.0034	1.0131	1.0082	0.0293
Feature Set2	0.9981	0.8990	0.9485	0.2759

(Feature Set1: P_{mean}/V_{mean} $(dp/dt)_{max}$ P_{mean} ΔP

Feature Set2: $(dp/dt)_{max}$ P_{mean} deltaP P_{max})

Prediction of change of E_{LV}

Similar calculations were performed to predict changes of E_{LV} (Table 7) with the result that, though the values are near unity, the standard deviations are rather large for both feature sets. This approach is less able to predict changes of E_{LV} accurately as compared to SVR. Table 8 shows the prediction performance when V_{ED} is taken as known. Smaller standard deviations are achieved with the mean values near 1. Therefore, to predict E_{LV}, it is better to measure V_{ED} and using it as input to parameter estimation.

Table 7 Prediction change of E_{LV}

$\dfrac{\partial P_{est}}{\partial P_{real}}$	ΔE_{LV} (-10%)	ΔE_{LV} (+10%)	Mean of $\pm$ 10% cases	Standard Deviation
Feature Set1	1.2125	0.9341	1.0733	0.6563
Feature Set2	1.3904	0.7734	1.0819	0.7675

Table 8 Fix V_{ED}, prediction change of E_{LV}

$\dfrac{\partial P_{est}}{\partial P_{real}}$	ΔE_{LV} (-10%)	ΔE_{LV} (+10%)	Mean of $\pm$ 10% cases	Standard Deviation
Feature Set 3	1.3502	0.9057	1.1280	0.3454
Feature Set 4	1.2983	0.8604	1.0794	0.3580

Conclusion

Hemodynamic parameter estimation based on non-invasive measurements in peripheral arteries is feasible with errors of < 10% when estimating SVR, E_{LV} and V_{ED} from computer generated brachial pressure and velocity data. Although most of the parameters used in the cardiovascular model are fixed, this scheme holds promise in the real setting since the fixed minor parameters have a relatively small effect on parameter estimation according to the sensitivity analysis. These errors can be reduced even further if V_{ED} is known.

In estimating using measured pressure and velocity, the parameter estimation accuracy will be largely related to accuracy of non-invasive measurement of P and V. As long as relatively precise measurement is assured, the above parameter estimation scheme should work well on providing hemodynamic parameter values non-invasively.

For the application of the parameter estimation scheme in continuous health monitoring in hospitals or homes, the major issue would be the calculation speed of this method, provided that pressure and velocity profiles can be obtained real-time. The

parameter estimation process generally needs one to two minutes, while the calculation of C.O. and S.V. takes three to five minutes using the cardiovascular model. Therefore, the current parameter estimation approach is applicable in the health monitoring where a five-minute or longer period is acceptable in between two estimations.

References

[1] Schmidt BM, Montealegre A, Janson CP and others; Short term cardiovascular effects of aldosterone in healthy male volunteers; *J Clin Endocrinol Metab*; 1999 Oct; 84(10): 3528-33

[2] Kasalicky J, Fabian J, Ressl J, Jebavy P, Stanek V; Left ventricular end-diastolic volume in advanced ischemic heart disease; comparison between healthy subjects and patients with mitral stenosis; *Cardiology* 1975;60(2):86-97

[3] Koelling TM, Semigran MJ, and others; Left ventricular end-diastolic volume index, age, and maximum heart rate at peak exercise predict survival in patients referred for heart transplantation; *J Heart Lung Transplant* 1998 Mar; 17(3):278-87

[4] Beards SC, Lipman J; Decreased cardiac index as an indicator of tension pneumothorax in the ventilated patient; *Anaesthesia* 1994 Feb;49(2):137-41

[5] Adams HR, Baxter CR, Izenberg SD; Decreased contractility and compliance of the left ventricle as complications of thermal trauma; *Am Heart J* 1984 Dec;108(6):1477-87

[6] Morita S, Kormos RL and others; Standardized ejection fraction as a parameter of overall ventricular pump function; *Jpn Circ J* 2000 Jul;64(7):510-5

[7] Stevenson L, Tillisch J; Maintenance of cardiac output with normal filling pressures in patients with dilated heart failure. *Circulation* 1986; 74(1):303-8.

[8] Omboni S; Smit AA; Wieling W; Twenty four hour continuous non-invasive finger blood pressure monitoring: a novel approach to the evaluation of treatment in patients with autonomic failure; *Br Heart J*; 1995 Mar; 73 (3): 290-2

[9] Belani K; Ozaki M; Hartmann T and others; Non-invasive blood pressure monitoring with the visotrac − results of a multicenter clinical trial; *Anesthesiology*; 1998 Sep; 89(3A)

[10] Stergiopulos N; Westerhof B; Westerhof N; Physical basis of pressure tranfer from periphery to aorta: a model-based study; *Am J of physiology*; 1998; 274(2); H1386

[11] Ozawa E., Bottom K. and Kamm R.D.; Numerical simulation of enhanced external counterpulsation Part I: The computational model;

[12] Bottom K., Ozawa E. and others; Numerical simulation of enhanced external counterpulsation Part II: Hemodynamic results;

[13] Senzaki H., Chen C. and Kass D.A.; Single-beat estimation of end-systolic pressure-volume relation in humans; *Circulation;* 94(10); Nov. 1996

[14] Yesilyurt S. and Patera A.T.; Surrogates for numerical simulations: optimization of eddy-promoter heat exchangers; *Computer Methods in Applied Mechanics and Engineering* 121, 231-257; 1995

[15] Franke R. and Nielson G.M.; Scattered data interpolation and applications: A tutorial and study in: H. Hagen and D. Roller, eds.; Geometric Modeling: Methods and Applications; (131-160); Springer-Verlag, Berlin; 1990

[16] Renka R.L.; Algorithm 660: QSHEP2D: Quadratic Shepard method for bivariate interpolation of scattered data; ACM TOMS; 14, (149-150); 1988

[17] Barton R. Ivey J; Nelder-mead simplex modifications for simulation optimization; *Management Science*; 42(7); July, 1996

Feature Extraction Methods

Feature extraction is an important step in parameter estimation. Features selected should be functions of the parameters and should be as independent of each other as possible. Since the minimized objective function is based on the difference of interpolated features and patient trace features, it requires that each feature have a relatively large sensitivity to changes of parameters. In addition, there should be no local maximum or minimum points in the ideal multi-dimensional space constructed by assuming each feature as a function of the parameters.

Feature selection needs extensive work since each possible combination of features should be evaluated by computing its related parameter estimation errors. Several feature extraction methods are presented and compared in this appendix.

Wavelet Transform

1. Basic theory

Wavelet transforms are integral transforms using integration kernels called wavelets. These transforms enable the study of non-stationary process (or signals) in that they have good localization properties both in time and frequency. Since the physiologic signal is non-stationary and the human cardiovascular system is nonlinear, this is a promising approach for feature extraction.

The wavelet transform is defined in a similar manner as Fourier transform. However instead of using the harmonics e^{iwt}, it uses wavelet bases. Wavelet transform decomposes a signal $f(t)$ onto a family of wavelet bases, and the weighting coefficients, $W_s[f(\tau)]$, represent the amplitudes at given location τ and frequency s. The process of wavelet transform goes essentially as follows. Sets of "wavelets" are combined to approximate a signal and each element in the set is a scaled (dilated or compressed) and translated (shifted) version of the basic (mother) wavelet. To obtain the appropriate weight of each element, the signal is projected onto each element. The result of each projection is a scalar number (real or complex) called wavelet coefficient or weighting

coefficient. Thus a signal is transformed to a combination of wavelets with different weights. Compared to the Fourier transform, $F(\omega)$, which depends only on frequency, the wavelet transform is a time frequency function which describes the information of $f(t)$ in various time windows and frequency bands. As a result, the wavelet transform is capable of capturing non-stationary information such as frequency variation and magnitude undulation, whereas the Fourier transform cannot.

2. Applications and evaluations

Wavelet transform is used widely in image processing and signal processing and there are many generated methods suitable for different applications. Two kinds of approaches to wavelet transform were tried on the pressure profiles and velocity curves: the Discrete Wavelet Transform (DWT), and the Wavelet Packet Method.

(a). Discrete Wavelet Transform

In DWT method that has multi-resolution structures, the signal is first split into low- and high-frequency components in the first level. The first low-frequency sub-band, containing most of the energy, is sub-sampled and again decomposed into low- and high-frequency sub-bands. This process can be continued into K levels. Fig. 1A.1 illustrates the multi-resolution decomposition structure with 3 levels. The coarsest signal is the one labeled LLL. Thus, a progression occurs from coarser to finer signal representation as high frequency "detail" is added at each level. The signal can therefore be approximately represented by different resolutions at each level of the tree.
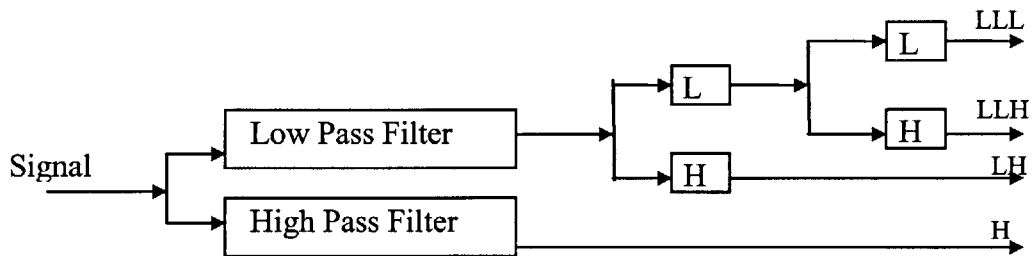

Fig. 1A.1 Multi-resolution Structure for 3 levels

36

Figure 1A.2 is the result of multi-resolution decomposition of a model-generated brachial pressure curve. Three decomposition levels were performed and "db3" wavelet basis was used. The second sub-plot of the figure contains all the coefficients obtained from DWT. "Approximated coefficients of level 3" correspond to level LLL in Fig. 1A.1. "Detailed coefficients level 3" correspond to level LLH in Fig. 1A.1, and "Det. Coeff. Level 2", "Detail Coeff. Level 1" correspond to level LH and H respectively. The advantage of wavelet transform – precise reconstruction – is demonstrated by the curve in the 3rd subplot of Figure 1A.2, which is reconstruction using all the coefficients of different level. This reconstructed curve is exactly the same as the original one if put into the same plot.
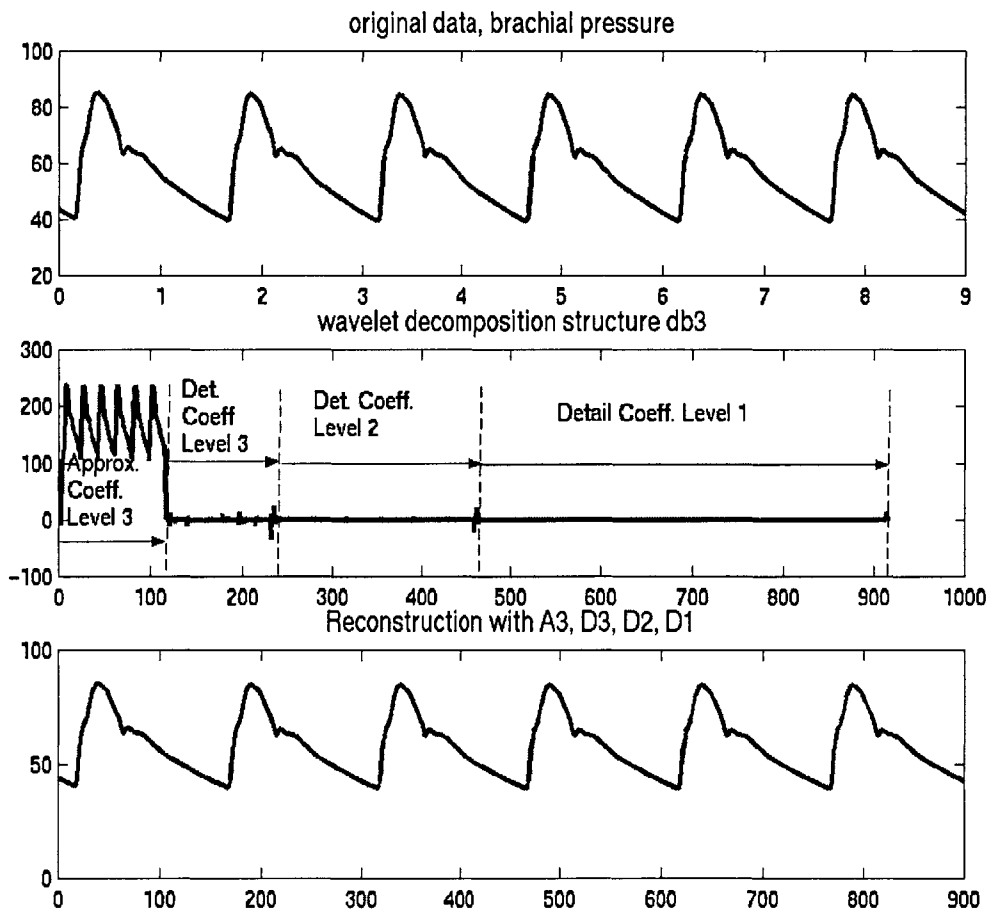

Fig. 1A.2 Multi-resolution decomposition example

Figure 1A.3 is the reconstruction result using each set of coefficient. The 2nd, 3rd, 4th, 5th subplots are the corresponding reconstruction of decomposition coefficients A3, D3, D2, D1 respectively. Note that the reconstruction of approximated coefficients of level 3 (A3) is very similar to the original signal. This makes it useful since only a limited number of features can be selected in parameter estimation and these features should contain as much information of the original signal as possible. This is discussed further below.
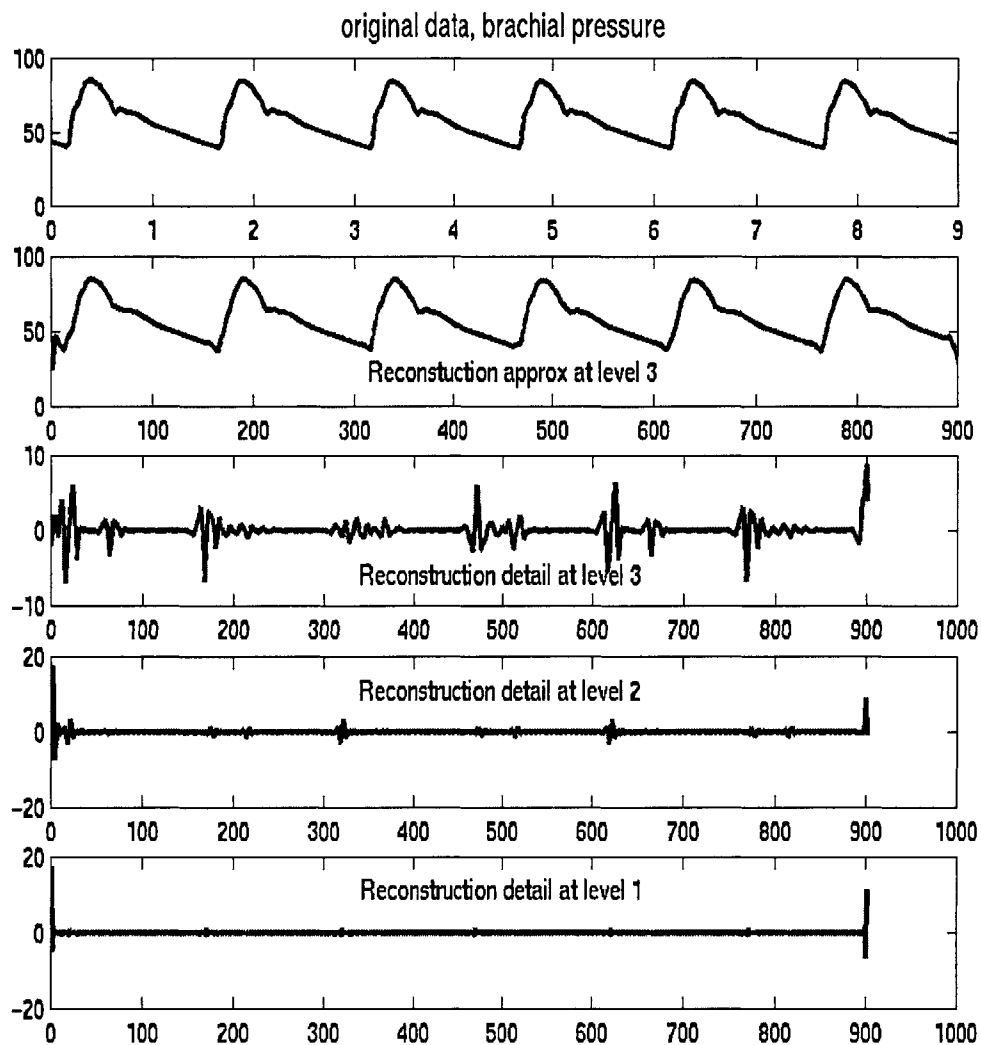

Fig. 1A.3 Reconstruction Results

(b). Wavelet Packet Method

In the Wavelet Packet method, at each level, both the low- and high-frequency sub-bands are decomposed again, so the original signal $f(t)$ is decomposed into small number of large packets at lower resolution and large number of small packets at higher resolutions. On the jth resolution, there are a total of 2^j packets. Signal reconstruction can be performed either by using the packets with the same size on the same resolution, or by using the packets with different sizes on different resolutions. Each wavelet packet represents certain signal information in a specific time-frequency window. Figure 1A.4 shows an example of wavelet packet transform. To do the transform, the original brachial pressure curve was shifted so that it has a mean value of zero. It can be seen that the reconstructed signal with all packets of level 6 is precisely the same with the original signal. The reconstructed signal with only 4 packets (who have largest amplitudes) of level 6 captures general information too (such as maximum, minimum values), but lost some of the details.

It shows that not all the packets in one level contain information, especially at higher resolutions, the coefficients of many packets are essentially zero. In feature extraction, the proposed method is to use the wavelet packets that contain large amounts of information as the features, called feature packets.

The DWT and wavelet packet methods are effective to analyze non-stationary and non-linear signals; they provide both frequency and time localized coefficients. However, in further study it proved not to be beneficial to employ those approaches in our work since it is difficult to extract 3 or 4 features from the detailed information they provide. In DWT, at each level, the wavelet representation always has the same number of data as the signal $f(t)$, each representation has a time and frequency scale, so after DWT, we obtained three times as much data as in the original signal. Although in the Wavelet Packet method, most of the packets are zero, even one nonzero feature packet contains much more information than can be expressed in 3 or 4 coefficients. We tried to use the first 3 or 4 largest coefficients as features, but all details were lost, which gives rise to large errors for parameter estimation.

39

The errors of parameter estimation using these two wavelets analysis are shown in Table 1A.1, together with that of other feature extraction methods that will be discussed in the following parts.

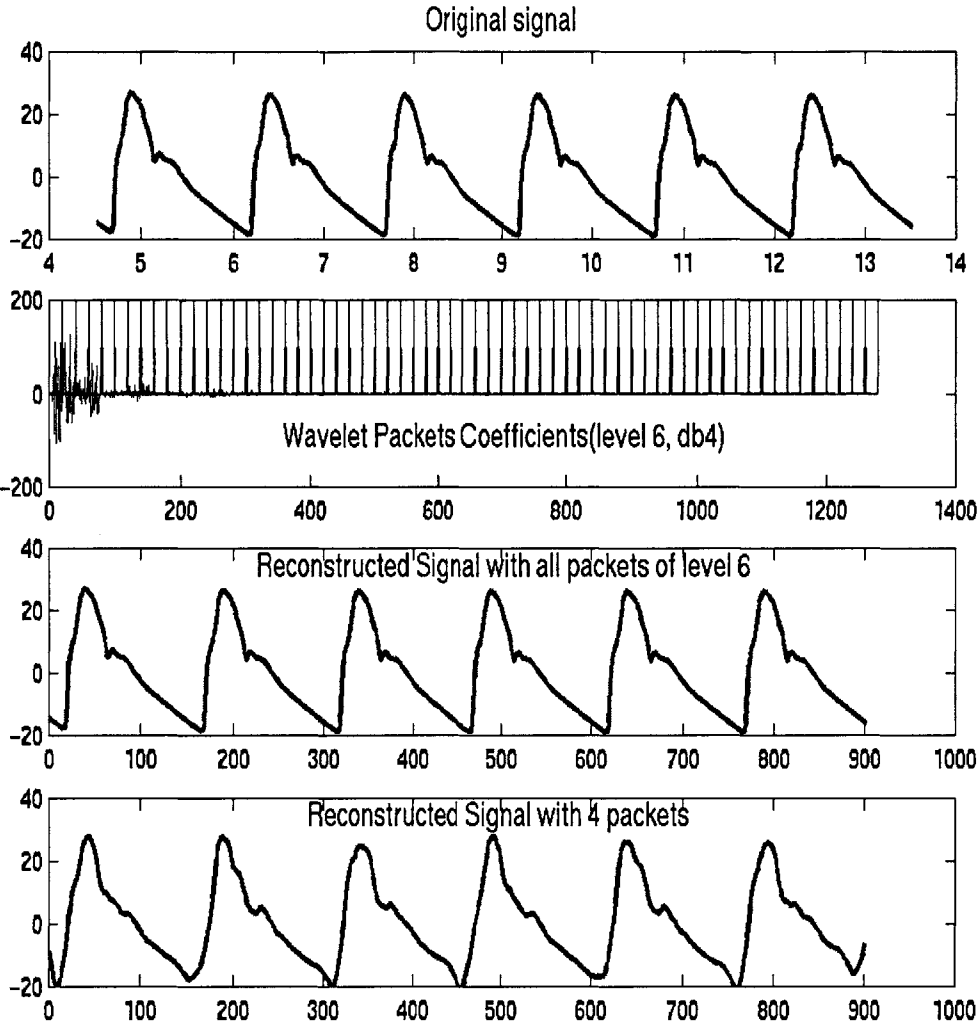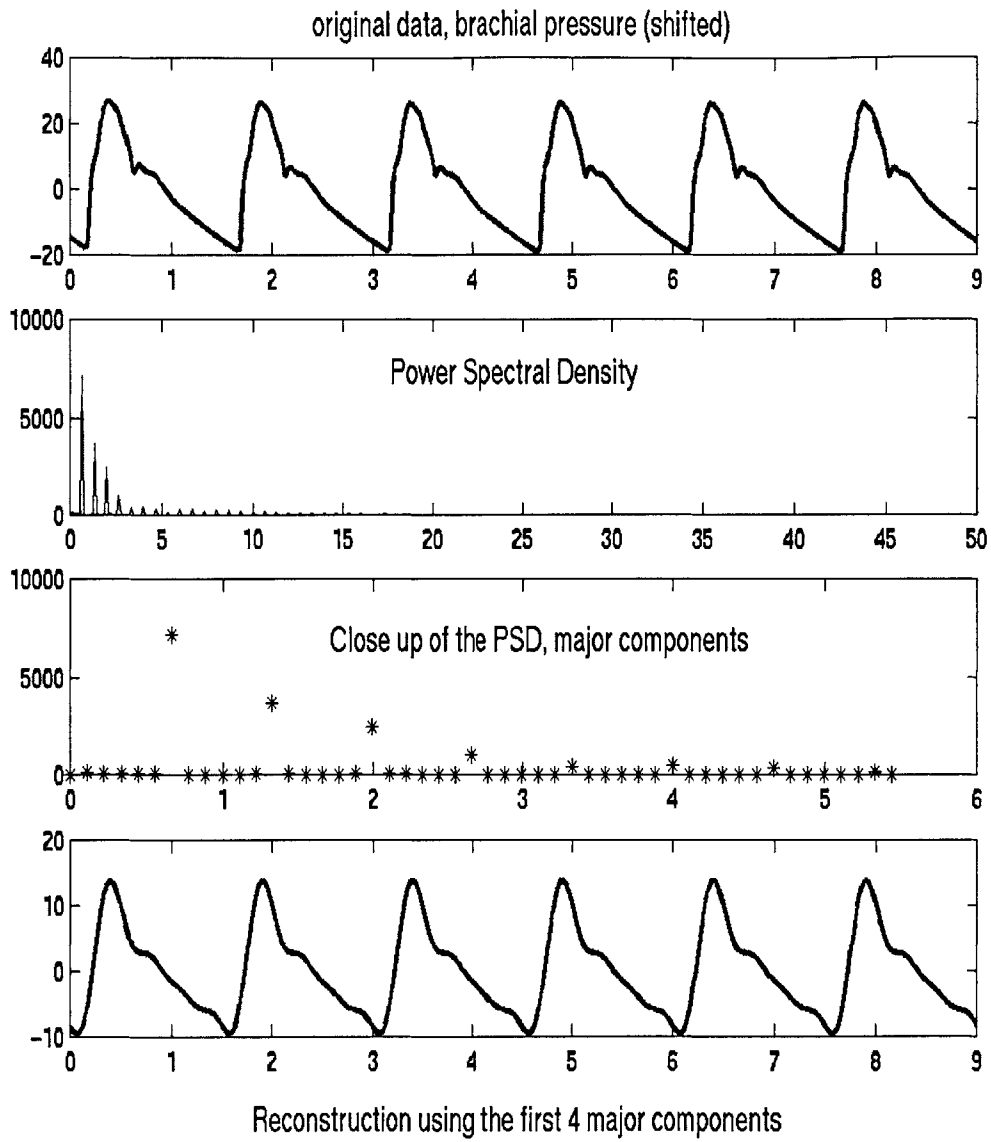Fig. 1A.4 Wavelet Packet Method Demonstration

original data, brachial pressure (shifted)

Power Spectral Density

Close up of the PSD, major components

Reconstruction using the first 4 major components

Figure 1A.5. Fourier Transform Example

41

Features\parameters	E_{LV}	V_{ED}	SVR
Wavelet Packet	42.0281	25.0410	32.1791
DWT	38.9784	28.0963	12.2098
FFT	31.8283	10.4340	2.5975
Waveform features	14.3867	6.2326	3.5520

Table 1A.1 Errors of parameter estimation using different feature sets.
(34 random points generated from model, estimated from pressure curve of
carotid artery. E_{LV}: Maximum value of left ventricle elasticity
V_{ED}: End Diastolic Volume, SVR: Systemic Vascular Resistance.)
(Noting these results were generated using a previous solution library
with smaller parameter space than that of being used now.)

Fourier Transform

In some respects, the Fourier transform can be considered a special form of a wavelet transform since it uses harmonics e^{iwt} as the "mother wavelet". Figure 1A.5 gives the FFT power spectral density and the reconstruction results using the coefficients of the dominant harmonics. The errors for parameter estimation using FFT are also listed in Table 1A.1. It is clear that they are not as small as those using waveform characteristics (discussed next). In addition, signals encountered in application are non-linear and non-stationary. As a result, this method was not viewed to be optimally suited to the current application.

Features from waveform characteristics

This led us to return to our previous approach using those features that physicians typically apply in their diagnosis of a patient. These may include mean pressure, peak systolic dP/dt, the slope of the pressure upstroke during early systole, and the systolic ejection period, or the time during the cardiac cycle that the left ventricle is actively contracting, the dP/dt of the pressure during diastole, etc.

Feature Evaluation

Ideally, the features should be independent of each other, adequate to specify a unique waveform, and each individually should be a monotonic function of the N parameters being estimated. However, in practice, the multi-dimensional relation between features and parameters makes it difficult to define an applicable criterion to evaluate the features. Many different combinations of feature sets were tried to do parameter estimations and the corresponding errors were compared. In this way, the performance of different features can be evaluated. Another way is to draw three-dimensional figures to show the relation of each feature to two parameters, which can give a direct impression how effectively the features can behave in estimation. This method was used at the beginning of the project when the computational model needed a longer time to finish and when much less points were contained in the solution library. The features considered include: mean pressure (P_{mean}), difference between maximum and minimum pressure (ΔP), peak systolic slope ($dPdt_{max}$), mean dP/dt during diastole ($dPdt_{dias}$), the time to reach peak pressure (T_{max}), the time to dicrotic notch, pressure at 2nd peak, maximum velocity, mean velocity, etc. The smallest set of errors in parameter estimation using four of those waveform features is listed in table 1A.1.

Figure 1A.6 is an example of evaluation of feature 1 (P_{mean}/V_{mean}) with initial dimensionless values of parameters as 0.2 0.4 0.5 0.6 0.7 respectively (noting it was generated using the old library mentioned above). It can be seen that many of these plots are not monotonic relations. For example, the last subplot is for feature 1 and parameters 4 and 5 (other parameters are fixed at their initial values), if parameter estimation is done near these values, larger errors will be resulted because of the non-monotonic feature of the surface. The ideal case is that all these 3D curves have shapes similar to the first subplot in Figure 1A.6.

From such evaluations, the best performing features are: ($dPdt_{max}$), (P_{mean}), (ΔP), while the worst performing ones are: (T_{max}) and $dPdt_{dias}$.

One-dimensional curves of feature and parameters can also be drawn to evaluate the linearity and sensitivity of the relationship. Figure 1A.7 is one of such plots. The initial values for the parameters are: 0.2 0.4 0.5 0.6 0.5 respectively. It can be seen that none of the features is sensitive to parameter 4 (systolic period). Therefore, it is difficult

to estimate this parameter using the listed features near the corresponding initial parameter values. For other parameters, there is at least one feature with relatively large sensitivity and linearity, which provide for a good assessment. Since the relationships of features and parameters are multi-dimensional in nature, different combinations of initial parameter values should be evaluated to judge the overall performance of a feature.
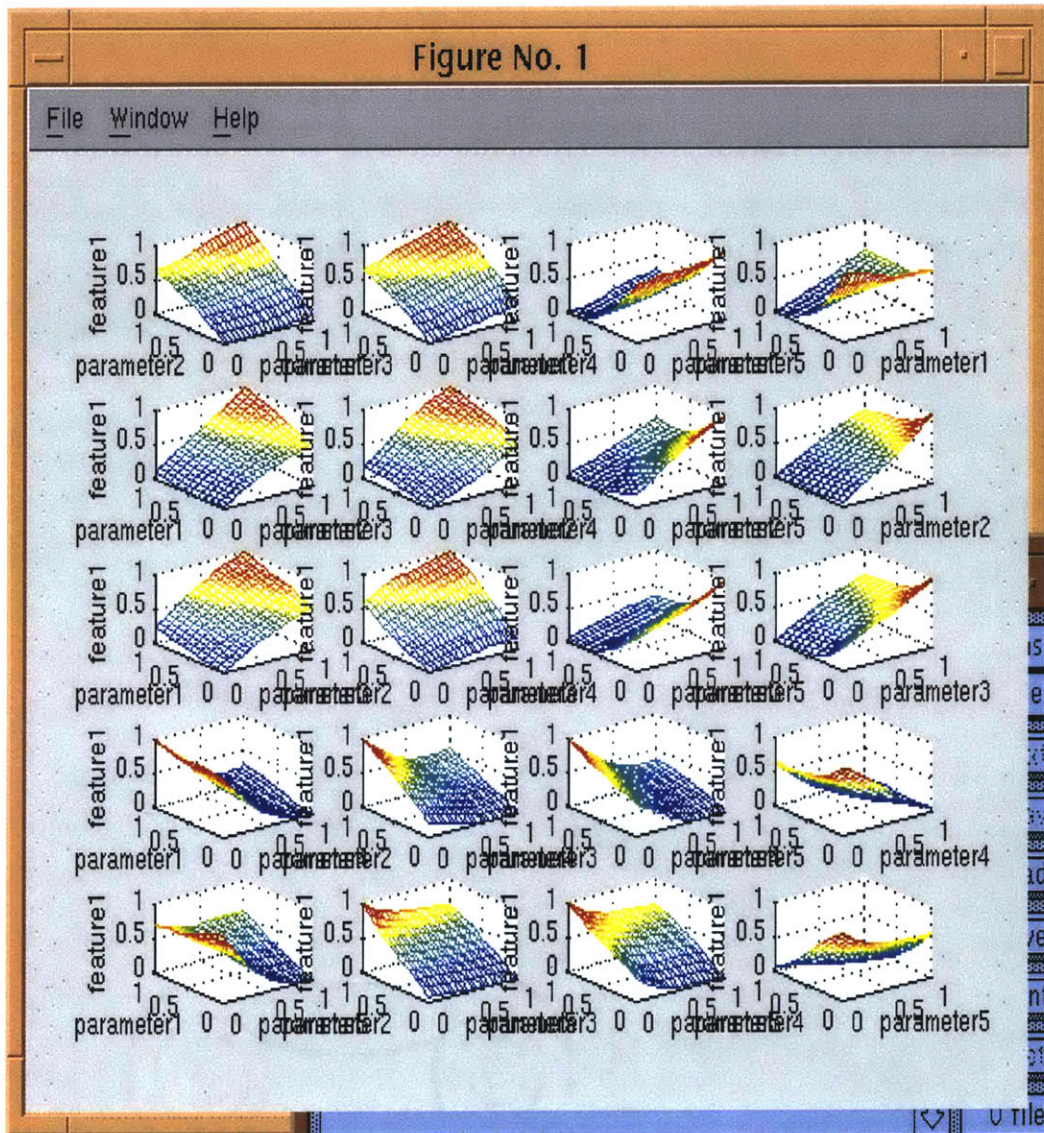
Fig. 1A.6 The 3D relationship of Feature1 (P_{mean}/V_{mean}) to parameters
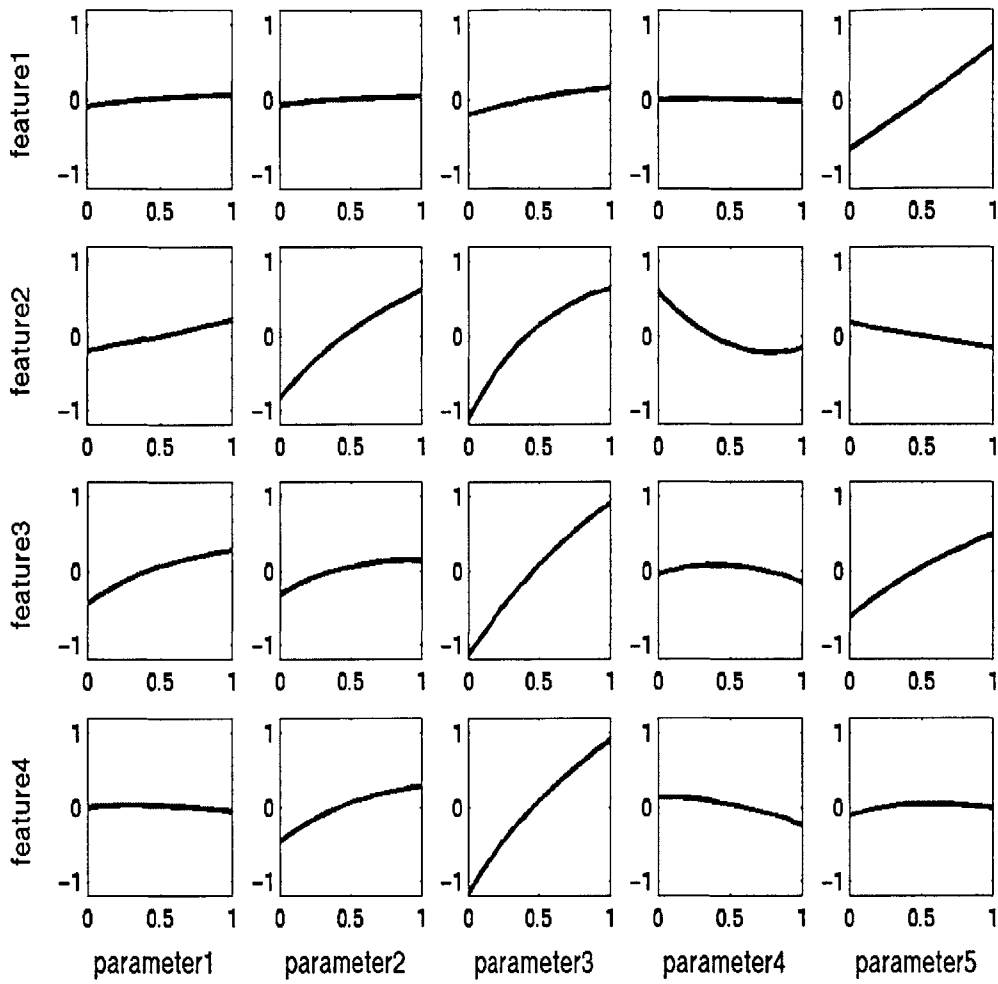
(1. HR; 2. E_{LV}; 3. V_{ED}; 4. Systolic Period; 5. SVR)

Fig. 1A.7 1D feature-parameters relation (Non-dimensionalized)

(Features 1 2 3 4 are P_{mean}/V_{mean}, $dPdt_{max}$, P_{mean}, deltaP respectively)

(Parmeters 1 2 3 4 5 are HR E_{LV} V_{ED} Systolic Period SVR respectively)

Discussion

Many different features have been evaluated and compared. The conclusion is that waveform characteristic features are among the best ones for our research objectives, for example, $dPdt_{max}$, P_{mean} and ΔP. They can give fairly small errors in parameter estimation of model-generated points.

However, it can not be guaranteed that these same features are good for measured pressure and velocity curves since it must depend on the applicability of the model assumptions and the limitations in measurement techniques.

Parameter estimation for measured pressure and velocity profiles will be discussed more intensively in later chapters.

Generation of Solution Library and Comparison of Models

Generation of solution library

As stated in the main part of the thesis, only sparse points can be saved into the solution library because of computational efficiency, while the more points presented, the more accurate are the interpolations. Thus, a compromise must be made between computation efficiency and interpolation accuracy.

Currently, the main program of the cardiovascular model written in C takes 5-10 minutes to finish simulation of 10 heart cycles for each given set of parameters. Note that this length of time depends on the value of Heart Rate (HR) for the specific run. The higher heart rate, the fewer computational points in one cycle and the less time it takes.

Table. 1B.1 gives the hemodynamic parameter scopes, the number of values used to generate solution library, and correspondingly, the steps between neighboring parameter values. After filtering the unreasonable parameter combinations using the lumped CV model, 2351 points are saved in the current solution library.

Table 1B.1. Hemodynamic parameter values in the solution library

	HR	E_{LV}	V_{ED}	SVR
Maximum Value	40 /min	300 dyn/cm^5	30 ml	300 dyn-sec/cm^5
Minimum Value	160 /min	15000 dyn/cm^5	400 ml	3500 dyn-sec/cm^5
Number of Grids	6	7	16	16
Value Steps	24 /min	980 dyn/cm^5	24.67 ml	533.3 dyn-sec/cm^5

Model discussion and comparison

An important issue needed to discuss is about the parameter η used in the model, as in equation (1B.1)

$$Ptm = Ptm(A^e) + \eta * \frac{\partial A}{\partial t} \qquad (1B.1)$$

The primary function of η is damping instabilities in the model. There is no evidence that suggests viscoelastic response is essential for capturing true physiological behavior in numerical models. Hence, the numerical value of η is not critical provided its value does not influence the result (K. Bottom).

For different hemodynamic parameters used in the model, η should have different values to ensure computational stability. For example, figure 1B.1 shows the results of aortic root pressures using different values of η (using the model modified by Karen Bottom). This model will be referred to as model II, while the original model by Edwin Ozawa will be referred as model I, and the new elastance model will be named model III).
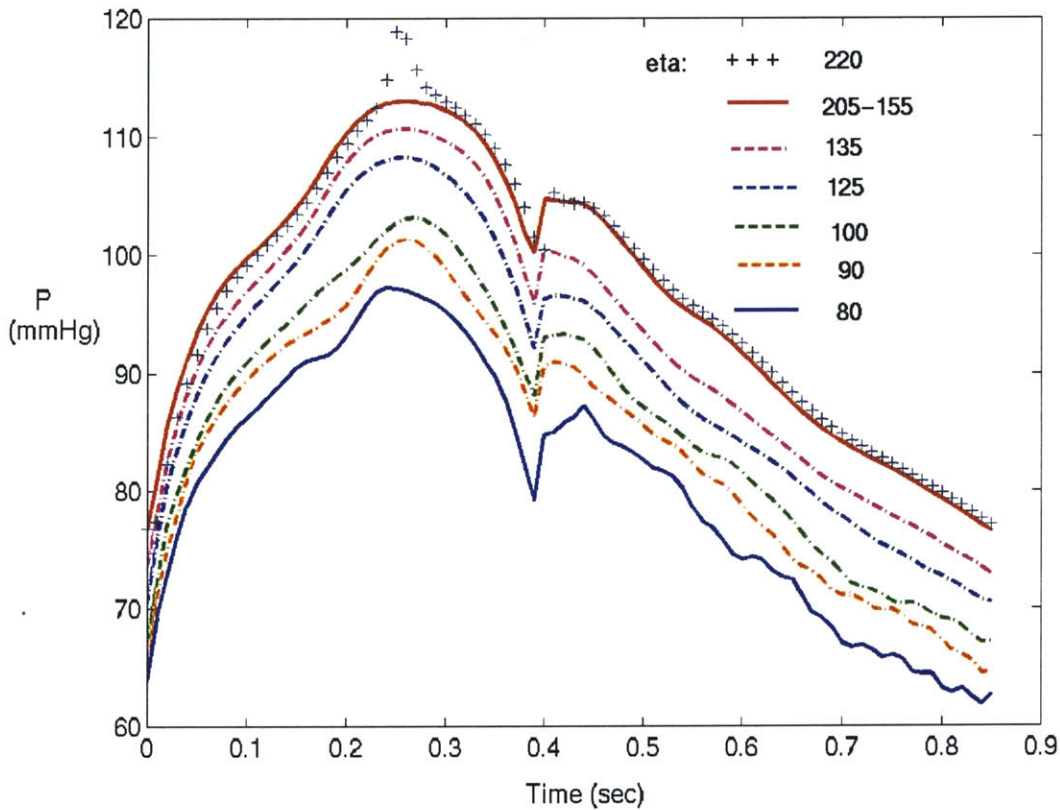

Fig. 1B.1 Effects of η on aortic root pressure curves

In the figure, different curves were generated using same input parameters list in Table 1B.2.

Table 1B.2. Parameter values for all curves in Figure B1

Parameters	HR	E_{LV}	V_{ED}	SVR
Values	70 /min	4500 dyn/cm^5	150 ml	1300 dyn-sec/cm^5

In Figure 1B.1, the solid red line (the upper solid line) can be generated using η values ranging from 205 to 155, i.e. the value of η doesn't affect the results as long as it is in this range. However, when η is as high as 205 or larger, numerical instabilities will occur and the pressure curve is distorted as shown. When η is lower than 155 but higher than 80, no instabilities in calculation, but the pressure values decreases as η decreases. When η reaches 80, instabilities occur again and oscillations can be seen in the pressure curve.

When generating a library, it is inefficient to adjust the value of η by trying the different values for each point by the user since there is over two thousand points. A uniform rule for value of η must be employed and it is better that the program can find a proper η automatically.

Since the problem of η arises when model I was improved into model II, the results of the new model can always be compared to those of the previous model. Assuming that model I gives reliable results, the right value of η to use can be decided using outputs of model I as reference.

Figure 1B.2 is a comparison of different model outputs using same parameters in Table 1B.2. It can be seen that the curve of model II with η = 205-155 is similar to the curve obtained from model I. Together with Figure 1B.1, it is obvious that when η is smaller than 155, the pressure curve would become more different from the assumed reference curve (that of model I).

Therefore, a criterion for value of η can be decided — the largest value of η with which there is no instability in calculation should be the desired value. The program is easily adapted to identify the value of η automatically in this way.
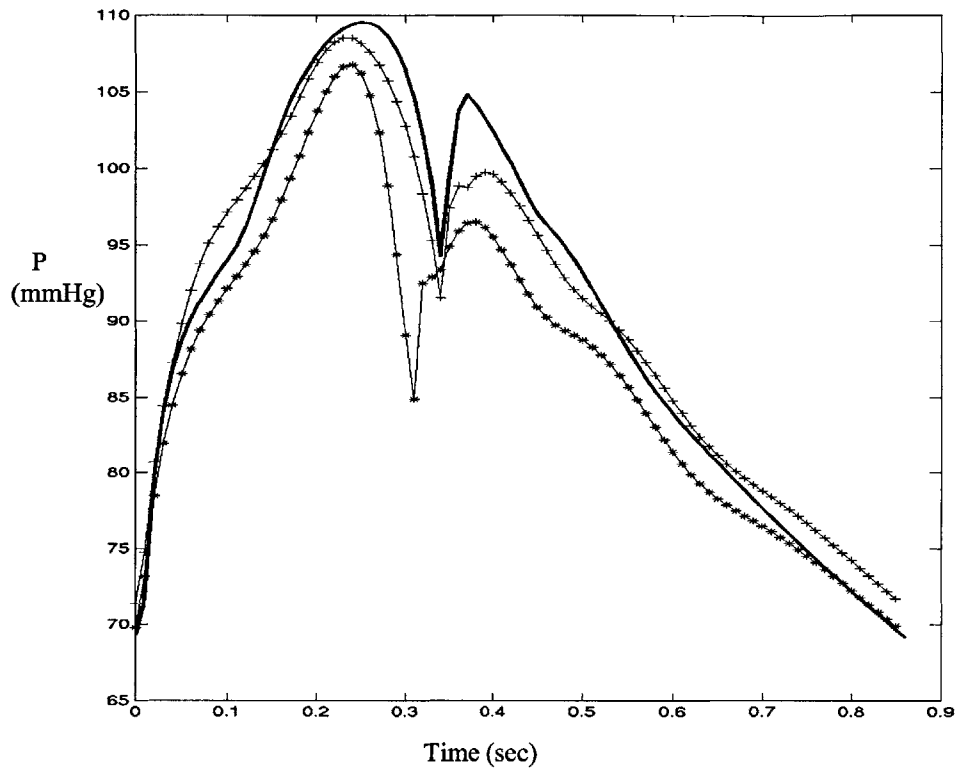
Figure 1B.2. Comparison of different model outputs

(solid line: aortic root pressure from model I

+ + line: aortic root pressure from model II, η = 205-155

** line: aortic root pressure from model III)

It should also be noted that by adjusting the value of η, the program takes more time to finish. If the proper η value is fairly small, this problem is significant since the value of η can only start from a high value (270, usually) to encompass all possibilities for library points.

In addition, figure 1B.1 is generated using model II, but the same rule about adjusting η is also applicable to model III.

Figure 1B.2 shows that model III gives a slightly lower pressure than the other two models. This is acceptable since model III is using different elastance theory for left ventricle and it is not unreasonable if the pressure changes from the old models. The most important thing is that this new model can enable more accurate parameter estimation for measured data, which will be shown in Chapter 2.

Further Comparison of Different Model Outputs

To further compare and evaluate the 3 models, their frequency responses were calculated. Numerous studies have been performed to characterize the frequency response of the arterial system. The most often used method is to define the input impedance of the system as the amplitude modulus, which is the ratio of pressure amplitude and the flow rate amplitude, as a function of frequency. The pressure and flow rate signals are transformed by Fourier decomposition.

Using the same parameters as listed in Table 1B.2, the aortic root pressure and flow rate traces are calculated respectively. After FFT (Fast Fourier Transform), the input impedances (Modulus and phases) were obtained. Figure 1B.3, 1B.4, 1B.5 are the results. Figure 1B.6 is a well-accepted result measured by Nichols, who recorded aortic blood flow and pressure invasively of normal subjects. The top panel of Figure B6 shows the modulus falls from its initial value to a minimum at 4Hz and rises again thereafter. The curve in the lower panel reaches a minimum negative value, indicating that flow is leading pressure, and then crosses over to become positive at approximately 3Hz. Comparing Figure 1B.6 to the other 3 figures, the model-based curves have similar shapes to that in 1B.6. In fact, in measurements, the impedance is affected by many factors, such as the peripheral resistance and the smooth muscle tone of the systemic arteries, and one individual's impedance may change frequently during a day.

Thus, we conclude that input impedance curve used in the new model does not adversely affect the results.
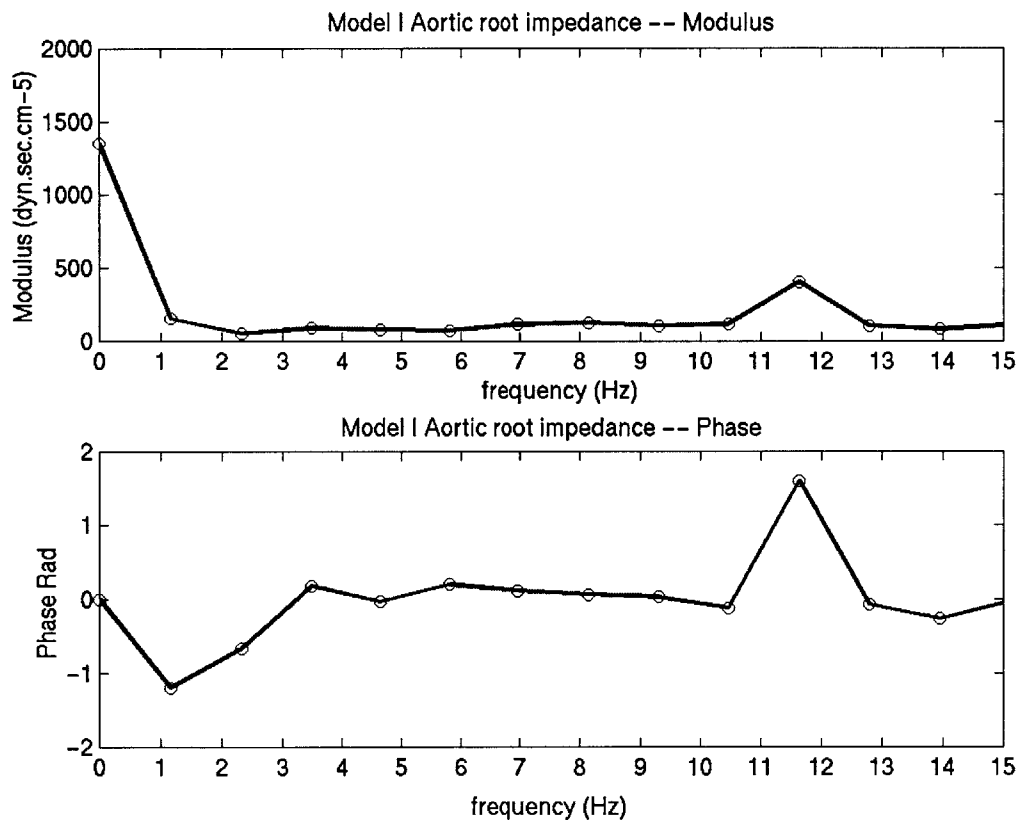
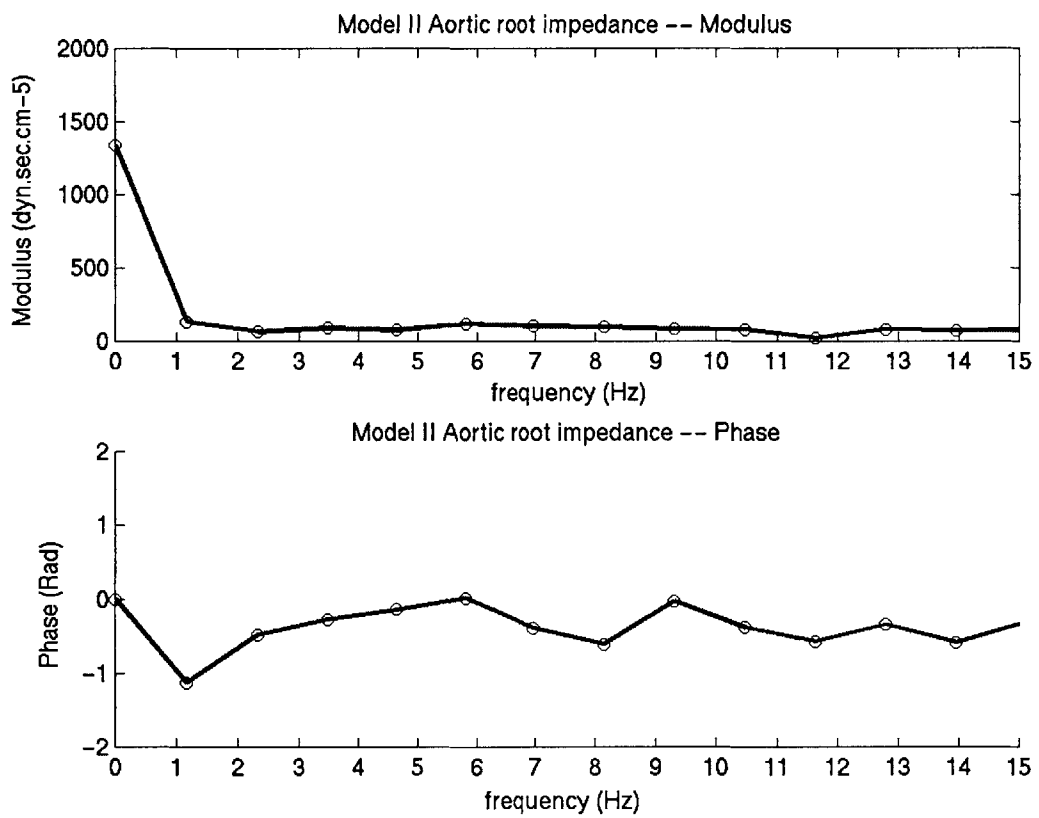Fig. 1B.3. Calculated aortic root impedance for model I

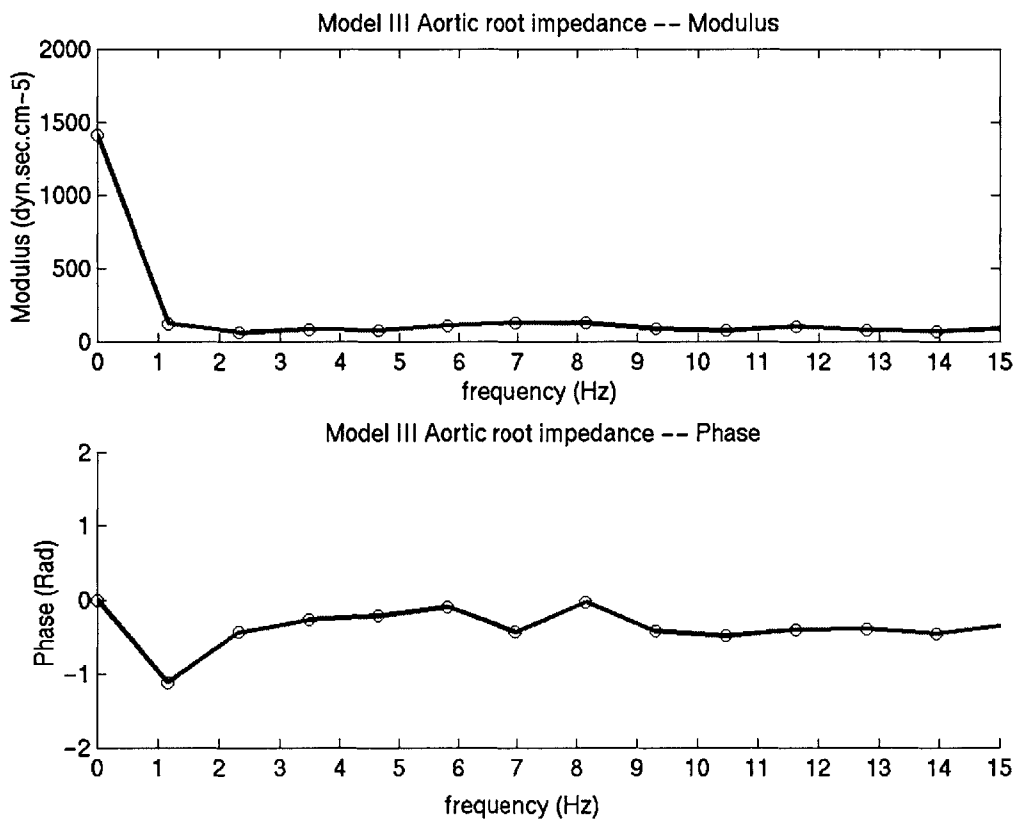Fig. 1B.4. Calculated aortic root impedance for model II

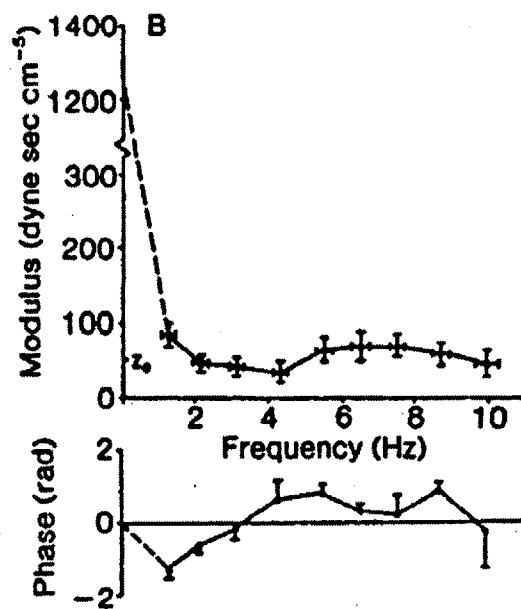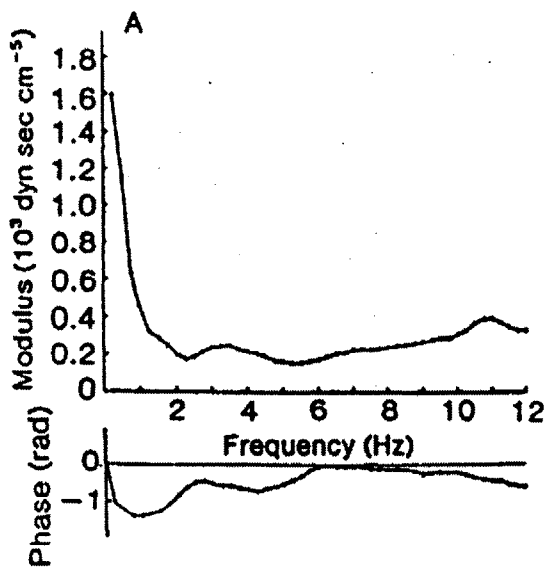Fig. 1B.5. Calculated aortic root impedance for model III

Fig. 1B.6 The input impedance of human arterial

system measured by Nichols et al. 1977

Additional Calculation Results

In addition to the results presented in Chapter 1, there are a few other calculations done to evaluate parameter estimation scheme.

<u>Sensitivity Analysis Results</u>

Figure 1C.1 is the sensitivity analysis results using feature set 4 when V_{ED} is taken as known. Recall that feature set 4 was got from 2 by omitting P_{max}. Compare this result with that in figure 7(2) (where parameter errors using feature set 2 was demonstrated), the sensitivity of V_0 is reduced, but other parameters' sensitivities are increased to various extents. Using V_{ED} as a known variable should make the parameter estimation more accurate. Therefore, it can be inferred that feature set 4 is actually sensitive to these parameters, while feature set 2, with P_{max} added, is less sensitive to the minor parameters. When estimating measured pressure curves to get patient's hemodynamic parameters, it will be better to use feature set 2 instead of feature set 4, even if V_{ED} is known from measurements.
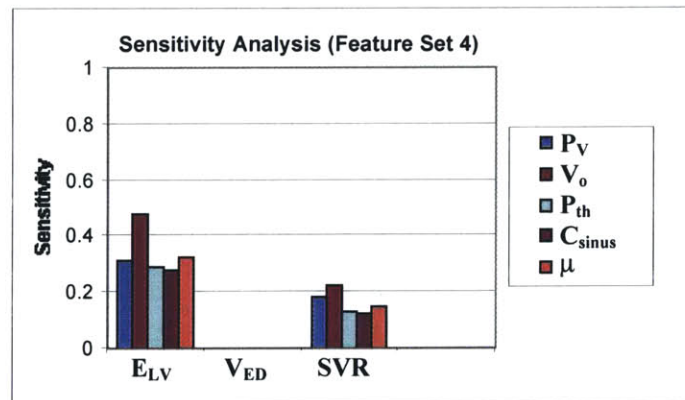

Figure 1C.1 Sensitivity analysis with V_{ED} known

(Feature Set 4: $(dp/dt)_{max}$ P_{mean} ΔP)

Prediction of Changes of SVR

Table 1C.1 is the results of predicting changes of SVR when V_{ED} is taken as known. The results are not of much difference from those when estimating V_{ED} shown in Table 5. Hence, in predicting changes of SVR, it is not necessary to measure V_{ED} first.

Table 1C.1 Predicting change of SVR when fixing V_{ED}

$\partial P_{est}/\partial P_{real}$	ΔSVR (-10%)	ΔSVR (+10%)	Mean of ± 10% cases	Standard Deviation
Feature Set 3	1.2016	0.9940	1.0078	0.0437
Feature Set 4	0.9067	0.8540	0.8804	0.3133

Table 1C.2 shows the results of predicting changes of SVR when the values of minor parameters are randomized in their respective ranges. The standard deviations using both feature sets are larger than 0.3. Table 1C.3 lists the values of the randomized parameters.

Table 1C.2 Prediction change of SVR with minor parameters randomized

$\partial P_{est}/\partial P_{real}$	ΔSVR (-10%)	ΔSVR (+10%)	Mean of ± 10% cases	Standard Deviation
Feature Set1	1.2171	1.0437	1.1304	0.3382
Feature Set2	1.1696	1.0432	1.1064	0.5313

From table 1C.3, it can be seen that randomized parameter values distribute widely in their corresponding ranges. In reality, one person seldom has all these parameters changed simultaneously. Thus, the standard deviations in table 1C.2 can be seen as the maximum values when estimating patient's hemodynamic parameters.

58

Table 1C.3 Random parameters for prediction changes of SVR

	P_V (mmHg)	V_0 (ml)	P_{th} (mmHg)	C_{sinus} (cm^5/dyn)	Blood Viscosity (cp)
Nominal	5.0	15	-5	0.00005	0.04
Rand. Set1	14.352688	46.177960	-24.424558	0.000098	0.036898
Rand. Set2	7.065009	10.240424	-8.649476	0.000144	0.052134
Rand. Set3	8.372989	56.414761	-12.662600	0.000051	0.049181
Rand. Set4	0.305479	49.785712	-14.797428	0.000187	0.038186
Rand. Set5	4.055304	13.248116	-10.565534	0.000064	0.023937
Rand. Set6	1.157826	23.524542	-4.982227	0.000015	0.020741
Rand. Set7	12.308647	52.795802	-2.084987	0.000151	0.022734
Rand. Set8	19.002586	15.409234	-10.484198	0.000104	0.060869

Table 1C.4 is the corresponding estimation results when fixing V_{ED}. The standard deviations are reduced slightly, but the overall results are approximately the same with those in table 1C.2. Measuring V_{ED} is not necessary when predicting changes of SVR.

Table 1C.4 Prediction change of SVR

With V_{ED} known and minor parameters randomized

$\partial P_{est} / \partial P_{real}$	ΔSVR (-10%)	ΔSVR (+10%)	Mean of $\pm$ 10% cases	Standard Deviation
Feature Set 3	0.9206	0.8831	0.9018	0.3298
Feature Set 4	0.8846	0.9261	0.9053	0.4760

Prediction of Changes of E_{LV}

Table 1C.5 is the results of predicting changes of E_{LV} when the minor parameters are randomized. The standard deviations are larger than 0.5. While in table 1C.6, the calculation was done by assuming V_{ED} was given, the standard deviations are decreased by about 0.2 each. These results are consistent with those in table 6 and 7 of Chapter 1.

59

The conclusion is that when predicting changes of E_{LV}, the estimation is more accurate if measuring V_{ED} first and take it as input to parameter estimation routines.

Table 1C.7 gives the randomized parameter values. Again, the errors shown in table 1C.5 and table 1C.6 can be seen as the maximum errors in reality.

Table 1C.5 Predict change of E_{LV}

With minor parameters randomized

$\partial P_{est} / \partial P_{real}$	ΔE_{LV} (-10%)	ΔE_{LV} (+10%)	Mean of ± 10% cases	Standard Deviation
Feature Set1	0.7711	1.2456	1.0084	0.6663
Feature Set2	0.8422	1.3079	1.0750	0.5662

Table 1C.6 Predict change of E_{LV}

With V_{ED} known and minor parameters randomized

$\partial P_{est} / \partial P_{real}$	ΔE_{LV} (-10%)	ΔE_{LV} (+10%)	Mean of ± 10% cases	Standard Deviation
Feature Set 3	0.7125	0.8943	0.8034	0.4020
Feature Set 4	0.7215	0.8886	0.8050	0.3756

Table 1C.7 Random parameters for prediction changes of E_{LV}

	P_v (mmHg)	V_0 (ml)	P_{th} (mmHg)	C_{sinus} (cm^5/dyn)	Blood Viscosity (cp)
Nominal	5	15	-5	0.00005	0.04
Rand. Set1	14.0548	36.43808	-14.8032	0.000143	0.04647
Rand. Set2	4.055304	13.24812	-10.56553	6.41E-05	0.023937
Rand. Set3	19.59494	18.09648	-19.93788	0.000177	0.052656
Rand. Set4	16.76237	1.309301	-8.499276	8.42E-05	0.057696
Rand. Set5	13.20455	22.79804	-18.94064	7.7E-05	0.041818
Rand. Set6	13.95797	25.22487	-3.733024	0.000173	0.04499
Rand. Set7	9.931049	59.98461	-4.756556	0.000134	0.056959

Parameter Estimation Errors

With the minor parameters randomized, simulations can be done and the pressure and velocity curves can be used to do parameter estimation. Since the estimations are obtained using the solution library in which all minor parameters are fixed, the estimation errors must be higher than those presented in chapter 1.

Figure 1C.2 gives the estimation errors when the minor parameters were randomized as listed in table 1C.3. It can be seen that all errors are less than 20% and the errors for SVR is much larger than those shown in chapter 1. As mentioned above, these parameter errors can be seen as the largest ones our method will have in estimating with measured pressure and/or velocity.

Figure 1C.2 Parameter Estimation errors when randomizing fixed parameters

Parameter estimation errors
with randomization of fixed parameters

Feature Set1
Feature Set2
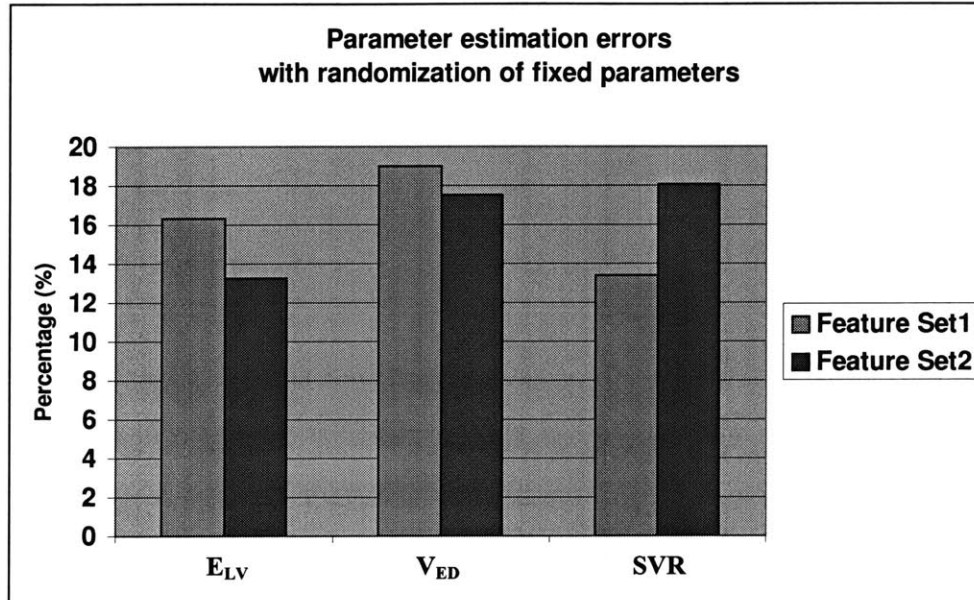
2. Measurement System and

Hemodynamic Parameter Estimation of Measured Data

Abstract

The non-invasive hemodynamic parameter estimation method presented in the section of *Noninvasive Assessment of Cardiovascular Health* is applied to estimate *SVR* (Systemic Vascular Resistance), E_{LV} (maximum Elasticity of Left Ventricle), V_{ED} (End Diastolic Volume), and to calculate *C.O.* (Cardiac Output) and *S.V.* (Stroke Volume). Measurements on healthy volunteers and patients were conducted in Brigham and Women's Hospital, Boston, MA. Carotid, brachial and radial pressures were measured by tonometry and velocities at corresponding locations were measured by ultrasound. Three heart failure patients and nine volunteers were studied. Parameter estimation results using feature sets 1 (P_{mean}/V_{mean} $(dp/dt)_{max}$ P_{mean} deltaP) and 2 ($(dp/dt)_{max}$ P_{mean} deltaP P_{max}) are presented, together with pressure and velocity waveforms reconstructed by inputting estimated parameters back to the CV model. Reasonable agreement is found between the measured pressure and velocity curves and the reconstructed ones. Invasive measurements of hemodynamic parameters are available for two of the patients, which are compared to predictions to evaluate the performance of parameter estimation routines.

Key words:
non-invasive, parameter estimation, pressure measurement, velocity measurement

Introduction

The application of the noninvasive hemodynamic parameter estimation method presented in chapter 1 of this thesis is demonstrated here providing a preliminary assessment of the method using real rather than computer-generated data. Measurements on volunteers and patients were made in collaboration with Drs. Richard Lee and Nancy Sweitzer in Brigham and Women's Hospital, Boston, MA.

In order to perform parameter estimation, carotid, brachial and radial pressure and velocity, EKG (at the same time when each pressure is measured), characteristic length (the length between measured locations on brachial and radial arteries) and brachial cuff blood pressure all must be measured. Subject's age, sex, height and weight may also be saved for reference. With the measured pressure and EKG, the subject's reference wave speed (aortic root wave speed at $P_{ref} = 100$ mmHg) and heart rate can be calculated. The above information is sufficient to do parameter estimations. Measurement and estimation results of 12 adult subjects (9 volunteers, 3 patients) will be presented in the following sections.

In addition, it is preferred to measure subject's V_{ED} non-invasively using ultrasound, either to compare with the estimated value or to do more accurate estimation of E_{LV} and SVR by taking V_{ED} as known. When the subject is a catheterized patient, the invasively measured hemodynamic data, such as SVR, C.O., should be recorded whenever possible to allow comparison and evaluation of the method. Among the subjects studied, V_{ED} was measured on two of them, and SVR, C.O. were measured invasively on two of the patients.

This paper describes the parameter estimation methods that are separated into the following topics: (1) Measurement hardware and software. (2). Pressure and velocity data processing. (3). Parameter estimation results and evaluation. (4). Discussion of parameter estimation scheme applied in measured data

Measuring System

In order to perform parameter estimation, arterial pressure and blood flow velocity in one of the peripheral arteries must be measured. Various methods can be used to obtain these measures as described next.

Pressure Measurement

Many non-invasive methods exist to monitor pressures in the peripheral arteries. Table 2.1 gives a brief list and introduction of some of the more popular ones [1].

Table 2.1 Pressure measurement methods

Method	Description
Auscultatory Method	Based on Korotkoff sound (first described in 1905), measures systolic and diastolic pressure, estimates mean
Oscillometric Method	Based on oscillations resulting from the coupling of the occlusive cuff to the artery, measures mean, estimates systolic and diastolic
Plethysmography	Measures the volumetric change associated with arterial distension since volumetric change causes change in the electrical impedance of the measured site
Tonometry	Using an array of sensors measuring pressure required to maintain the flattened shape of artery when external pressure is applied. Continuous waveform can be measured.

Selection of a pressure measuring device that can give reliable continuous traces is crucial to parameter estimation. A Millar tonometer was chosen because, unlike some of the other methods, it can give continuous pressure profiles similar to catheter measurement. Figure 1 gives a view of the pencil-like probe of this tonometer (SPT-301, Millar Instruments Inc., Houston, TX).
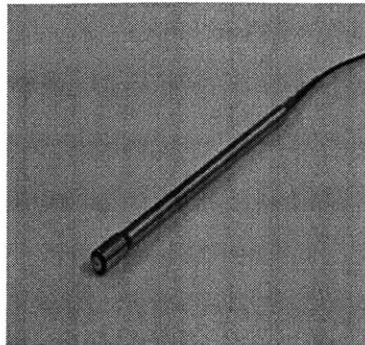
Figure 1 Millar Tonometer

Measurement of arterial pressure using the Millar tonometer is based on the principle of applanation tonometry, as is commonly used in the measurement of intra-ocular pressure [2]. When one flattens or applanates (Figure 2) the curved surface of a pressure-containing structure, the pressure difference across the vessel wall is eliminated and the sensor registers the true intra-arterial pressure [3]. The wall flattening is important since force from the intra-arterial pressure needs to be evenly distributed to the force-sensing area without distortion from circumferential stresses inherent in a curved wall [4]. With applanation achieved, the circumferential forces are rendered normal to the direction of the probe and hence balance to zero. If flattening is not achieved, no consistent signal is obtained. Excessive flattening produces a high amplitude excursion signal [5, 6].
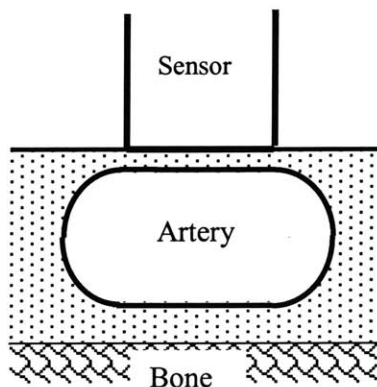

Figure 2 Diagram of applanation tonometry process

Tonometry has several limitations. First, it is sensitive to sensor position and angle, contributing to reduced inter- and intra- operator reproducibility. Secondly, since the pressure registered by a tonometer is related to the applanation force applied to the probe, tonometry requires calibration via an initial blood pressure measurement obtained by an independent technique. Thirdly, a tonometer can only be used on superficial arteries supported by a rigid bony structure in order to provide a contact force between the skin and the sensor area equal to the intra-arterial pressure.

Another important concern with tonometry is that the applied external force distorts the artery wall and may also change the contours of the pressure trace. However, distortion of the arterial wall is required in tonometry since it measures the normal contact stress that is equal to the instantaneous intraluminal pressure when the artery wall is optimally flattened [5, 6]. Driscoll et al studied the influence of recording force on arterial pressure pulses and showed that mean arterial pressure pulse contours remained stable until the force applied at the brachial arterial site exceeded approximately 60% (or 4.28±0.46 N) of the largest brachial force used [5]. Also, it was found that the larger the applied force, the smaller the measured pulse pressure. Therefore, in clinical studies, proper flattening of the arterial wall is determined empirically, i.e. by obtaining a consistent and large amplitude signal [4,7].

The Millar tonometer used in the present studies (FDIC proved, MIKRO-TIP Pressure Transducer, together with Model TCB-500 control unit) uses piezoelectric transducers to detect artery wall deflection transmitted through the skin. It converts pressure to DC voltage with a measurement range of 0 to +300mmHg (0 to 40kPa), sensitivity of $5\mu V/V/mmHg$ (nominal, $37.6\mu V/V/kPa$) and natural frequency of 35kHz.

Velocity Measurement

Velocity profiles are measured using Doppler Ultrasound. The Doppler effect is a shift in the observed frequency of a radiated acoustic wave when there is relative movement between the source of radiation and the observer. The Doppler shift (the difference between the observed and the transmitted frequency) is proportional to the velocity of the scatterer [8]. In medical Doppler ultrasound the scatterer (e.g. red blood

cell) is often moving at an angle to the transmitter and receiver beams as illustrated in Figure 3. The Doppler shift frequency is given by:

$$f_d = \frac{-2Vf_0 \cos(\theta)\cos(\delta/2)}{c} \qquad (1)$$

where

V = Scatterer velocity

f_0 = Transmitted frequency

c = Speed of ultrasound

θ = Angle between the bisector of the transmitter and receiver beams and the direction of movement.

δ = Angle between the transmitter and receiver beams.

The negative sign indicates that the Doppler shift is negative (transmitted frequency shifted to a lower frequency) if the direction of movement is in the conventionally positive direction (away from the transducer).

Since the angle (δ) between the beams is usually sufficiently small so that cos(δ/2) is close to 1.0, the above equation is often simplified to:

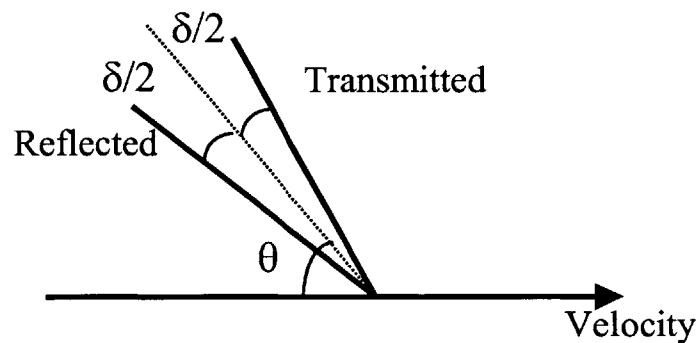$$f_d = \frac{-2Vf_0 \cos(\theta)}{c} \qquad (2)$$

Figure 3 Mechanism for velocity measurement

In the studies presented in this paper, velocity data were obtained by the use of Hewlett-Packard Sonos 2000 echocardiography machine with a 7.5 MHz linear array transducer probe. In each patient, the artery of interest is identified using M-mode ultrasound with color Doppler overlay [9]. Once the transducer is positioned over the artery, PW (Pulse Wave) Doppler measurements are obtained over several cycles, which can be recorded or transmitted to a data acquisition system. Data are processed offline using a laptop computer. Figure 4 is the typical HP Echo machine used in the experiments.
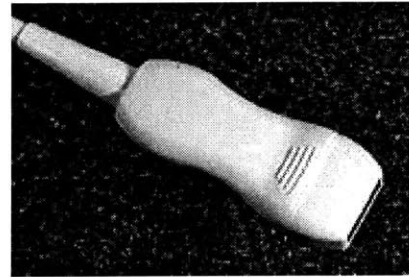
(a)   (b)

Figure 4 Velocity measuring system

(a). HP Echo machine. (b). A typical probe.

Figure 5 Pressure data acquisition

Data acquisition system

A Macintosh Powerbook G3 equipped with a data acquisition card (DAQCard-516, National Instrument Corp. Austin, TX) and related accessories are used. The signal from the pressure transducer is ported to the computer through DAQCard, the National Instrument DAQ software, and LabVIEW software, converting analog signals into digital ones that are then saved in a readable plain text format. Velocity related information (Doppler sound signal) is ported through the computer's "sound in" port and collected using Ultra-Recorder software. Figure 5 is demonstration of the data acquisition system when measuring radial pressure.

Data processing

Pressure

1. Averaging the measured data

The Millar tonometer measures pressure continuously and data are stored in real time. Usually, more than 10 relatively stable cycles are saved. When processing pressure data, it can often be found that no two cycles are precisely the same, or obvious differences, in terms of amplitudes, shape of contours, etc, exist among the assumed

stable cycles. In these cases, a mean cycle of more than 10 cycles is taken. Figure 6 is an example of the pressure data measured. 13 cycles were taken in this example.
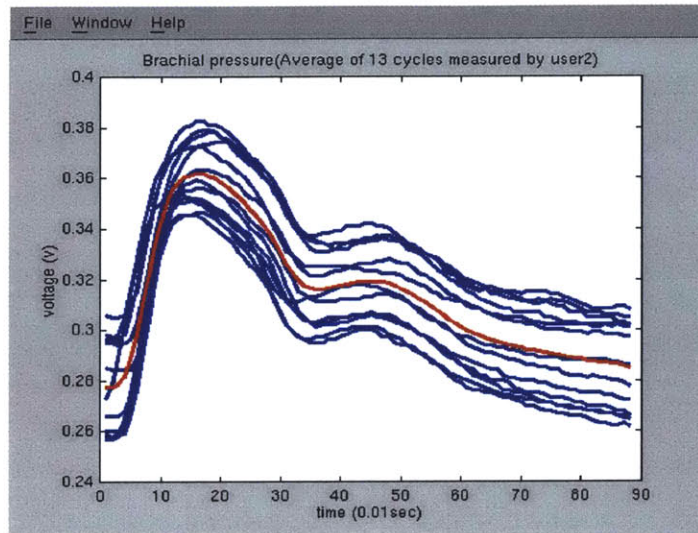

Figure 6 Example of pressure measured

(Brachial pressure of a volunteer.

Blue: 13 individual measurements; red: average of all 13 cycles)

2. Calibration

Note in Figure 6, the "pressure" is actually voltage values obtained directly from the Millar tonometer before calibration. With the assumption that the contour of the pressure trace is unchanged by the application of external force, the measured voltage can be converted into pressure with brachial systolic and diastolic pressure measured using the auscultatory method. For the measurements of Figure 6, auscultation indicated the blood pressure to be 132/84 mmHg, the mean pressure trace can be linearly scaled so that it has maximum and minimum values of 132, 84 mmHg, respectively.

For locations other than the brachial artery, e.g. radial or carotid, no convenient auscultatory device is generally available. To calibrate pressures at these locations, a mean pressure and a scale factor are needed. Mean pressure is estimated to be the same at the brachial and radial arteries. For the scale factor, the nominal one specified by Millar can be used. Outputs from Millar tonometer is pre-amplied through the TCB-500 control box, which has an internal calibration circuit to provide an electrical zero as well

as 20 and 100 mmHg calibration signals. It is given that the pressure output signal from the control box is nominally 0.2V/100mmHg. This scale factor can be used for calibration.

However, this nominal scale factor is only applicable when the optimal applanation of the artery is achieved. Our clinical studies showed that when external force increases, the measured absolute pressure values will go up, while the pulse pressure ($P_{max} - P_{min}$) measured will go down, as shown in Figure 7. In this figure, during the measurements of radial pressure, the external force applied to hold the tonometer was increased three times. It can be seen that the absolute pressure value goes up and the pulse pressure goes down as the force is increased.
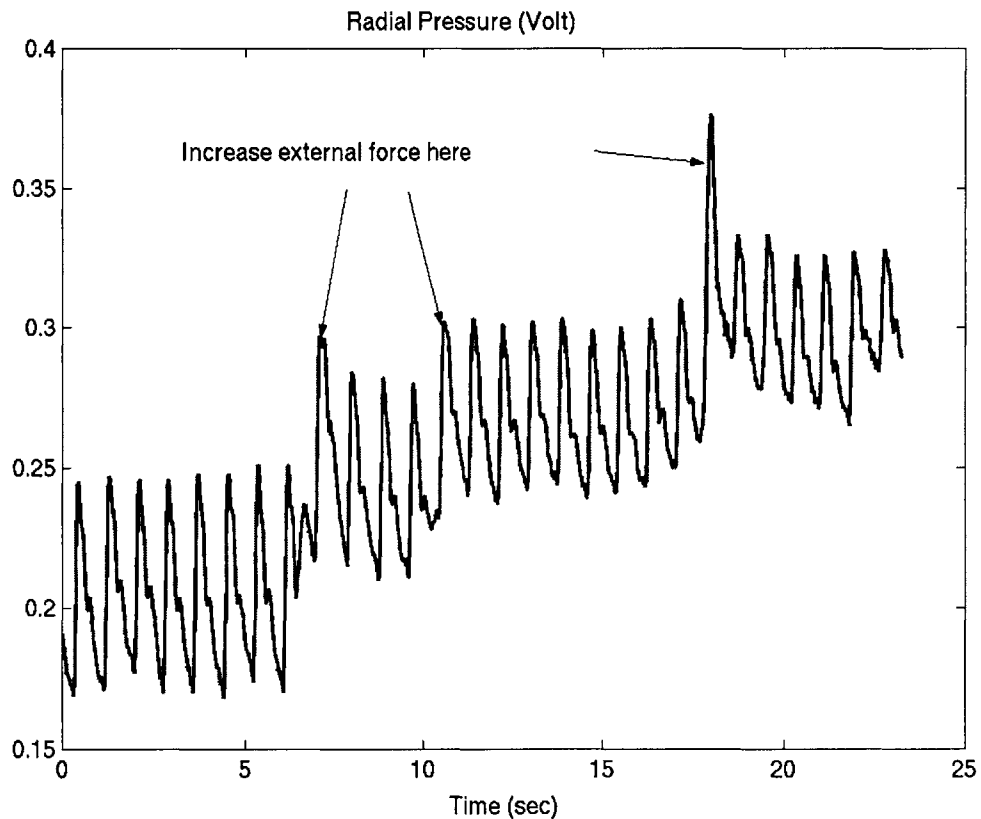

Figure 7 Effects of external force on pressure measurement

If the same scale factor is used for all cycles in figure 7, different pressure values will be resulted for cycles with different external forces applied. As discussed in

72

PRESSURE MEASUREMENT, optimal applanation should be the one that gives the largest amplitude pressure. The nominal scale factor can not be used when optimal applanation is not reached in measurement.

Another possible way to calculate the scale factor for locations other than the brachial artery is by assuming that the value of scale factor for brachial artery applies to all other locations, although it is different from the nominal one specified by the instrument. As an example, for the brachial measurement demonstrated in figure 6, the measured pulse pressure using ascultation is (132-84) = 48 mmHg. The "pulse voltage", as shown in the figure, is (0.36-0.28) = 0.08V approximately. Therefore, a scale factor of (0.08/48) * 100 = 0.167 V/100mmHg can be calculated, which is different from the nominal one and it can be inferred that excessive applanation was reached because of large external force. In our clinical study, the calculated scale factor for brachial pressure is usually less than 0.2 V/100mmHg and varies in the range of 0.05 to 0.2 V/100mmHg. There are two reasons that optimal applanation is difficult to achieve for the brachial artery. (1). Brachial artery lies deeper in the tissue than radial or femoral arteries where tonometry is usually used. (2). The presence of the biceps brachii muscle makes it difficult to be applanated against the humerus bone (as shown in figure 2, a bone is needed to support the applanated artery).

This assumption that the same scale factor for brachial artery can be applied to other arteries breaks down when different external forces are applied at different measurement locations. This is often the case since there is no sensor in the tonometer to measure external force and the operator can hardly ensure that the external forces applied on different arteries are consistent. In our clinical study, we found it necessary to apply higher forces on the brachial artery than on radial artery presumably because the brachial artery lies deeper in the tissue than radial. When the external force on the brachial artery is larger than that on other arteries, the scale factor calculated using brachial pressure data would be small. If a smaller factor is used to calibrate pressure, unrealistically high pulse pressures will be predicted.

To summarize, neither of these methods for determining the calibration can be applied reliably. The specified nominal scale factor of 0.2V/mmHg is only applicable when the applanation is correct and the external force is within a certain range, while the

calculated factor from brachial pressure data can be only applied to other locations when external forces are consistent. Therefore, to calibrate pressures at radial or carotid artery accurately, either optimal applanation or measurement of external force is required.

The technique for optimal applanation can only be gained through practice. Studies showed that after 4 to 6 weeks' use of the tomometer, intra-observer variability was 4.5% and inter-observer variability was 11.6% in measuring radial pulse waveforms in adult humans [4].

It is possible to improve the measurement accuracy by designing a micro-manipulator as presented by Kelly et al [4] to ensure accurate and consistent placement of the tonometer on arteries. Alternatively, a sensor and feedback system may be incorporated into the probe so that the applanation force that yields maximal pulse pressure can be automatically determined [5, 6].

At present, for most patient or volunteer cases presented in this paper, only the brachial measurements are being used to do parameter estimation because of inaccurate calibration of radial or carotid pressure. The brachial pressures were calibrated using the systolic and diastolic pressures measured by auscultatory method.

Velocity

1. General data processing

As mentioned before, velocity is measured by Doppler ultrasound. After the measurement, data processing is completed offline. First, FFT analysis is performed on the acoustic signal (frequency shift) stored in the computer. Then, after filtering noise, eliminating aliasing and late diastole discontinuity, equation (2) (repeated below) is used to calculate the desired velocity.

$$f_d = \frac{-2Vf_0\cos(\theta)}{c} \qquad (2)$$

The known variables are the emitted frequency, f_0, acoustic speed in tissue c (1540 m/sec) and angle θ. In our experiments, $f_0 = 5.5\text{MHz}$ and $\theta = 60°$. Hence, velocity can be calculated once f_d is known.

74

Figure 8 is an example of the original acoustic signal after FFT and Figure 9 is the corresponding velocity obtained from this signal after eliminating noise (note that there is aliasing in the frequency spectrum, which will be discussed in the next session).
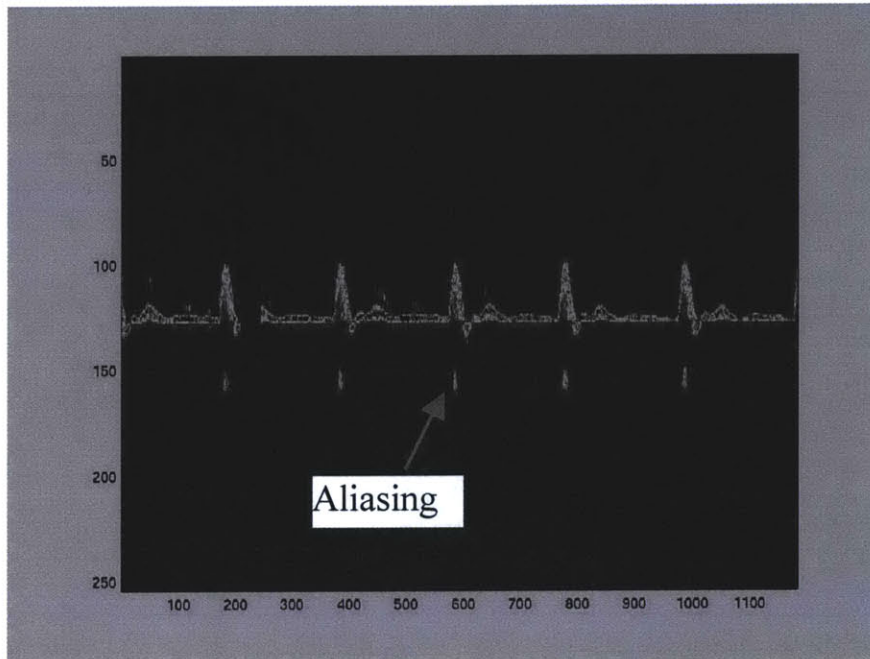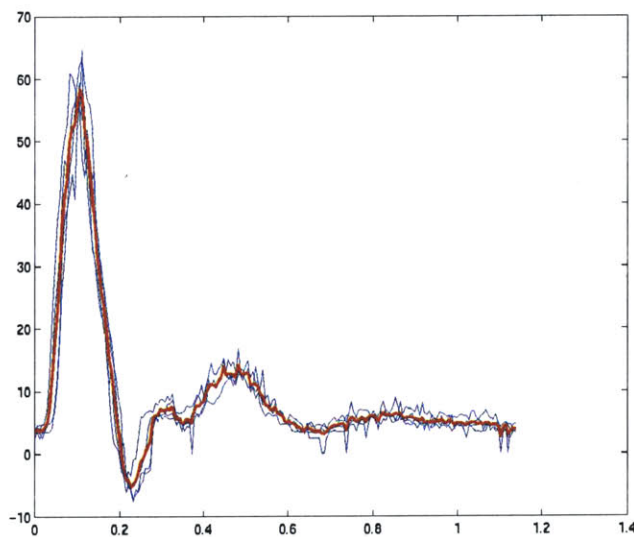

Figure 8 Frequency spectrum

Figure 9 Velocity profile (Red curve is the mean trace)

2. Noise elimination

Three methods are included in the program to correct for or remove noise from the velocity data: aliasing correction, wall artifact correction and late diastole correction.

(a). Correction for Aliasing

A problem that is peculiar to pulsed Doppler instruments is that of aliasing. The pulsed system inherently has a pulse repetition frequency (PRF) that determines how high a Doppler frequency the pulse system can detect; signals need to be sampled at least twice per cycle of their highest frequency component in order to unambiguously resolve that component. This means that the highest Doppler shift frequency that the pulsed Doppler instrument can measure is equal to half of the pulse repetition frequency of the instrument. The inability of a pulsed Doppler system to detect high-frequency Doppler shifts is known as "aliasing" [8]. If Doppler frequencies above this limit are present, they will be displayed as spurious frequencies equal to the Doppler shift minus the pulse repetition rate. They will appear within the limits of plus and minus half the pulse repetition frequency and changed in sign. Figure 8 shows an example of aliasing.

To eliminate aliasing, the program unwraps the data — the user indicates the region that has aliased and the velocities are corrected in the data array. Figure 10 is the counterpart of Figure 8 after correcting for aliasing.

(b) Wall artifacts correction

This procedure is designed to eliminate the velocity signal from the vessel wall that is of low-frequency, but can be prominent, especially in systole, and corrupt the measurements of blood velocity. The user identifies this region and the program can filter out low velocities, as illustrated in Figure 11.
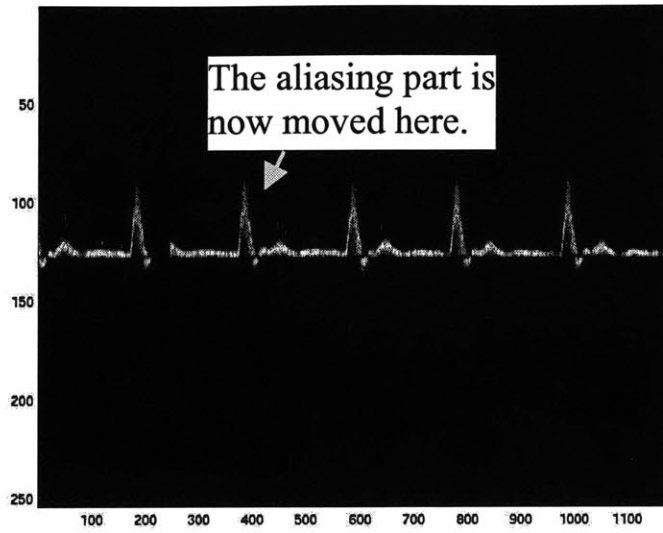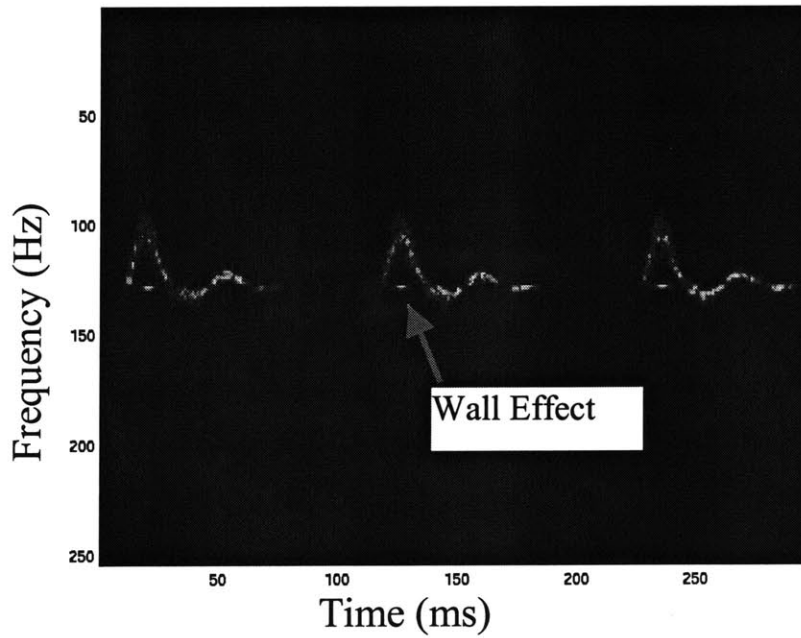
Figure 10 Corrected Aliasing

Figure 11: Wall velocity effect (Doppler frequency)

(c). Late diastole correction

In late diastole, since there is little flow, a weak and sporadic velocity waveform is often seen and the noise usually overwhelms desired velocity data. The program identifies the late diastole region and the data are set to zero so that other noise is eliminated.

The above three methods for noise reduction address the major obstacles to obtaining velocity by Doppler. There are however still some factors. For example, there is usually some background noise in the acoustic signal that is inevitable because the quality of the instrument is not perfect. Such noise can be easily eliminated by filtering out the low frequency components.

Measurement/Calculation of C_0 and L

As mentioned in chapter 1, to reduce the number of significant parameters, the method of non-dimensionalization was used. Three parameters were selected as basic variables to non-dimensionalize other parameters. They are aortic root wave speed C_0 at reference pressure 100 mmHg, characteristic length L (the length between distal ends of radial and brachial arteries) and blood density ρ. ρ is assumed to be constant and equal to 1.06 g/cm^3, while C_0 and L may vary from subject to subject and must be measured/calculated. Obviously, L can be measured directly using externally visible anatomical landmarks, but aortic root wave speed poses a more difficult problem.

To estimate C_0, measurements from which the mean wave speed between carotid and radial artery at normal arterial pressure can be calculated were first obtained. Since the patient is lying still and the time a set of measurements needs is not long (typically 30 minutes), one can assume that the patient's EKG doesn't change, so that it can be used as a timing tool. That is, both EKG and pressure traces are measured on the carotid and radial arteries. The time difference between EKG and the starting of systole on pressure trace can be measured from the curves for both the carotid and radial data. (In EKG, P wave represents depolarization of the atria and QRS complex represents depolarization of the ventricular muscle cells [10]. However, any point on EKG can be used as long as it is consistent for carotid and radial EKGs). Denoting this time difference as $\Delta t_{carotid}$ and

Δt_{radial} respectively, together with the difference between travel distance from the heart to carotid artery and that from the heart to radial artery, the mean wave speed (C_{mean}) traveling between these two artery can be calculated:

$$C_{mean} = (\Delta t_{radial} - \Delta t_{carotid})/ \Delta L_{carotid,radial} \qquad (3)$$

Figure 12 and Figure 13 are examples of the measured EKG and pressure at carotid and radial respectively. In the studies presented in this paper, a kind of "0-1" type EKG connector was used, which means that the measured EKG does not have the usual shape, but only zero (when EKG voltage is 0) or a non-zero constant (in the cases of figure 12 & 13, it is 0.55) (when voltage is not 0), which is adequate and convenient for our timing purpose.
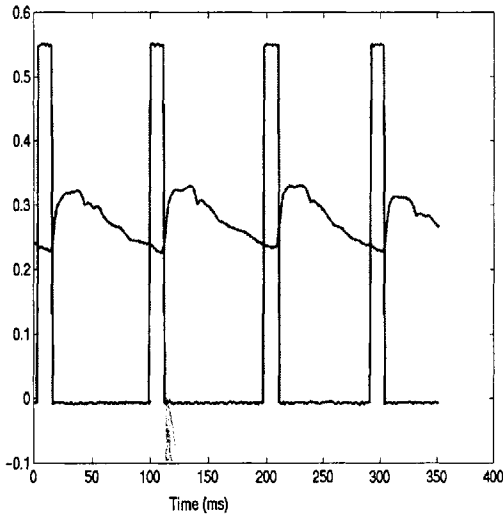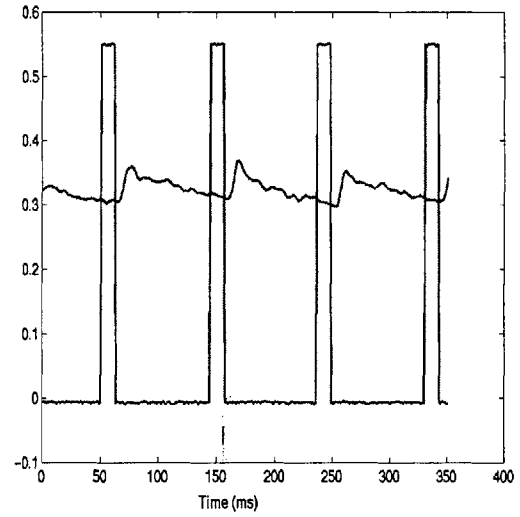

Figure 12 Carotid pressure and EKG   Figure 13 Radial pressure and EKG

From these figures, it can be seen that Δt_{radial} is larger than $\Delta t_{carotid}$.

After obtaining C_{mean}, a relationship of C_0 at aortic root $(P_{ref} = 100 \text{ mmHg})$ and C_{mean} must be used to calculate C_0. In the case of the model, this relationship could be determined precisely, based on the expressions used for the distribution of wave speed through the arterial network and the dependence of wave speed on transmural pressure in the computational model. However, in the application of this method to real subjects, the

relationship is unknown and is likely to vary from subject to subject. For this reason, an empirical approach was needed that was independent of the computational model. For library points generated from the computational model, C_o = constant = 462 cm/sec. Considering the fact that changes in wave speed are related to arterial pressure changes [11], a relationship of (C_{mean}/C_o) and (P/P_{ref}) may be found, where P can be the brachial/radial mean pressure, systole pressure or diastole pressure. This is an assumption that needs to be tested further.

Compared to other combinations, brachial diastolic pressure ($P_{dias,bra}/100$) and (C_{mean} / 462) for library points exhibit a nearly linear relationship. Figure 14 shows the distribution of 2351 library points on these two variables. Blue dots represent individual library points and the red curve is the 6-degree polynomial fit of the distribution. From this figure, we obtain the relationship of C_o and $P_{dias,bra}$ as the following:

$$Co = C_{mean} / (-2.4292 * (P_0)^6 + 10.5840 * (P_0)^5 - 17.5862 * (P_0)^4 + 13.8310 * (P_0)^3$$
$$- 4.9651 * (P_0)^2 + 1.2423 * (P_0)^1 + 0.5491)$$

$$(4)$$

Where P_0 represents ($P_{dias,bra}/100$).

To test this formula, it was used to calculate C_o of all the library points and compare the results to the known value 462cm/sec. Figure 15 plots the calculated C_o value of each point.
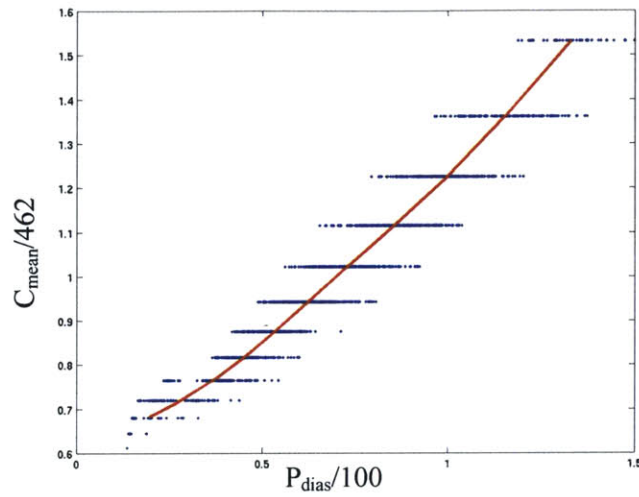
80

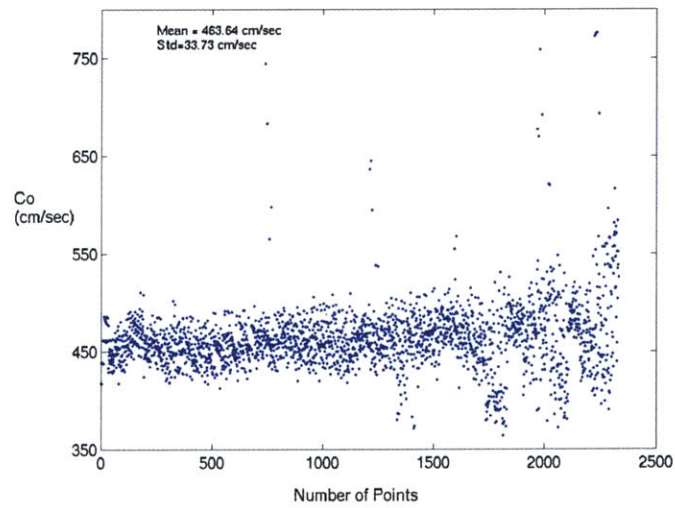Figure 14 Relationship of ($P_{dias,bra}/100$) and ($C_{mean} / 462$) for 2351 library points.

Figure 15 Calculated Co for library points.

(Mean value: 463.64cm/sec, Standard Deviation: 33.73cm/sec)

From figure 15, it can be seen that C_0 for most of the library points calculated in this way lie in the range 463.64 ± 33.73 cm/sec. This is acceptable for our purpose since the measurements of Δt and calculation of C_{mean} can have a relative error larger than this. However, if the measurements are improved in the future, this calculation of C_0 will take a more significant part in the errors of parameter estimation[*].

Measurement of V_{ED}, SVR and CO

For the purpose of evaluating the parameter estimation accuracy, V_{ED} was measured non-invasively using ultrasound in some subjects studied. Estimations with V_{ED} as a known variable can be done additionally. It represents another potential piece of information that can be used to refine the parameter estimation procedure.

C.O. and SVR for catheterized patients were recorded to compare with estimated values. For the patients in this study, cardiac outputs were measured using the Fick method, which uses arterial and mixed venous saturations to determine oxygen extraction, under an assumed basal metabolic rate of 125 $mlO_2/min/m^2$. SVR is a calculated value using the equation:

$$SVR = (P_{MA} - P_{RA})/C.O. \qquad (4)$$

Where P_{MA} is Mean Arterial Pressure, P_{RA} is Right Atrial Pressure, both of which are measured by indwelling catheters, and C.O. is Cardiac Output.

Feature Selection for Measured Data

Feature selection discussed in previous chapters pertains to model-generated pressure and velocity profiles. If the model were perfect, those discussions would apply to measured data as well. However, due to numerous simplifying assumptions made in the course of model development, and in the inaccuracies noted above in the measurement techniques and/or data processing, the model-based evaluation of parameter

---

[*] The relatively small number of points that lie far from the mean were likely cases for which the program incorrectly identified the start of systole.

82

estimation performance may not be directly applicable to real measurements. In particular, the feature sets found to have the lowest parameter estimation errors for model-generated data may not be optimal when applied to real subject data. Therefore, different feature sets are considered for each set of measurement to compare their performance.

In the following, 12 sets of measured data will be presented, and the parameter estimation results are presented using feature set 1 (P_{mean}/V_{mean} $(dp/dt)_{max}$ P_{mean} deltaP) (if both pressure and velocity were measured) and feature set 2 ($(dp/dt)_{max}$ P_{mean} deltaP P_{max}) (pressure only). Details will be presented in RESULTS and DISCUSSION.

Results

Measurements were obtained on 12 adult subjects (3 patients, 9 volunteers). Table 2 lists the available data of all the subjects for reference. Parameter estimations used brachial artery pressure and/or velocity. Because of the problem in calibration of radial pressure mentioned before, it is not recommended to use radial data to do parameter estimation. Velocity profiles are not provided for all subjects since some of the original Doppler data are of poor quality and did not give realistic velocities.

Table 2 Subject data

Patient	Height (cm)	Weight (lb)	Sex	Age	Health Status
#281	180	160	M	32	Healthy
#512	183	188	M	37	Healthy
#y11	168	125	F	29	Healthy
#h11	183	185	M	39	Healthy
#471	183	250	M	36	Healthy
#472	178	138	M	33	Healthy
#h22	158	110	F	24	Healthy
#4201	183	187	M	38	Healthy
#sa418	N/A	110	M	56	Heart failure patient
#mc417	N/A	N/A	M	60	Heart failure patient
#671	190.5	110	M	30	Heart failure patient
#730	170	180	M	42	Healthy

Tables 3 through 38 contain subject information and parameter values estimated using both feature sets 1 and 2. The objective function in these tables is the one to be minimized in parameter estimation routine. It is defined as:

$$\sqrt{\sum_{i=1}^{n}(1-\frac{f_e}{f_m})^2} \tag{5}$$

Where n is the number of features used in estimation, f_e is the estimated feature value, and f_m is the measured feature value.

For all 12 cases below, objective functions obtained from estimations using feature set 1 are much larger than those from using feature set 2. The significance of objective function will be mentioned in DISCUSSION. Reconstruction was done for each parameter estimation using feature set 2, and the reconstructed P, V curves are drawn to compare with the measured ones (Figures 16 through 29). Cardiac Output (C.O.) and Stroke Volume (S.V.) values (calculated from reconstruction) are also listed.

Note that the values listed in Tables 31 for subject 671 is the mean value based on 3 measurements right after the pressure and velocity measurements were finished. The original values are 227, 281, 283 ml. For subject 730, only one measure was performed, the value was 192ml, as listed in table 35.

Table 3 Measured data of male subject 281

(Healthy volunteer)

Height (cm)	Weight (Pound)	Char. Length (cm)*	BP (mmHg)
180	160	27	108/66
HR (/min)	Wave Speed (cm/sec)	Young's Modulus (dyn/cm^2)	V_{ED} (ml)
57.44	440.05	3.63×10^6	N/A

*Char. Length is the length between measurement location on brachial and radial arteries, usually it is the distance of the distal points.

Table 4 Estimated and calculated parameters of subject 281

(Feature Set 2: (dp/dt)$_{max}$ P$_{mean}$ deltaP P$_{max}$)

Objective function = 0.0039

E_{LV} (dyn/cm^5)	V_{ED} (ml)	SVR (dyn/cm^5.sec)	C.O. (l/min)	S.V. (ml)
5081.76	156.85	1162.85	5.49	77.26

Table 5 Estimated and calculated parameters of subject 281

(Feature Set 1: P$_{mean}$/V$_{mean}$ (dp/dt)$_{max}$ P$_{mean}$ deltaP)

Objective function = 0.3707

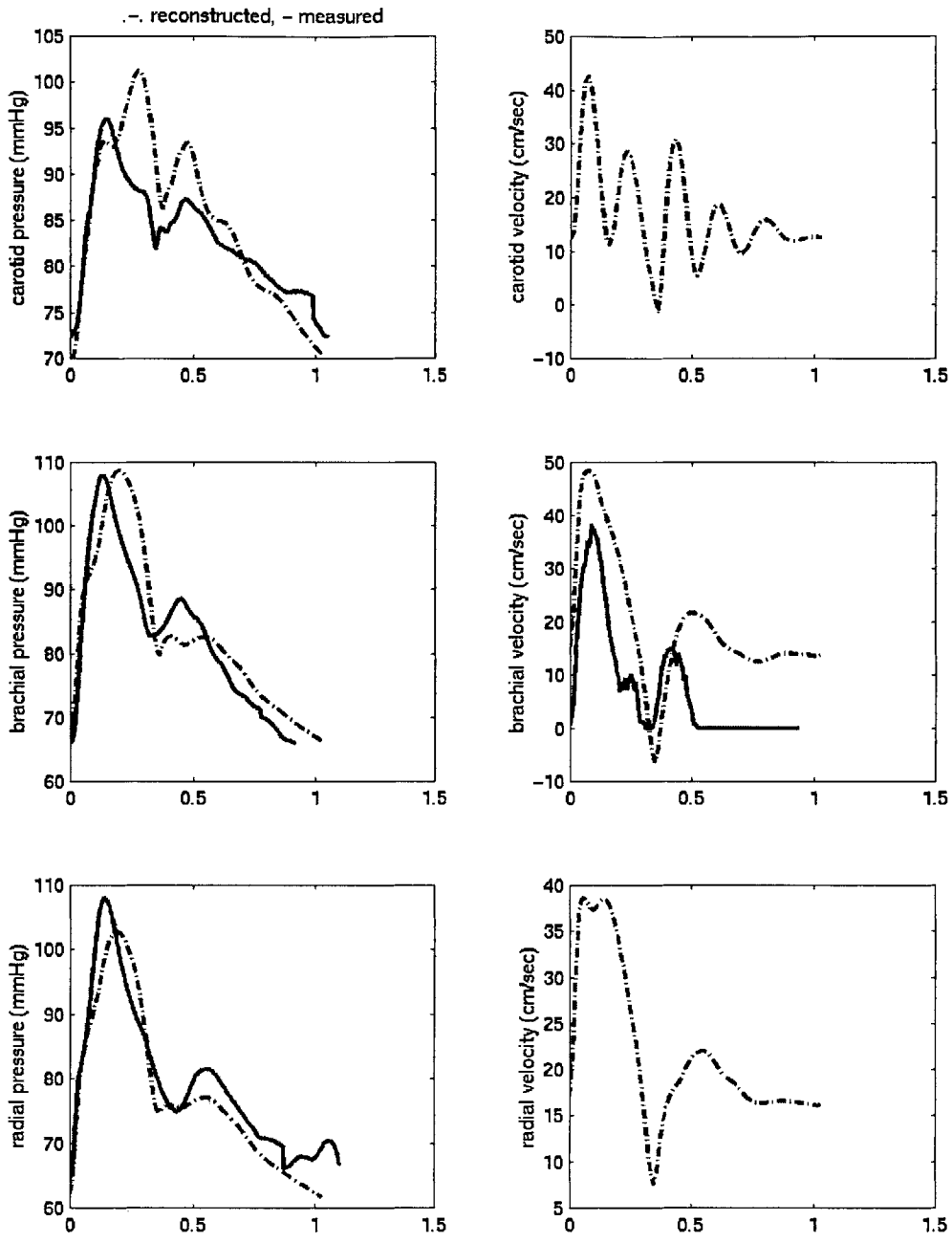| E_{LV} (dyn/cm^5)	V_{ED} (ml)	SVR (dyn/cm^5.sec)	C.O. (l/min)	S.V. (ml)
8304.15	104.52	2313.29	N/A	N/A

Figure 16 Reconstruction of subject 281

Table 6 Measured data of male subject 512

(Healthy volunteer)

Height (cm)	Weight (Pound)	Char. Length (cm)	BP (mmHg)
183	188	30	132/82
HR (/min)	Wave Speed (cm/sec)	Young's Modulus (dyn/cm^2)	V_{ED} (ml)
56.7	490	4.5×10^6	N/A

Table 7 Estimated and calculated parameters of subject 512

(Feature Set 2: $(dp/dt)_{max}$ P_{mean} deltaP P_{max})

Objective function = 0.0087

E_{LV} (dyn/cm^5)	V_{ED} (ml)	SVR (dyn/cm^5.sec)	C.O. (l/min)	S.V. (ml)
3752.66	222.36	1117.5	7.06	101.3

Table 8 Estimated and calculated parameters of subject 512

(Feature Set 1: P_{mean}/V_{mean} $(dp/dt)_{max}$ P_{mean} deltaP)

Objective function = 0.4184

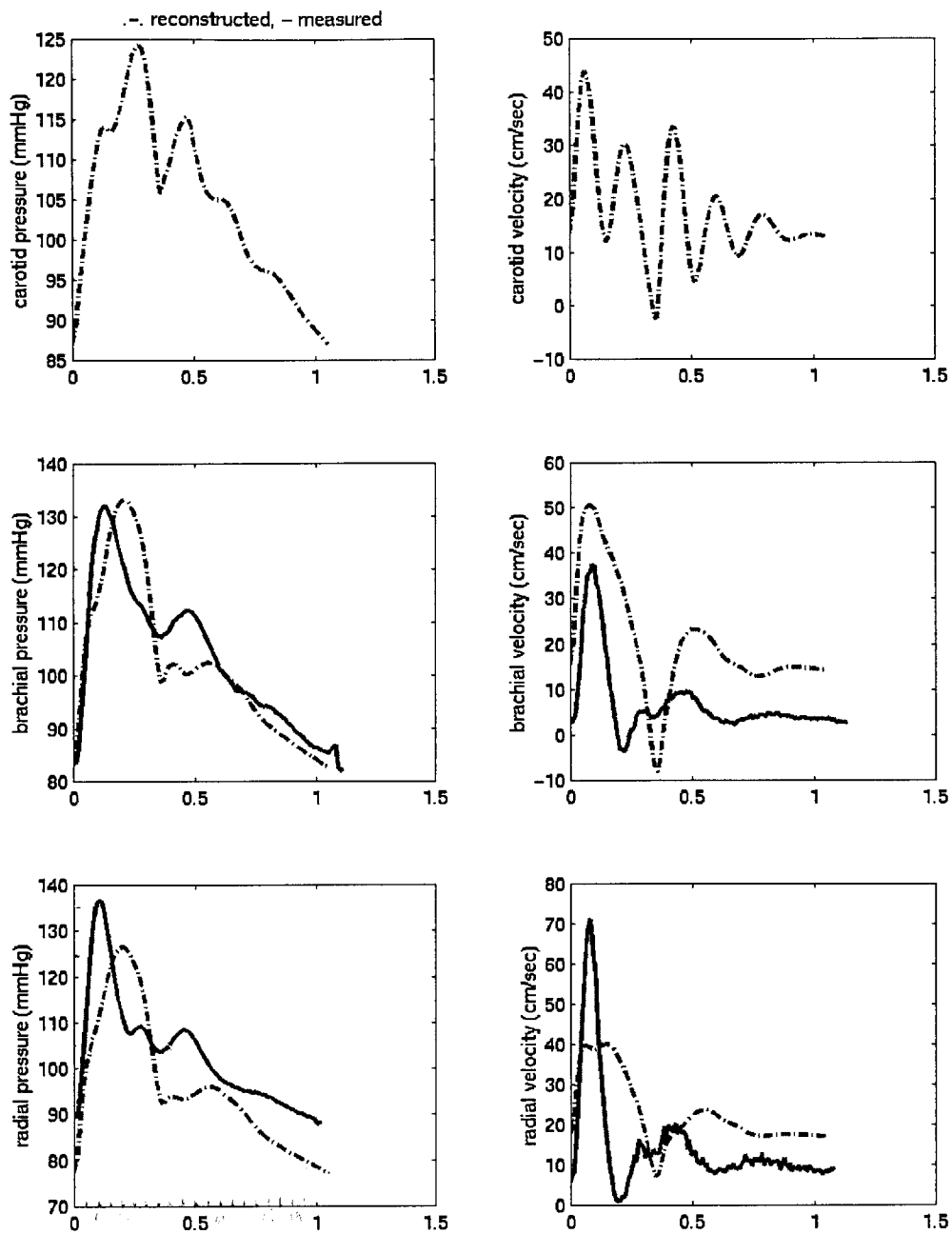| E_{LV} (dyn/cm^5)	V_{ED} (ml)	SVR (dyn/cm^5.sec)	C.O. (l/min)	S.V. (ml)
7504.12	139.35	2162.77	N/A	N/A

Figure 17 Reconstruction of subject 512

Table 9 Measured data of female subject y11

(Healthy volunteer)

Height (cm)	Weight (Pound)	Char. Length (cm)	BP (mmHg)
168	125	27	104/76
HR (/min)	Wave Speed (cm/sec)	Young's Modulus (dyn/cm^2)	V_{ED} (ml)
63.8	510.6	4.89×10^6	N/A

Table 10 Estimated and calculated parameters of subject y11

(Feature Set 2: $(dp/dt)_{max}$ P_{mean} deltaP P_{max})

Objective function = 0.1217

E_{LV} (dyn/cm^5)	V_{ED} (ml)	SVR $(dyn/cm^5.sec)$	C.O. (l/min)	S.V. (ml)
6723.09	76.47	2812.19	2.19	34.68

Table 11 Estimated and calculated parameters of subject y11

(Feature Set 1: P_{mean}/V_{mean} $(dp/dt)_{max}$ P_{mean} deltaP)

Objective function = 0.2471

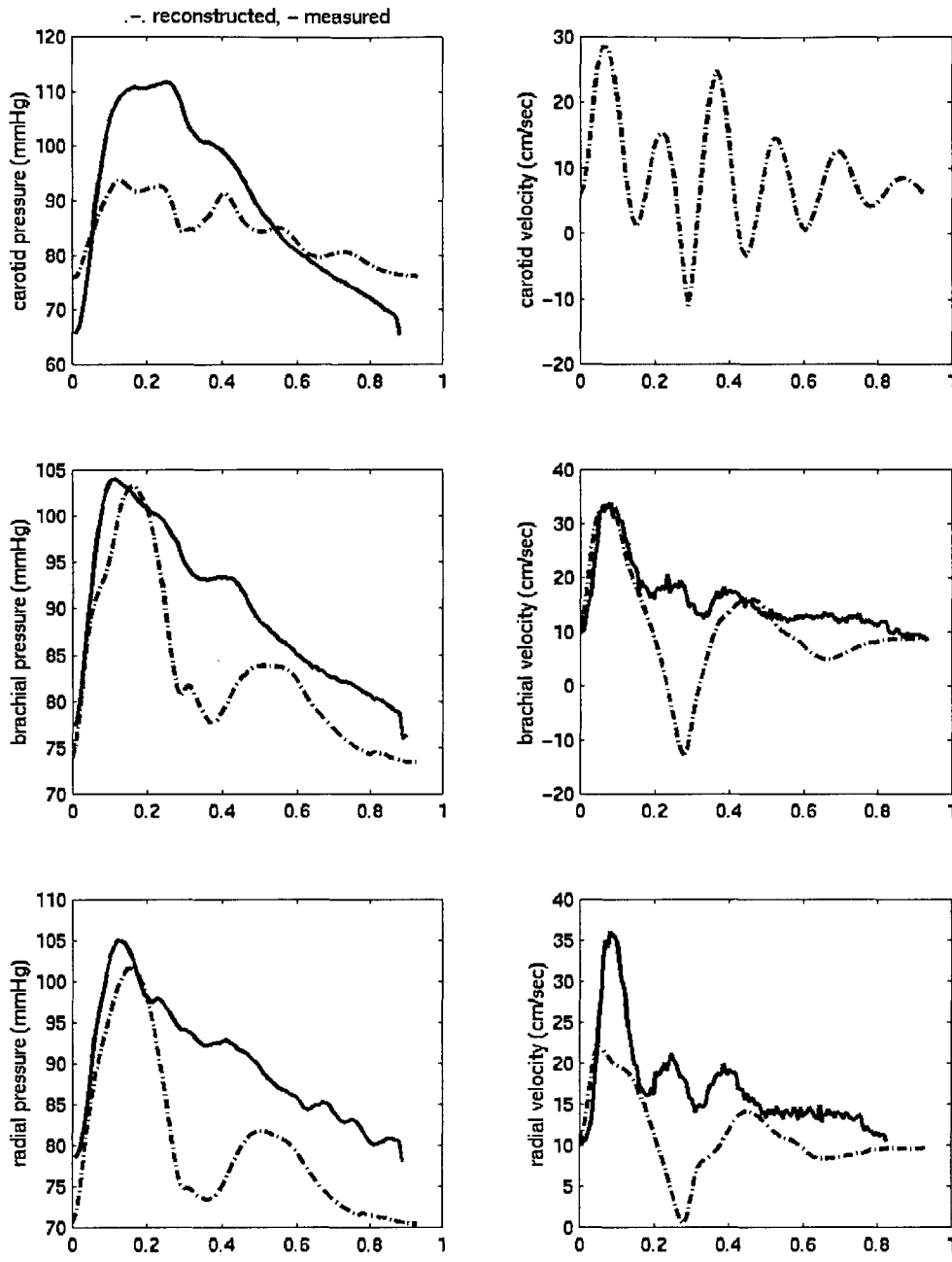| E_{LV} (dyn/cm^5)	V_{ED} (ml)	SVR $(dyn/cm^5.sec)$	C.O. (l/min)	S.V. (ml)
5360.89	83.4	2260.6	N/A	N/A

Figure 18 Reconstruction of subject y11

Table 12 Measured data of male subject h11

(Healthy volunteer)

Height (cm)	Weight (Pound)	Char. Length (cm)	BP (mmHg)
183	185	27	124/82
HR (/min)	Wave Speed (cm/sec)	Young's Modulus (dyn/cm^2)	V_{ED} (ml)
77.0	586.7	6.45×10^6	N/A

Table 13 Estimated and calculated parameters of subject h11

(Feature Set 2: $(dp/dt)_{max}$ P_{mean} deltaP P_{max})

Objective function = 0.0305

E_{LV} (dyn/cm^5)	V_{ED} (ml)	SVR $(dyn/cm^5.sec)$	C.O. (l/min)	S.V. (ml)
5411.1	107.63	2030.91	3.60	50.22

(Brachial velocity is not available for this subject, so parameter estimations using feature set 1 couldn't be performed.)
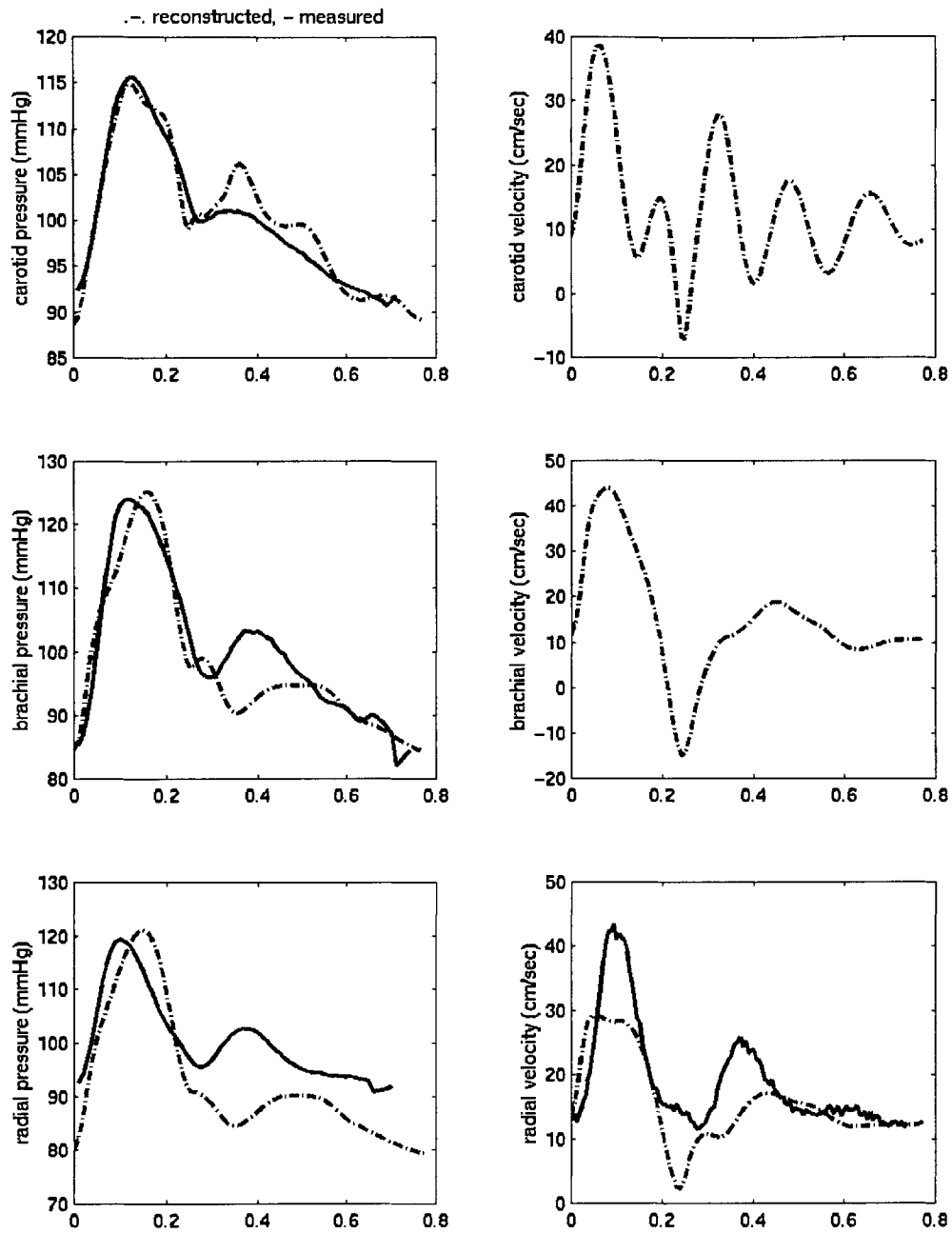
Figure 19 Reconstruction of subject h11

92

Table 14 Measured data of male subject 471

(Healthy volunteer)

Height (cm)	Weight (Pound)	Char. Length (cm)	BP (mmHg)
183	250	28	126/72
HR (/min)	Wave Speed (cm/sec)	Young's Modulus (dyn/cm^2)	V_{ED} (ml)
62	592	6.57×10^6	N/A

Table 15 Estimated and calculated parameters of subject 471

(Feature Set 2: $(dp/dt)_{max}$ P_{mean} deltaP P_{max})

Objective function = 0.0330

E_{LV} (dyn/cm^5)	V_{ED} (ml)	SVR $(dyn/cm^5.sec)$	C.O. (l/min)	S.V. (ml)
3899.0	166.38	1228.0	5.46	87.85

Table 16 Estimated and calculated parameters of subject 471

(Feature Set 1: P_{mean}/V_{mean} $(dp/dt)_{max}$ P_{mean} deltaP)

Objective function = 0.3298

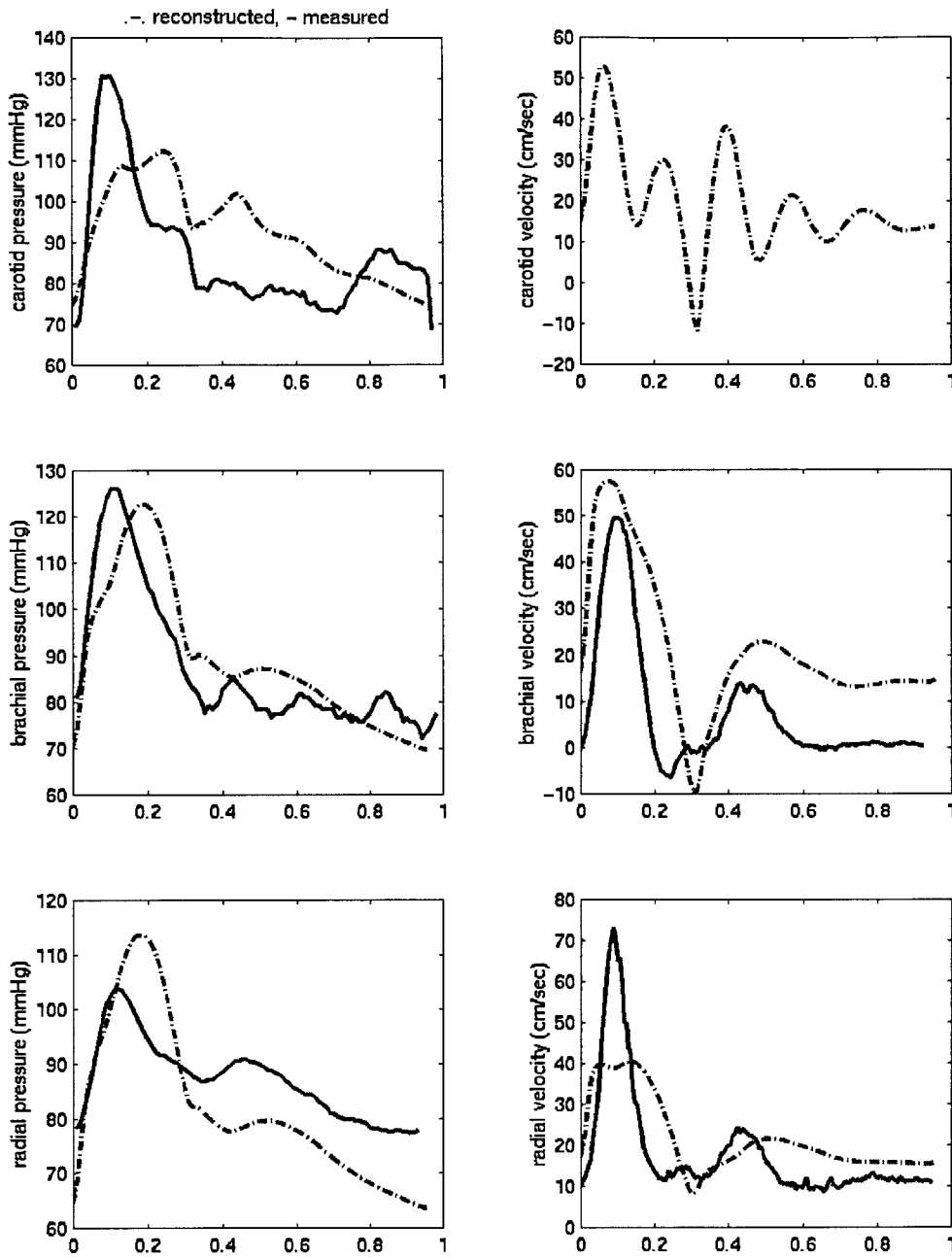| E_{LV} (dyn/cm^5)	V_{ED} (ml)	SVR $(dyn/cm^5.sec)$	C.O. (l/min)	S.V. (ml)
10714.2	87.78	2813.41	N/A	N/A

Figure 20 Reconstruction of subject 471

Table 17 Measured data of male subject 472

(Healthy volunteer)

Height (cm)	Weight (Pound)	Char. Length (cm)	BP (mmHg)
178	138	25	122/72
HR (/min)	Wave Speed (cm/sec)	Young's Modulus (dyn/cm^2)	V_{ED} (ml)
80	473	4.19×10^6	N/A

Table 18 Estimated and calculated parameters of subject 472

(Feature Set 2: $(dp/dt)_{max}$ P_{mean} deltaP P_{max})

Objective function = 0.0490

E_{LV} (dyn/cm^5)	V_{ED} (ml)	SVR $(dyn/cm^5.sec)$	C.O. (l/min)	S.V. (ml)
3012.8	205.9	1297.4	5.65	70.38

Table 19 Estimated and calculated parameters of subject 472

(Feature Set 1: P_{mean}/V_{mean} $(dp/dt)_{max}$ P_{mean} deltaP)

Objective function = 0.3175

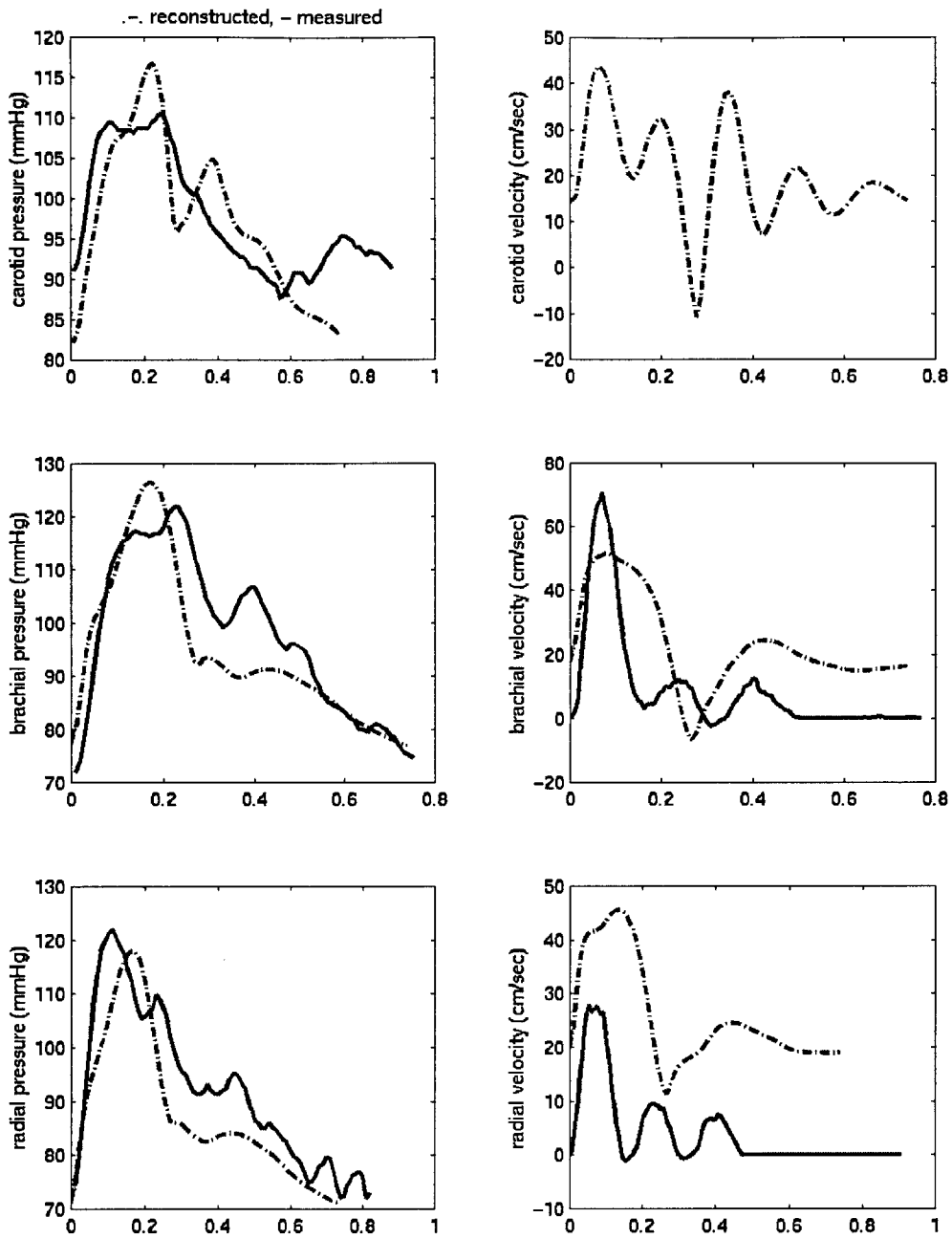| E_{LV} (dyn/cm^5)	V_{ED} (ml)	SVR $(dyn/cm^5.sec)$	C.O. (l/min)	S.V. (ml)
11966.4	72.81	2991.65	N/A	N/A

Figure 21 Reconstruction of subject 472

Table 20 Measured data of female subject h22

(Healthy volunteer)

Height (cm)	Weight (Pound)	Char. Length (cm)	BP (mmHg)
158	110	22.5	116/78
HR (/min)	Wave Speed (cm/sec)	Young's Modulus (dyn/cm^2)	V_{ED} (ml)
62	497	4.63×10^6	N/A

Table 21 Estimated and calculated parameters of subject 472

(Feature Set 2: (dp/dt)$_{max}$ P$_{mean}$ deltaP P$_{max}$)

Objective function = 0.0055

E_{LV} (dyn/cm^5)	V_{ED} (ml)	SVR (dyn/cm^5.sec)	C.O. (l/min)	S.V. (ml)
7436.0	78.3	2929.9	2.47	39.86

(Brachial velocity is not available for this subject, so parameter estimations using feature set 1 couldn't be performed.)
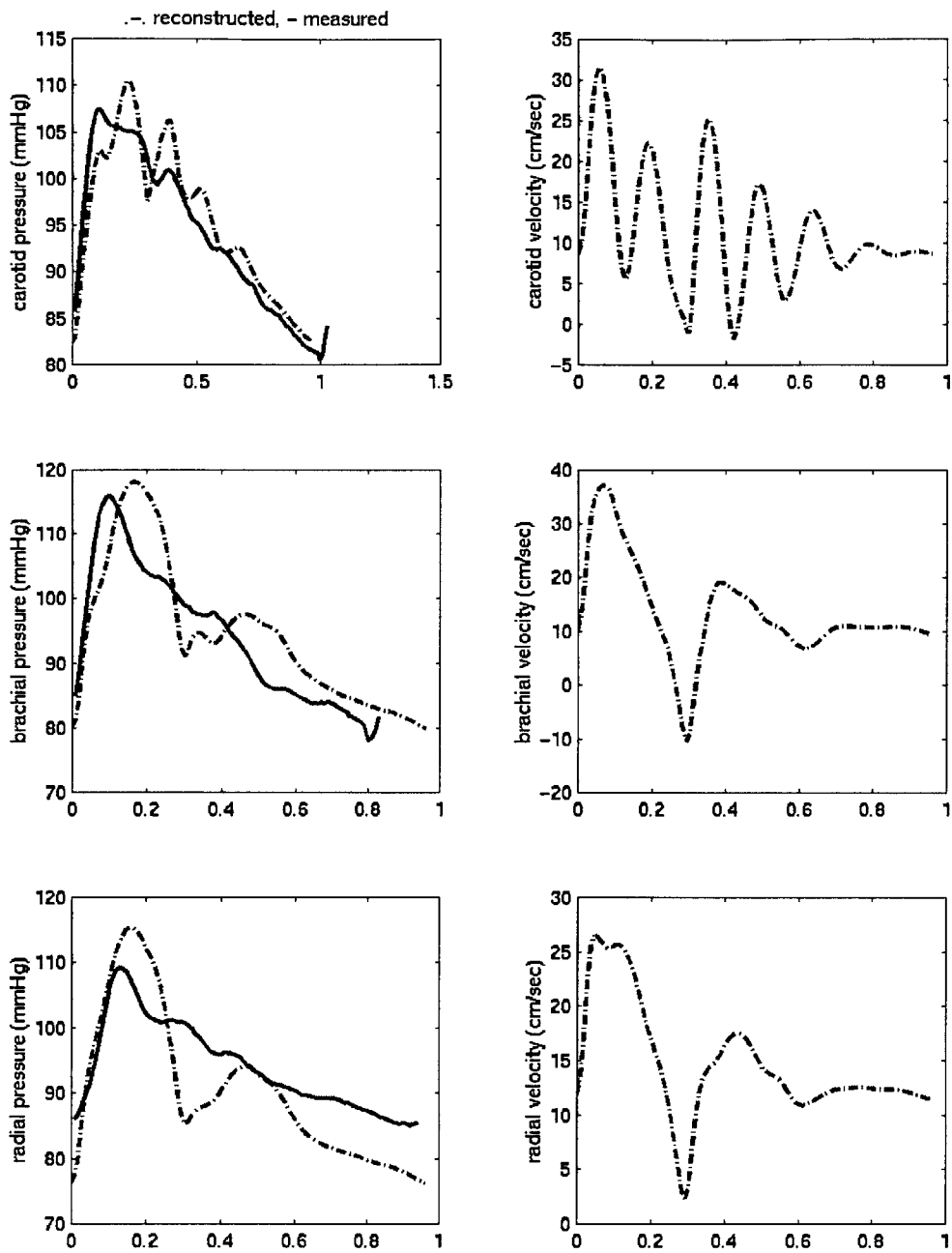
Figure 22 Reconstruction of subject h22

Table 22 Measured data of male subject 4201

(Healthy volunteer)

Height (cm)	Weight (Pound)	Char. Length (cm)	BP (mmHg)
183	187	33	132/84
HR (/min)	Wave Speed (cm/sec)	Young's Modulus (dyn/cm^2)	V_{ED} (ml)
61	590	6.52×10^6	N/A

Table 23 Estimated and calculated parameters of subject 4201

(Feature Set 2: $(dp/dt)_{max}$ P_{mean} deltaP P_{max})

Objective function = 0.0115

E_{LV} (dyn/cm^5)	V_{ED} (ml)	SVR $(dyn/cm^5.sec)$	C.O. (l/min)	S.V. (ml)
3455.5	209.1	1181.6	6.44	105.55

Table 24 Estimated and calculated parameters of subject 4201

(Feature Set 1: P_{mean}/V_{mean} $(dp/dt)_{max}$ P_{mean} deltaP)

Objective function = 0.5559

E_{LV} (dyn/cm^5)	V_{ED} (ml)	SVR $(dyn/cm^5.sec)$	C.O. (l/min)	S.V. (ml)
6150.13	146.27	2151.5	N/A	N/A
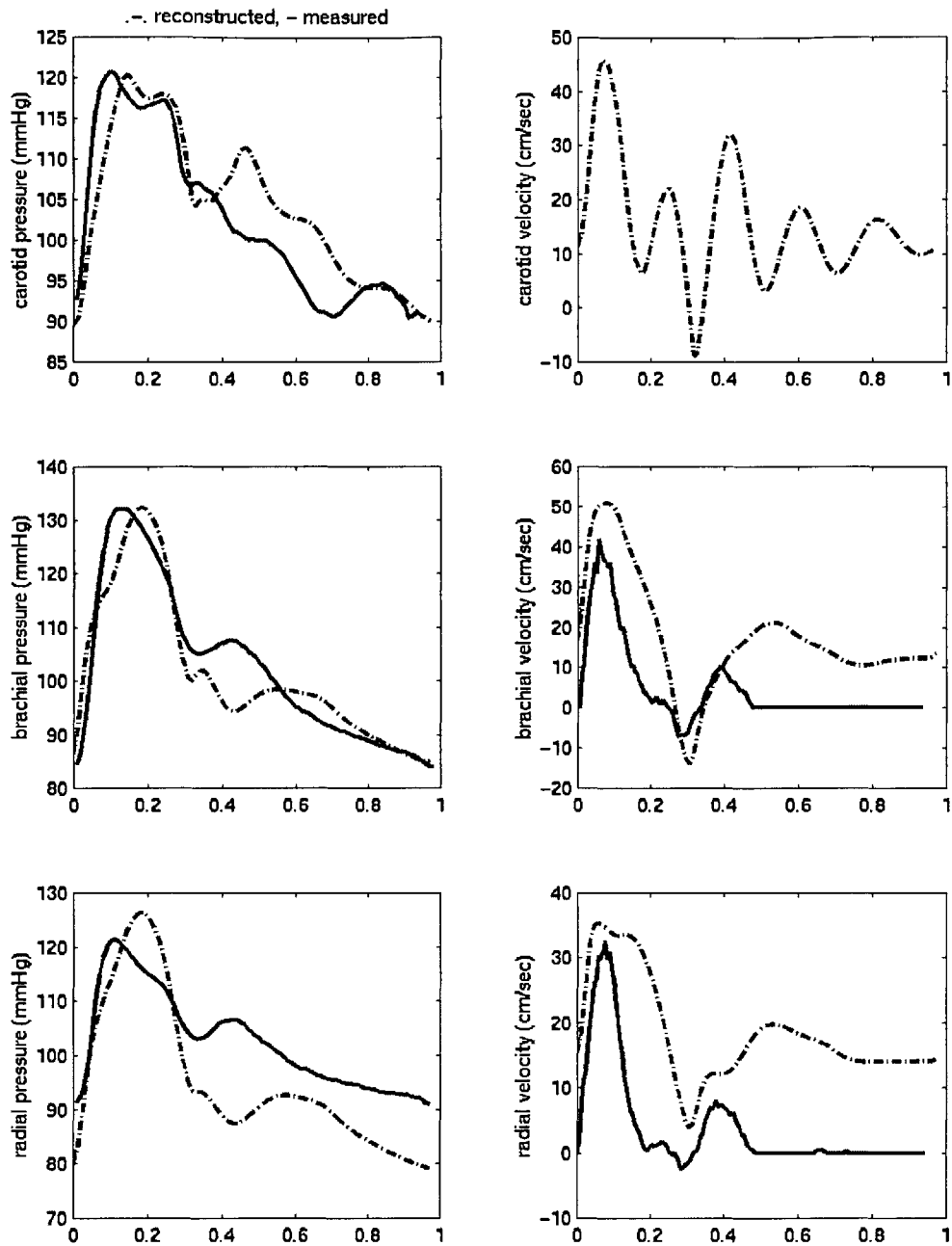
Figure 23 Reconstruction of subject 4201

100

Table 25 Measured data of male subject sa418 (56 yo)

(Heart failure patient)

Height (cm)	Weight (Pound)	Char. Length (cm)	BP (mmHg)
N/A	110	27	92/65
HR (/min)	Wave Speed (cm/sec)	Young's Modulus (dyn/cm^2)	V_{ED} (ml)
76	443	3.68×10^6	N/A

Table 26 Estimated and calculated parameters of subject sa418

(Feature Set 2: (dp/dt)$_{max}$ P$_{mean}$ deltaP P$_{max}$)

Objective function = 0.0600

E_{LV} (dyn/cm^5)	V_{ED} (ml)	SVR (dyn/cm^5.sec)	C.O. (l/min)	S.V. (ml)
943.1	255.0	2134.3	2.55	36.62

(Brachial velocity is not available for this subject, so parameter estimations using feature set 1 couldn't be performed.)

Table 27 Measured hemo-data of subject sa418

	C.O. (l/min)	SVR (dyn/cm^5.sec)
12:30PM	4.4	1096
4:00PM	2.4	1975
8:30PM	3.4	1349

(The pressure and velocity measurement was taken at ~2.30PM)
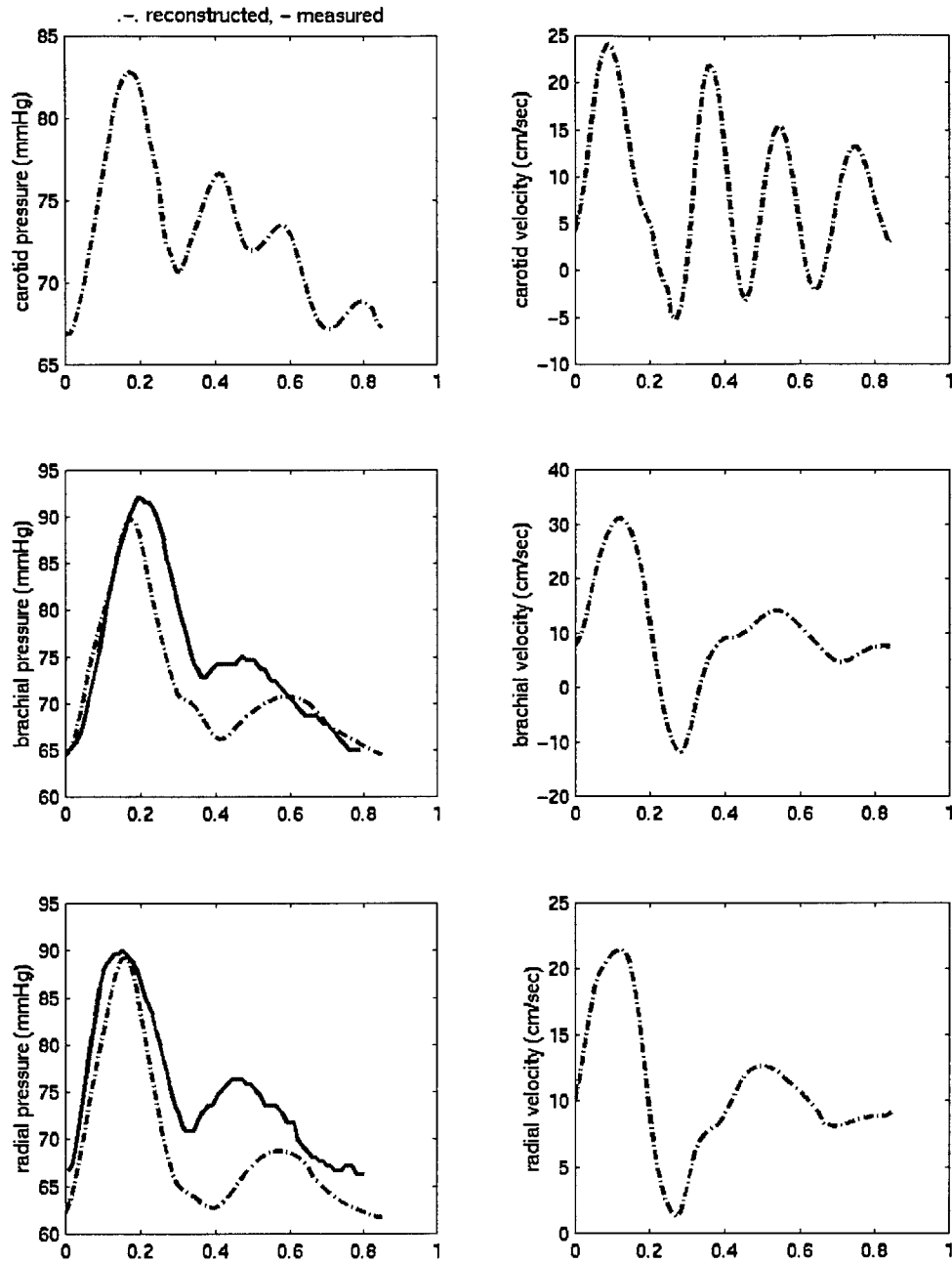
Figure 24 Reconstruction of subject sa418

Table 28 Measured data of male subject mc417 (60 yo)

(Heart failure patient)

Height (cm)	Weight (Pound)	Char. Length (cm)	BP (mmHg)
N/A	N//A	25	99/64
HR (/min)	Wave Speed (cm/sec)	Young's Modulus (dyn/cm^2)	V$_{ED}$ (ml)
69.4	403	3.04×10^6	N/A

Table 29 Estimated and calculated parameters of subject mc417

(Feature Set 2: (dp/dt)$_{max}$ P$_{mean}$ deltaP P$_{max}$)

Objective function = 0.0092

E$_{LV}$ (dyn/cm^5)	V$_{ED}$ (ml)	SVR (dyn/cm^5.sec)	C.O. (l/min)	S.V. (ml)
3267.9	150.9	1417.3	4.23	60.92

(Brachial velocity is not available for this subject, so parameter estimations using feature set 1 couldn't be performed.)

Table 30 Measured hemo-data of subject mc417

	C.O. (l/min)	SVR (dyn/cm^5.sec)
12:30PM	4.2	1104
7:00PM	3.7	1219

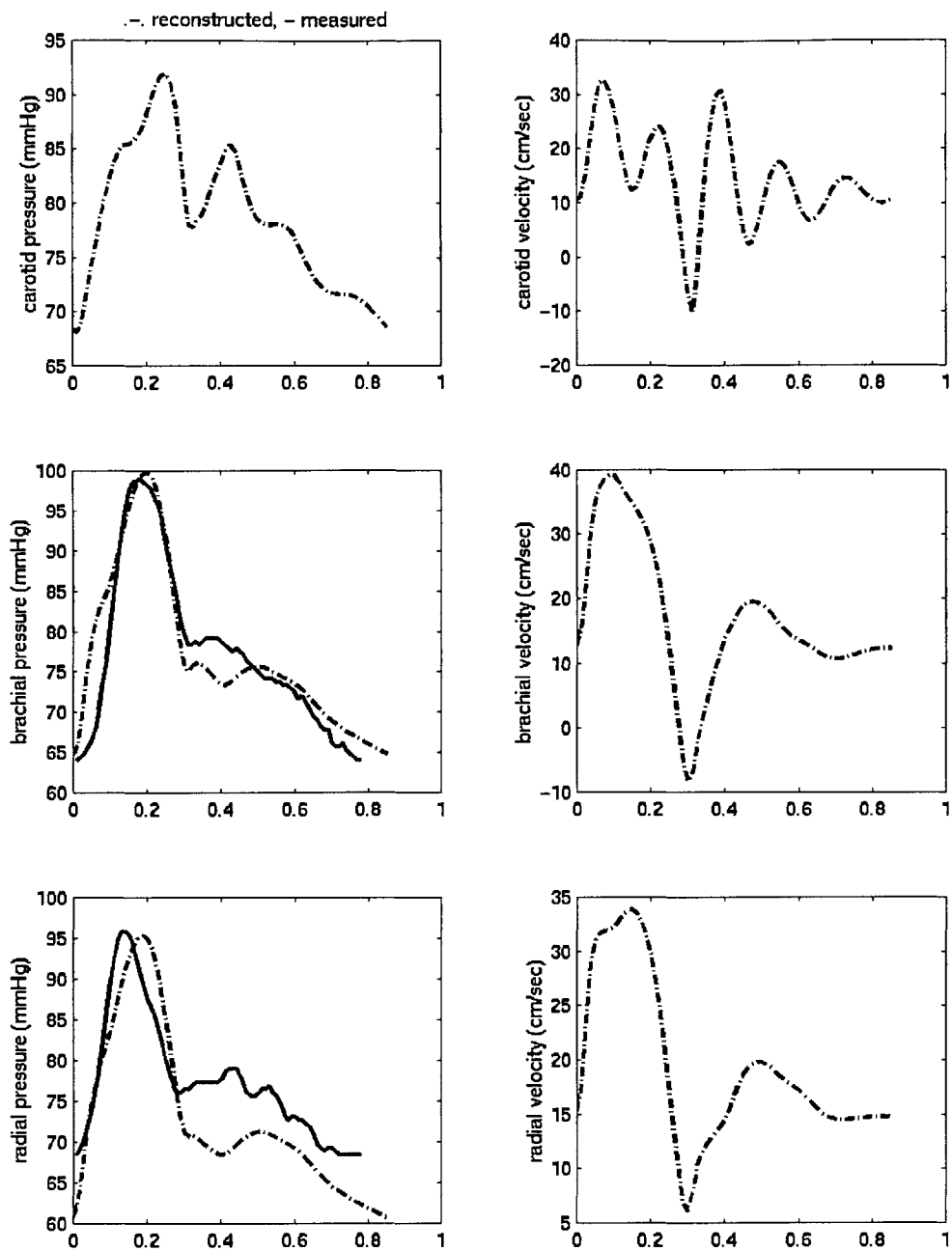(The pressure and velocity measurement was taken at ~2.30PM)

Figure 25 Reconstruction of subject mc417

Table 31 Measured data of male subject 671

(Heart failure patient)

Height (cm)	Weight (Pound)	Char. Length (cm)	BP (mmHg)
190.5	110	28	102/74
HR (/min)	Wave Speed (cm/sec)	Young's Modulus (dyn/cm^2)	V_{ED} (ml)
101	472.54	4.1846×10^6	254

Table 32 Estimated and calculated parameters of subject 671

(Feature Set 2: $(dp/dt)_{max}$ P_{mean} deltaP P_{max})

Objective function = 0.0318

E_{LV} (dyn/cm^5)	V_{ED} (ml)	SVR $(dyn/cm^5.sec)$	C.O. (l/min)	S.V. (ml)
1024.6	323.7	1520.8	4.16	41.06

Table 33 Estimated and calculated parameters of subject 671

(Feature Set 1: P_{mean}/V_{mean} $(dp/dt)_{max}$ P_{mean} deltaP)

Objective function = 0.6339

E_{LV} (dyn/cm^5)	V_{ED} (ml)	SVR $(dyn/cm^5.sec)$	C.O. (l/min)	S.V. (ml)
2334.3	166.98	2394.25	N/A	N/A

Figure 26 Reconstruction of subject 671

106

Table 34 Estimated and calculated parameters of subject 671

(Feature Set 3: $(dp/dt)_{max}$ P_{mean} deltaP)

(V_{ED} as known)

Objective function = 0.0318

E_{LV} (dyn/cm^5)	V_{ED} (ml)	SVR (dyn/cm^5.sec)	C.O. (l/min)	S.V. (ml)
1371.5	254.0	1537.9	4.13	40.8
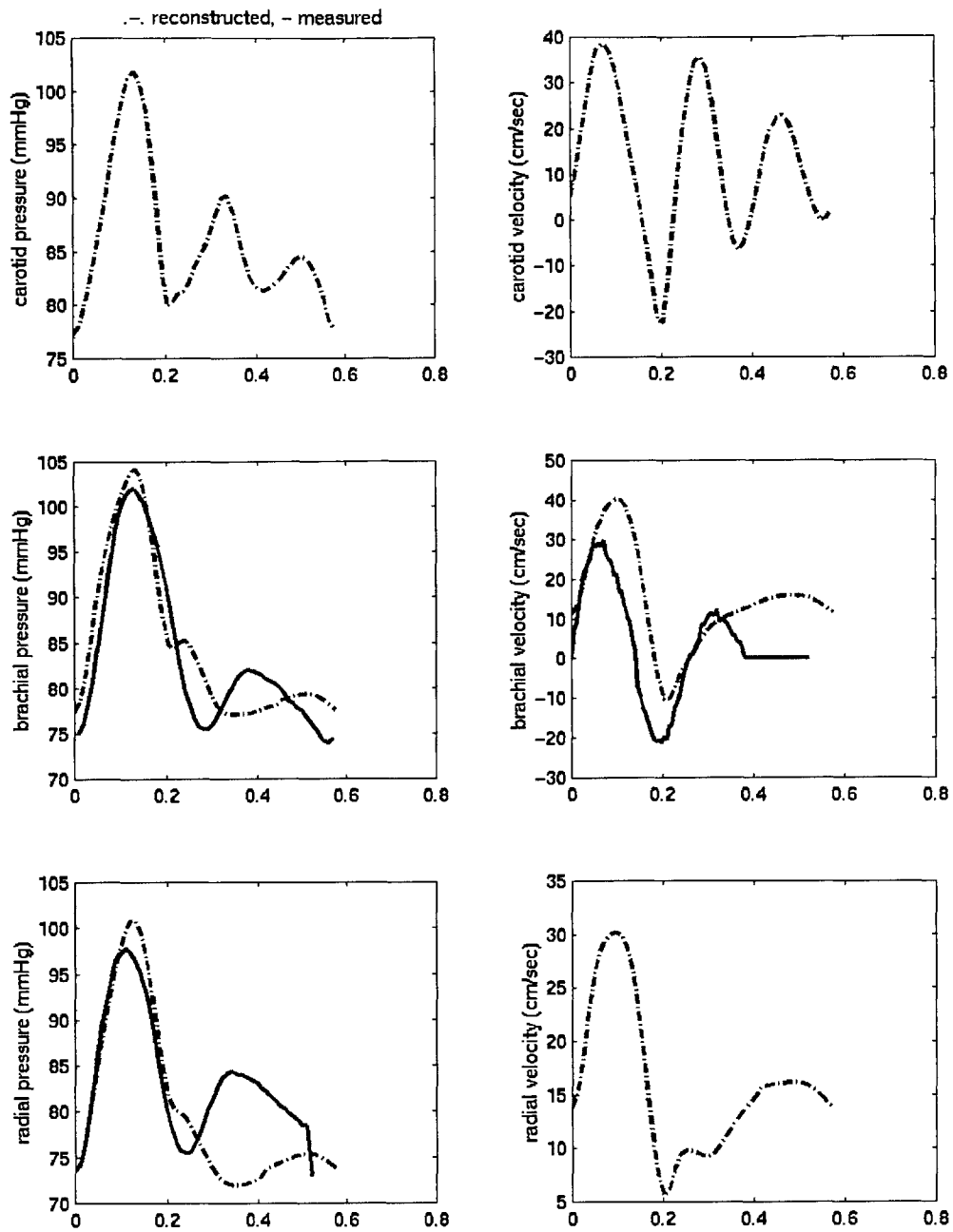
Figure 27 Reconstruction of subject 671

(V_{ED} as known)

108

Table 35 Measured data of male subject 730

(Healthy volunteer)

Height (cm)	Weight (Pound)	Char. Length (cm)	BP (mmHg)
156	180	27	118/72
HR (/min)	Wave Speed (cm/sec)	Young's Modulus (dyn/cm^2)	V_{ED} (ml)
60.0	489	4.4812×10^6	192

Table 36 Estimated and calculated parameters of subject 730

(Feature Set 2: $(dp/dt)_{max}$ P_{mean} deltaP P_{max})

Objective function = 0.0238

E_{LV} (dyn/cm^5)	V_{ED} (ml)	SVR (dyn/cm^5.sec)	C.O. (l/min)	S.V. (ml)
2643.8	201.8	1373.9	5.11	85.03

Table 37 Estimated and calculated parameters of subject 730

(Feature Set 1: P_{mean}/V_{mean} $(dp/dt)_{max}$ P_{mean} deltaP)

Objective function = 0.6011

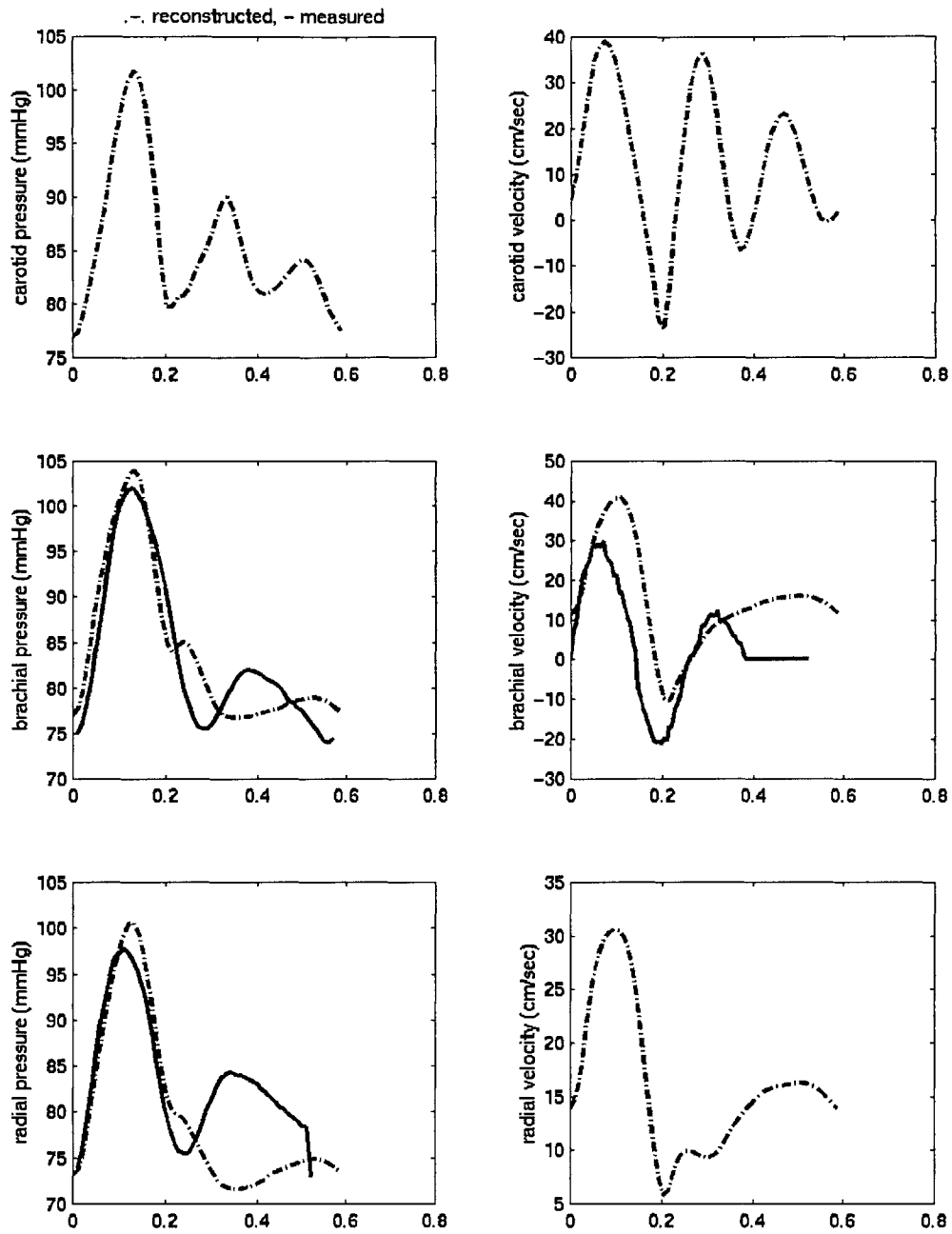| E_{LV} (dyn/cm^5)	V_{ED} (ml)	SVR (dyn/cm^5.sec)	C.O. (l/min)	S.V. (ml)
7030.66	102.85	2664.58	N/A	N/A
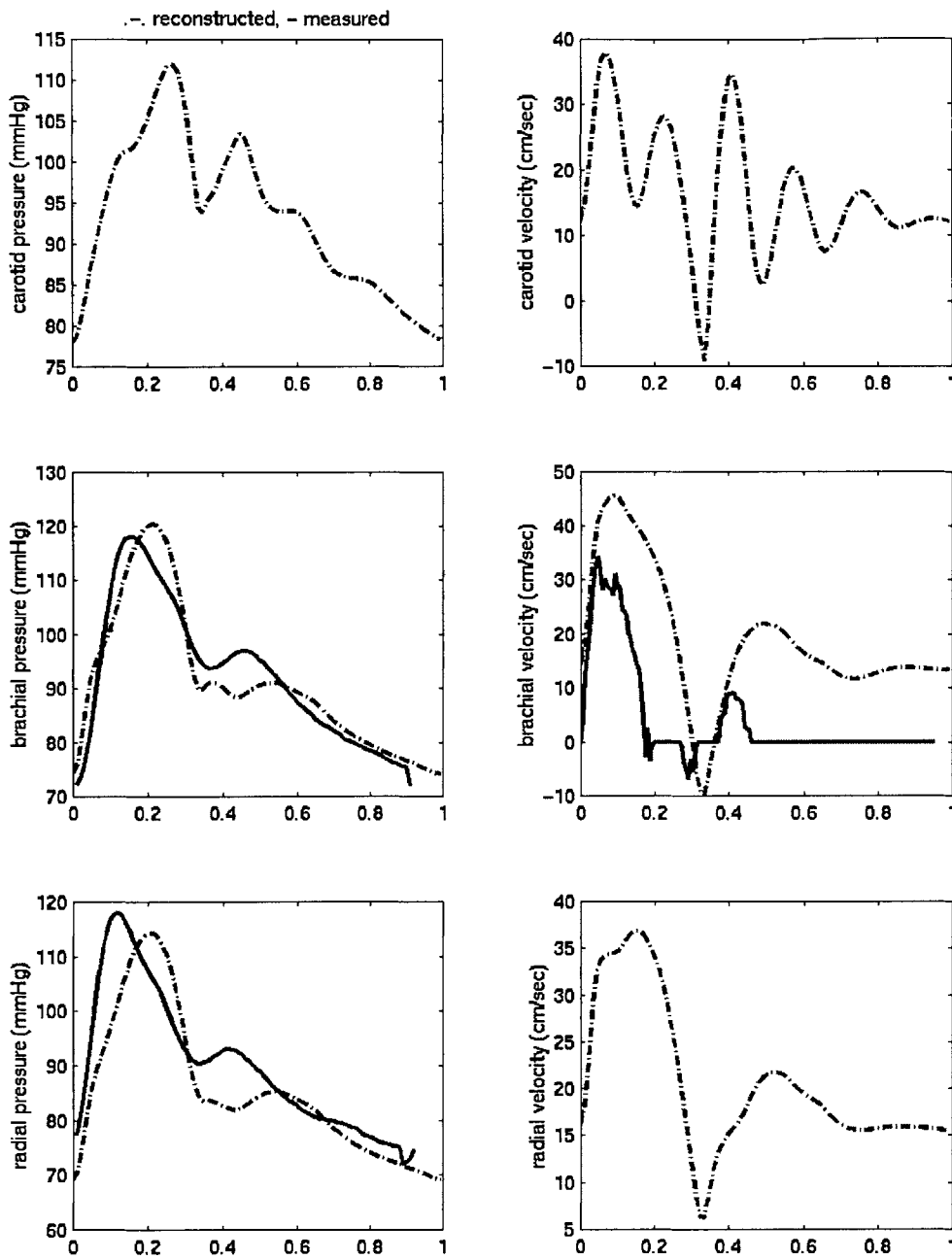
Figure 28 Reconstruction of subject 730

Table 38 Estimated and calculated parameters of subject 730

(Feature Set 3: (dp/dt)$_{max}$ P$_{mean}$ deltaP)

(V$_{ED}$ as known)

Objective function = 0.0146

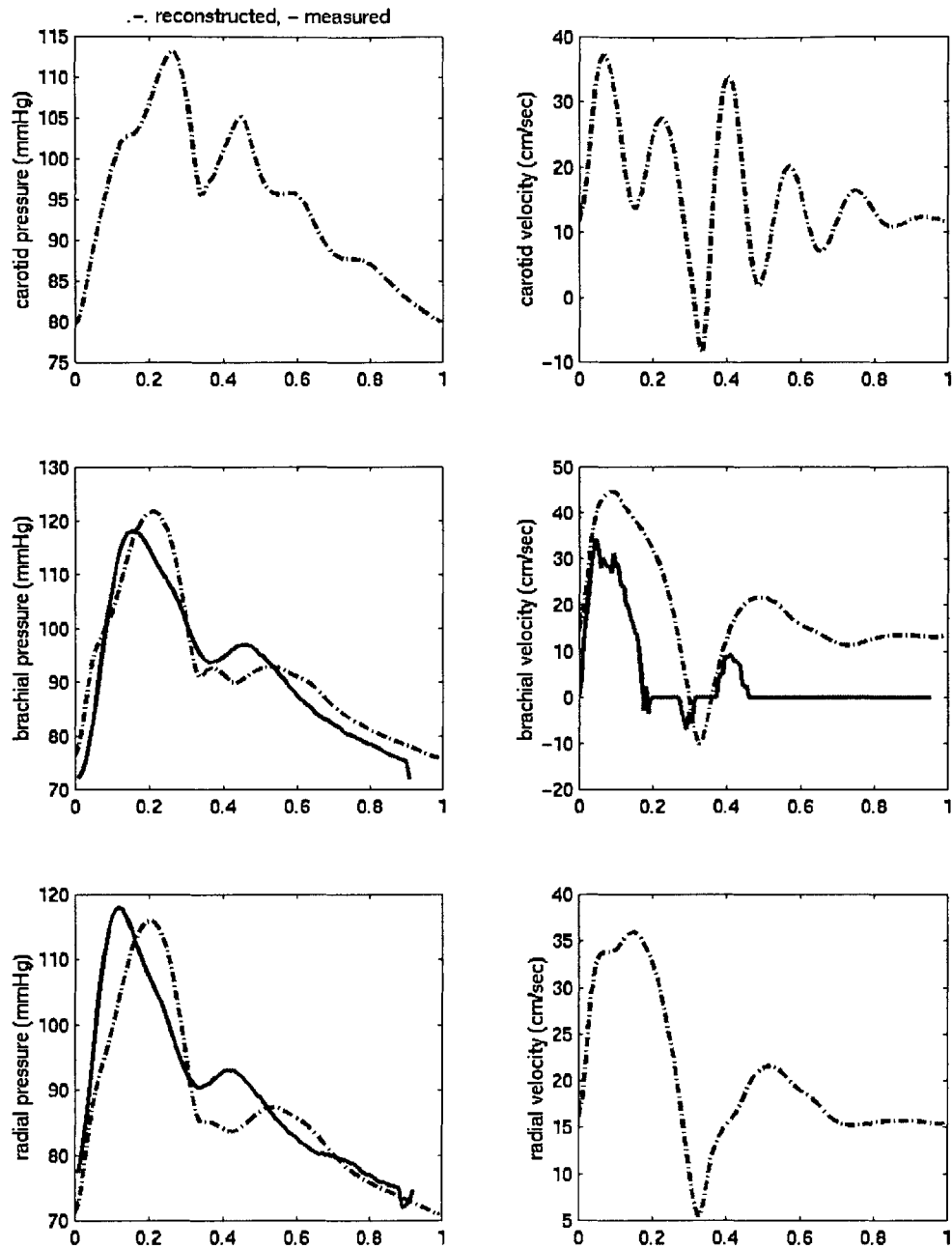| E$_{LV}$ (dyn/cm^5)	V$_{ED}$ (ml)	SVR (dyn/cm^5.sec)	C.O. (l/min)	S.V. (ml)
2843.2	192.0	1432.3	4.99	83.11

.-. reconstructed, – measured

Figure 29 Reconstruction of subject 730

(V_{ED} as known)

112

Discussion

Comparison of the Feature Sets

The accuracy of parameter estimation in human subjects can be assessed by a variety of methods. Although a direct comparison of the predicted parameter values to an accurate, possibly invasive, measurement is the most effective evaluation, this is not often possible. Alternatively, since the objective function provides a measure of the error between the measured and predicted waveforms, its value is one indicator of the degree of agreement. Parameter estimation results in tables 3 to 38 show that feature set 2 usually gives smaller objective functions than feature set 1. Most of the objective functions using this feature set are less than 0.1, while those using feature set 1 are larger than 0.3. The value of the objective function that the estimation reached can be a necessary measure of accuracy of parameter estimation, but it is not sufficient since it is possible that multiple combinations of parameters might yield the same features. Additionally, because the relation of features and parameters is non-linear and may have multiple minima, the search process may wind up some point far from the real parameter values in the feature-parameters space. Still, it seems reasonable that a smaller objective function represents a closer fit, and experience indicates that a correct estimation should have an objective function with a value less than 0.1.

It therefore follows that feature set 2 generally provides a better estimate from the measured data since the objective functions obtained using this set (based solely on pressure data) are smaller than those using feature set 1 (based on both pressure and velocity waveforms). This contradicts the findings presented in chapter 1, where it was found that feature set 1 produced smaller errors in parameter estimation of model-generated pressure and velocity curves. There are several possible explanations for this inconsistency. One is that noise in the measured acoustic signal affects data processing process and compromises the accuracy of velocity data. This problem is quite obvious in some cases producing velocity data that are clearly unreasonable. Another reason may be that the velocity calculated by the computational model is not realistic, i.e. it is not consistent with the realistic velocity of human with the same hemodynamic parameters. Measured velocities were found to be consistently higher than the calculated values, lending some credence to this hypothesis.

Meanwhile, if it proves correct that pressure-related features alone (feature set 2) can yield fairly accurate estimates of the subject's parameters, it would simplify the measuring and data processing procedures required by the parameter estimation routine since velocity measurement would not be necessary.

Evaluation of Parameter Estimation Accuracy

To evaluate the accuracy of the estimated parameters, the most direct method is to compare them with the clinically measured values. Among the parameters estimated or calculated with our approach, V_{ED} can be measured non-invasively using ultrasound, SVR and C.O. are generally measured invasively in hospitals, while E_{LV} is not used in usual diagnosis and can only be measured in specific research labs in hospitals. Below we discuss cases in which several of these comparisons were made.

Cases with V_{ED} measured

Among the 12 subjects presented in this paper, we have measured values for V_{ED} for only 2, subject 671 and 730. For subject 671, the mean measured V_{ED} is 254ml (three measures were taken: 227, 281, 283ml, as mentioned in RESULTS), while our estimated value is 324ml using feature set 2 (Table 2.32). For subject 730, the measured V_{ED} is 192ml, while our estimated value is 202ml using feature set 2 (Table 2.36). Both values are within acceptable limits.

When the parameter estimation procedure was repeated for these two subjects with V_{ED} specified, the estimated results are very similar to the original estimations (when V_{ED} is estimated), which shows that taking V_{ED} as known is of little advantage indicating that the first estimation is sufficiently accurate. However, in chapter 1, figure 5 does show that when V_{ED} is known, the parameter estimations will be more accurate. Therefore, for these two measured cases, it may be a coincidence that it doesn't improve much with V_{ED} known. More comparisons should be made to study the effect of V_{ED} in estimation.

Cases with SVR and C.O. measured

Three heart failure patients were presented, subjects sa418, mc417 and 671. For the former two, C.O. and SVR were measured invasively.

For subject sa418, estimated SVR is 2134 dyn/cm^5.sec and the calculated C.O. is 2.55 l/min, compared to values of 1975 dyn/cm^5.sec (relative error: (2134.3-1975)/1975*100% = 8.07%) and 2.4 l/min (relative error: 5.81%) respectively, measured at 4:00PM. Since the pressure and velocity measurements were made at about 2:30PM, it is not clear what the actual values of SVR and C.O. were at that time, but the estimated results are promising. In addition, E_{LV} was estimated to be 943.1 dyn/cm^5, a low value consistent with the patient's condition.

For subject mc417, estimated SVR is 1417.3 dyn/cm^5.sec and calculated C.O. is 4.23 l/min. These compare favorably with the values of 1104 dyn/cm^5.sec (relative error: 28.4%) (or 1219 dyn/cm^5.sec, relative error: 16.3%, measured at 7:00PM) and 4.2 l/min (relative error: 0.71%) respectively, measured at 12:30PM. Again, it should be noted that the pressure and velocity measurements were made at about 2:30PM, so that the values of SVR and C.O. at the precise time of waveform measurement are unknown. The estimated value of E_{LV} for mc417 is 3267.9 dyn/cm^5, a little bit higher for this patient, but still lower than healthy values.

Estimation Evaluation for Volunteers

For volunteers who are not catheterized, invasive measurements of hemodynamic data were not available. Estimation accuracy was assessed in three ways (1). by comparing estimated values to normal ranges for healthy subjects, (2). by inspecting the objective function and (3). by comparing the reconstructed pressure and velocity curves with the measured one.

Normal values for V_{ED} in healthy male subjects should be in the range of 110 to 200ml depending on size and physical condition [12]. For females, this value will be smaller. For E_{LV} and SVR, the empirical normal ranges (coming from our clinical study) are 3800 ~ 6500 dyn/cm^5 and 1000 ~ 2000 dyn/cm^5-sec respectively. From the tables about estimation results on volunteers, it can be seen that most of the estimated parameter values for volunteers are in or near the normal ranges.

The objective functions for most estimations using feature set 2 are less than 0.1. As for the comparison of reconstructed and measured curves, no criterion for judgement exists. However, that the agreement appears reasonable, at least for brachial pressures (the one used for parameter estimation). When comparing the reconstructed and

measured profiles, note that because of measurement and data processing limitations, the velocity data for some of the cases were unreliable, and the amplitudes of radial or carotid pressures are not accurate because of calibration problems.

Significance of the Feature (dp/dt)$_{max}$

In other results not presented here using an early version of the CV model in which the time-dependence of left ventricular elasticity was approximated by a half sinusoid, we found $(dp/dt)_{max}$ to be an unreliable feature despite the fact that it proved useful in estimating model-generated data. In the current model, a new elasticity relation was employed for the left ventricle as mentioned in Chapter 1. This elastance curve was obtained from extensive experiments on patients and is likely to be a more accurate model for left ventricular elasticity. Using the current model and its generated solution library, we found that the use of $(dp/dt)_{max}$ improves the accuracy of parameter estimation on measured data. One reason feature set 2 including $(dp/dt)_{max}$ performs quite well is because it reflects the contractility of the left ventricle. If the latter is modeled accurately, the measured $(dp/dt)_{max}$ is consistent with the ones in the library, so that it can be useful in characterizing the pressure curve. This strongly suggests that the current left-ventricle-elasticity model is more appropriate than the former one.

In summary, the accuracy of parameter estimation for measured data critically depends on the accuracy of pressure and velocity measurement. In this section, all parameter estimation results are based exclusively on brachial data because we experienced pressure calibration problems at other measuring locations. Estimation using brachial pressure only (feature set 2) appears to give the most accurate results. In spite of the problems existing in measurement and the model, the current parameter estimation scheme looks promising in estimation of both volunteer data and patient data.

Reference:

[1] Geddes, L.A. The direct and indirect measurement of blood pressure. Chicago: Year Book Medical Publishers, Inc.; 1970

[2] Mackey RS, Marg E, Oechsli R. Automatic tonometer with exact theory: various biological applications. Science 1960; 131:1688-89

[3] Drzewiecki GM, Melbin J, Noordergraaf A: Deformational forces in arterial tonometry. IEEE Front Eng Comput Health Care 1984; 28:642-645

[4] Kelly R, Hayward C, Gans J, Daley J, Avolio A. Noninvasive registration of the arterial pressure pulse waveform using high-fidelity applanation tonometry. J Vasc Med Biol 1989; 1:142-9.

[5] M.Darcy Driscoll, J. et al ;Determination of appropriate recording force for non-invasive measurement of arterial pressure pulses; clinical science (1997) 92, 559-566

[6] Drzewiecki GM, Melbin J, Noordergraaf A. Arterial tonometry: review and analysis. J Biomech 1983; 16: 141-52

[7] Kelly R, Hayward C, Avolio A, O'Rourke M. Noninvasive determination of age-related changes in the human arterial pulse. Circulation 1989; 80: 1652-9.

[8] Fish, Peter. Physics and instrumentation of diagnostic medical ultrasound; Chichester; New York: Wiley; c1990.

[9] Feigenbaum, Harvey; Echocardiography; Lea & Febiger; 4th ed; 1986

[10] Lilly L.S.; Pathophysiology of Heart Disease; Williams & Wilkins; 2nd ed. c1997

[11] Gribbin B, Steptoe A, Sleight P. Pulse Wave Velocity as a Measure of Blood Pressure Change. Psychophysiology 1976; 13-1;

[12] Guyton and Hall; Textbook of Medical Physiology; Saunders; 9th ed. 1996

Graphical User Interface for CV Modeling and Parameter Estimation

To make the simulation and estimation programs easy to use by those who are not familiar with the model theory and the inner structure of the software, we designed a set of Graphical User Interface (GUI) in collaboration with Mr. Stanley Liang during his brief stay in Prof. Kamm's group. These programs were written in MATLAB under UNIX platform. It makes the whole software package friendly for users.

The interface consists of two parts: one is model simulation, the other is parameter estimation. The first one, as shown in Figure 2A.1, is to do simulations using the model by specifying the four input parameters: HR, E_{LV}, V_{ED}, SVR. The outputs of simulations are pressure and velocity curves at any location of the cardiovascular system. The second interface – parameter estimation interface, as shown in Figure 2A.2, can be used to input the measured pressure and/or velocity curves and to do parameter estimation using the model-generated library. The estimated parameter values will be listed in the interface and the user can choose to do simulation using the first interface to compare the measured pressure and velocity curves and the model reconstructed ones. In this way, the accuracy of parameter estimation can be evaluated and other desired parameters, such as Cardiac Output, can be calculated using the model.

No details about the GUI programming will be included in this thesis, only the guide for using this interface will be presented below.
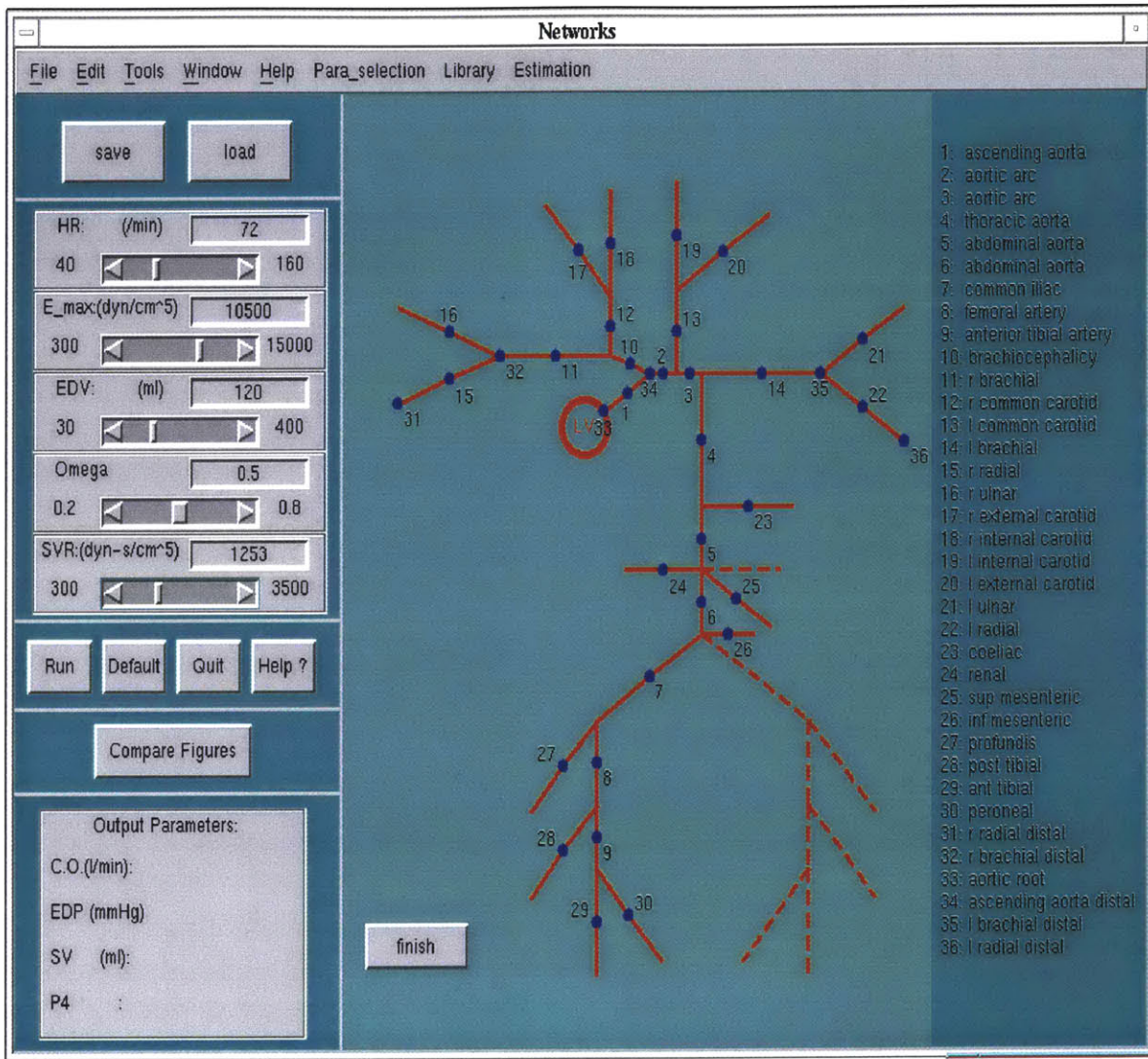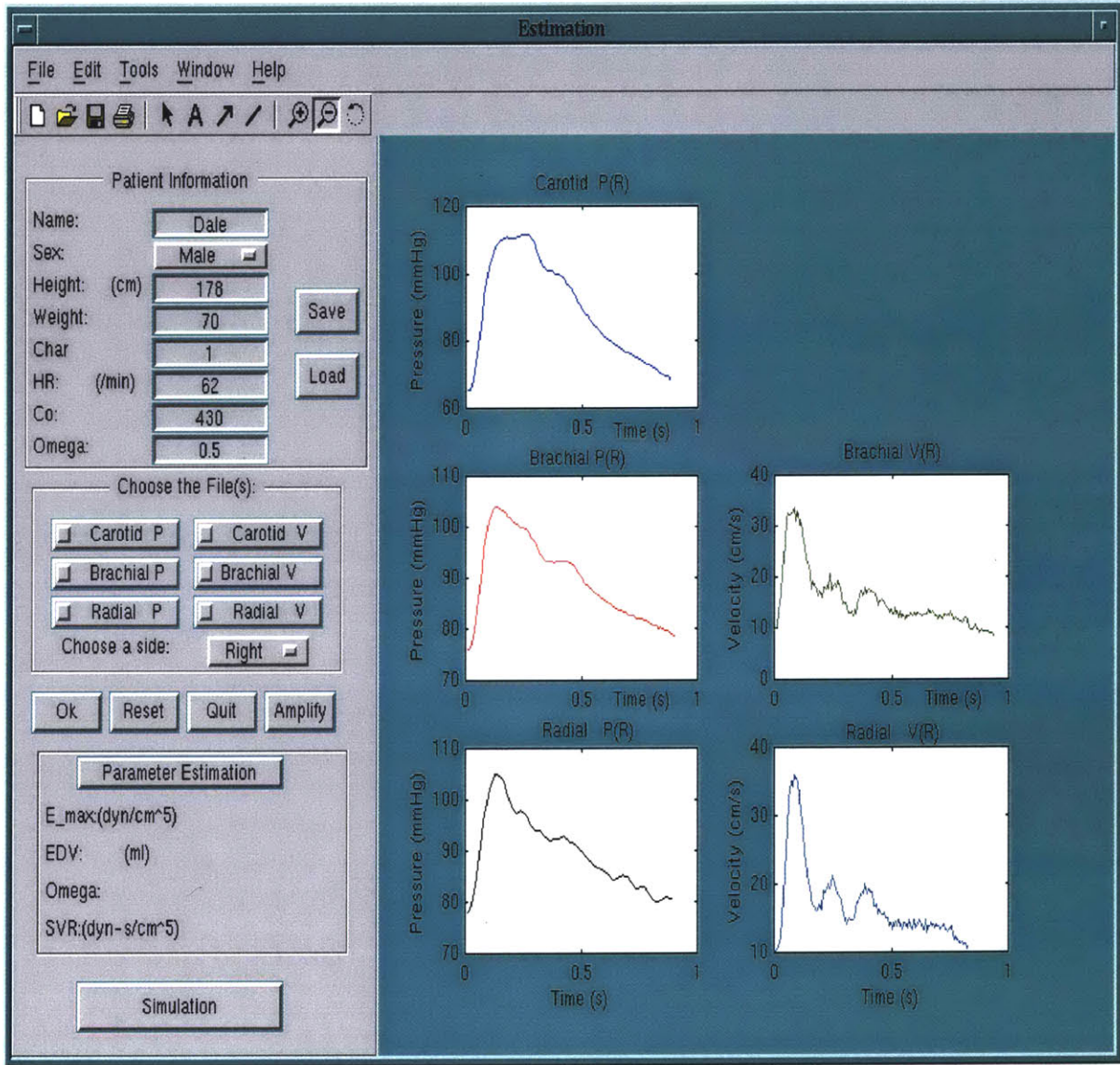
Figure 2A.1 GUI of Model Simulation

Figure 2A.2 GUI of Parameter Estimation

(Curves in the subplots are measured ones.

Carotid velocity was not measured for this subject.)

Guide for Using the CV Modeling and Parameter Estimation Software

a. Model Simulation

1. Run gui.m file and select "simulation", the Networks window will appear.
2. Specify parameter values for HR, E_{LV}, V_{ED}, SVR.
3. Push 'Run' button. If the parameter values specified are not physiologically reasonable, the program can not finish and it will tell the user to change the values.
4. Generally, it will take 3-8 minutes to finish a run in Dec Alpha workstation.
5. After it finishes, the user can save the parameters and output data file into one file, push 'save' button on top of the window. Each big dot on the arterial tree represents a point on the artery that can be selected. Pressure and/or Velocity and/or area as a function of time can be plotted. After selecting all the points the user wants to display, push 'finish', the curves will be shown in separate windows. Choosing 'compare', curves of different locations can be displayed in one window to compare their differences.

Notes: there will be warning messages like the following when running the model,

cycle 2

WARN- velocity approaching c, element 1, node 6

WARNING II - velocity exceeding c, element 1

......

These are normal messages. They are showing that the program is adjusting one of the parameter η for computational stability and finally when it reaches stable, these warning messages will disappear.

After the program is finished, it gives C.O. (Cardiac Output) SV (Stroke Volume) values. Discard EDP and P4 since they have no practical meanings here.

b. Parameter Estiamtion (P. E.)

1. Run gui.m file and select "Estimation", the parameter estimation interface appears. In this interface, the user needs to input patient data first. Some of the data are necessary for calculations, such as: HR (Heart Rate), Char (Character length -- the length from the elbow to the end of radial artery, 22.9 cm in the model), C_o (wave speed). Other data are just for reference. (The parameter Omega was once used as an input to the estimations, but now it is not needed, however, when using the current GUI, this item should be filled with any value between 0 and 1. Revision of the GUI is needed to update).

   After inputting patient information, the user can save them to a file, and load them later.

2. Next step, choose the pressure and velocity files, and the side (left or right arms) on which measurements were done. Push "Ok", the P, V profiles will be plotted in the window.

3. Now, ready to choose "Parameter Estimation", after this is done, the estimated parameter values will appear in the window. 3-6 minutes are needed for it to finish.

4. After parameter estimation, Simulation can also be done using the estimated parameter values to generate the pressure, velocity and area curves at any artery of this person. This procedure is called "Reconstruction" for convenience.

Notes: The programs for parameter estimation are mainly in "outputs" directory. The current version of estimation uses features from brachial pressure only, but can be easily modified to use both pressure and velocity features.

For patient parameter estimation, we are using brachial pressure/velocity, current package only has qshep*, c_out*, mods_out* files for this location. To get these files for other locations, run "libindex*" file manually, this procedure is not included in GUI.

In this package, a set of patient measurement data is provided. To use it, 'load' 'demo1' file for patient information, and load pressure file: 'demopre281bracali', and velocity file: 'demovel281bradata' and use location 2 to do parameter estimation.

An important issue is that the simulation is currently designed for Co=462cm/sec, Leng=22.9cm only, so if after parameter estimation, the user want to see "reconstruction" results, the P, V curves from model simulation should be converted to "realistic" values by using:

$$P_{real}=P/462/462*Co*Co$$
$$V_{real}=V/462*Co$$

Only P_{real} and V_{real} can be compared with the measured P and V. Further improvement is needed on the GUI and related programs to include this function.

3. Conclusions and Future Work

Hemodynamic parameters such as SVR and E_{LV} are often resources used by physicians for diagnosis and to adjust treatment plans. These parameters are usually measured and/or further calculated invasively is inconvenient and often cause discomfort. A non-invasive hemodynamic parameter estimation method has been developed and tested. Parameter estimation errors for model-generated pressure and velocity curves are less than 10% for E_{LV}, V_{ED}, and less than 3% for SVR using brachial pressure. 12 subjects have been studied in hospital to preliminarily test the method. As presented in part 2, promising results have been achieved on estimating the measured brachial pressure profiles.

However, there is still much opportunity to refine the cardiovascular model and to improve the parameter estimation accuracy on measured data.

Problems existing in the CV model

The current model uses a new elastance curve E*(t) for left ventricle as mentioned in part 1. This curve was got from experiments on patients, and the relation for E(t) and pressure of left ventricle was assumed as shown in equation 3.1, where there is no viscoelastic term.

$$P_{LV} = E(t) \times (V_{LV} - V_0) \qquad (3.1)$$

and $\quad E(t) = E*(t) \times E_{LV}$

In previous models, the expression including a viscoelastic term is:

$$P_{LV} = E(t) \times (V_{LV} - V_0) + (1 - \sigma) \times (-\partial V / \partial t) \qquad (3.2)$$

When incorporating the new E*(t) curve into the CV model, however, the viscoelastic term in the previous model was not changed in a manner consistent with

125

equation 3.1. In this way, the meaning of E_{LV} is the same as in the previous model and the model output is similar to that of previous ones, as shown in Figure B2. In changing the elastance model by deleting viscoelastic terms, the meaning of E_{LV} must be changed too. For example, if with viscoelastic term, a value of 4500 dyn/cm^5 of E_{LV} is viewed as normal, without visco-term, the normal value should be lower than 4500. Otherwise, the generated pressures will be very large since the damping is left out, as shown in Figure 3.1.

From figure 3.1, not only the amplitude of the 4th curve changed from the previous models, but also the shape of the profile changed greatly. Therefore, further work should be done to study how to incorporate the relation of equation 3.1 into the CV model. Other modifications may also be necessary.

Another problem existing in the current model concerns the radial velocity. The simulated velocity (often with a peak of around 20 cm/sec) seems to be smaller than our measured ones. Although there is not a reliable reference for radial velocity values, we suspect that to the peak values should be in the range of 40-60 cm/sec for normal subjects, based on our own measurements.

In addition, to solve the problem of instability in the current model, two small elements located in the aortic arch were added near the aortic artery to make calculations more stable. However, the addition of these two elements were found to introduce new oscillations in the carotid pressure and velocity (while having no obvious results on brachial and radial ones), as can be see in figures 2.18 through 2.31. Further study is needed to identify the source of these oscillations and, if determined to be artificial, to eliminate them.
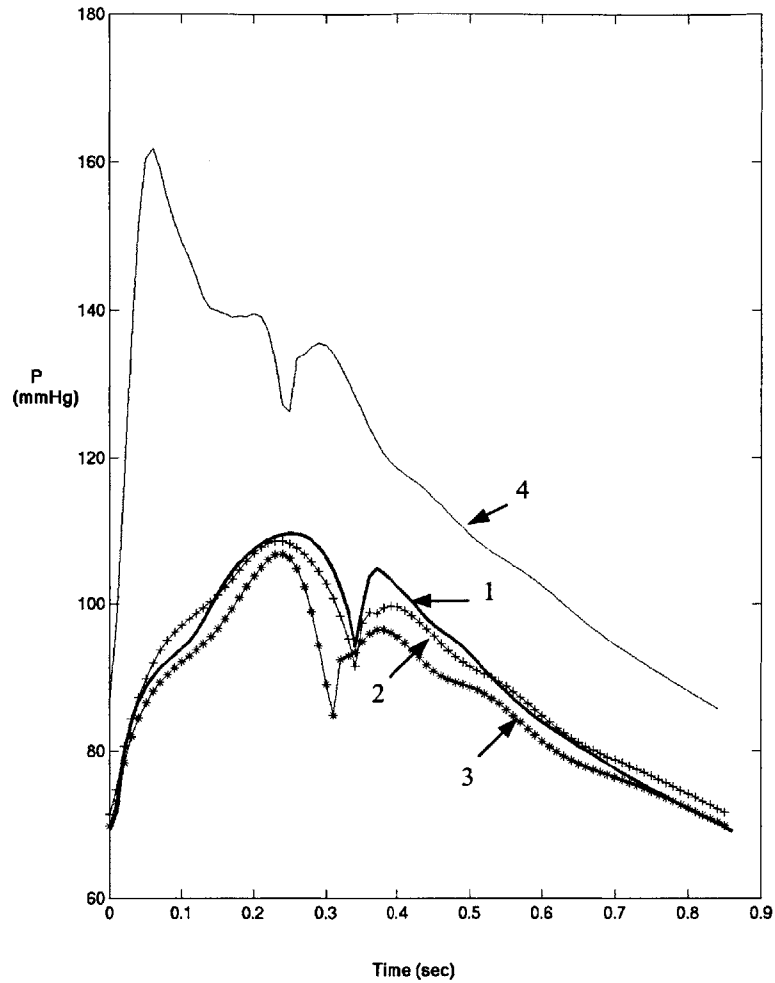
Figure 3.1 Comparison of model outputs

(Curves 1 to 3 are the same curves shown in figure B2 generating

from 3 models, the 3rd one is the one used in this thesis. Curve 4 is the

pressure curve when using the same value of E_{LV} in the elastance model

without viscoelastic term, shown in equation 3.1)

Problems in measurement and data processing

Although the Millar tonometer yields a continuous pressure trace, the acquisition of stable ones requires considerable practice. As mentioned in part 2, the measured pressure depends on the external force applied, the direction of the probe, etc. Any deviation from the optimal applanation position will result in errors in measured pressure. What's more, the tonormeter is incapable of measuring absolute pressure values with precision in our experience. We emphasized in part 2 that because of the inaccurate calibration, carotid and radial pressures are not reliable and should not be used in parameter estimation. To solve this problem, either new equipment is needed or improvement on the current tonometer is needed. For example, by making a mounting and adding an external force sensor for this tonometer, the external force can be controlled and the applanation position can be adjusted accordingly. In this way, errors in calibration can be reduced and no any more strict requirement on the operator's experience.

For velocity data, the original Doppler signal is often accompanied by considerable noise, thus, the velocity measurement accuracy will heavily rely on and be affected by data processing technique. This problem may be inevitable for non-invasive measurement. However, careful study of the usage of ultrasound probes (or maybe by using another probe) may help.

Since one of the ultimate objectives of this project is for automatic healthcare monitoring at home, wearable pressure and velocity measuring probes will be needed and real-time automatic data processing of pressure and velocity will be a major challenge (note that the current data processing techniques need operator interference).

Additional parameter estimation errors are introduced due to uncertainty in the measurement location. We have assumed that the pressure and velocity measurements are made at the distal ends of the brachial and radial artery and the mid-point of carotid artery. However, in reality, the locations can be easily different from distal ends, since no one can detect for sure where the distal point is. For pressure, this may be not a serious problem, since calculations show that pressures of other points near the distal end

are very similar to that of the distal end. However, for velocities, significant differences might arise. Velocity increases gradually away from the distal end and approaching the mid-point of the artery (the point of largest velocity amplitude). A difference of 5-10 cm/sec may be found between mid and distal velocities. Whenever possible, efforts should be made to ensure that pressure and velocity measurement for each artery are done at approximately the same location in one test, and this location should be near distal point.

In summary, although the current parameter estimation method gives encouraging results in estimating both model-generated and measured data, both the CV model and the measurement process could be improved. Further work, both numerical and experimental is needed to evaluate the entire approach further, including evaluation of parameter estimation accuracy and the ability to predict changes in all critical hemodynamic variables.